

Review

Advanced Gas Turbine Cooling for the Carbon-Neutral Era

Kenichiro Takeishi ^{1,*} and Robert Krewinkel ²

¹ Department of Mechanical Science and Engineering, Graduate School of Engineering Science, Osaka University, Toyonaka 560-8531, Japan

² Faculty of Mechanical Engineering and Economic Sciences, Graz University of Technology, Inffeldgasse 25, 8010 Graz, Austria; robert.krewinkel@tugraz.at

* Correspondence: takeishi@mech.eng.osaka-u.ac.jp

Abstract: In the coming carbon-neutral era, industrial gas turbines (GT) will continue to play an important role as energy conversion equipment with high thermal efficiency and as stabilizers of the electric power grid. Because of the transition to a clean fuel, such as hydrogen or ammonia, the main modifications will lie with the combustor. It can be expected that small and medium-sized gas turbines will burn fewer inferior fuels, and the scope of cogeneration activities they are used for will be expanded. Industrial gas turbine cycles including CCGT appropriate for the carbon-neutral era are surveyed from the viewpoint of thermodynamics. The use of clean fuels and carbon capture and storage (CCS) will inevitably increase the unit cost of power generation. Therefore, the first objective is to present thermodynamic cycles that fulfil these requirements, as well as their verification tests. One conclusion is that it is necessary to realize the oxy-fuel cycle as a method to utilize carbon-heavy fuels and biomass and not generate NO_x from hydrogen combustion at high temperatures. The second objective of the authors is to show the required morphology of the cooling structures in airfoils, which enable industrial gas turbines with a higher efficiency. In order to achieve this, a survey of the historical development of the existing cooling methods is presented first. CastCool[®] and wafer and diffusion bonding blades are discussed as turbine cooling technologies applicable to future GTs. Based on these, new designs already under development are shown. Most of the impetus comes from the development of aviation airfoils, which can be more readily applied to industrial gas turbines because the operation will become more similar. Double-wall cooling (DWC) blades can be considered for these future industrial gas turbines. It will be possible in the near future to fabricate the DWC structures desired by turbine cooling designers using additive manufacturing (AM). Another conclusion is that additively manufactured DWC is the best cooling technique for these future gas turbines. However, at present, research in this field and the data generated are scattered, and it is not yet possible for heat transfer designers to fabricate cooling structures with the desired accuracy.

Keywords: carbon neutrality; industrial gas turbine; turbine cooling; double-wall cooling; additive manufacturing; hydrogen; ammonia; CCGT; IGCC; Oxy-fuel combustion; HAT cycle



Citation: Takeishi, K.; Krewinkel, R. Advanced Gas Turbine Cooling for the Carbon-Neutral Era. *Int. J. Turbomach. Propuls. Power* **2023**, *8*, 19. <https://doi.org/10.3390/ijtp8030019>

Academic Editors: Tony Arts and Rodolfo Bontempo

Received: 29 January 2023

Revised: 2 May 2023

Accepted: 12 June 2023

Published: 24 June 2023



Copyright: © 2023 by the authors. Licensee MDPI, Basel, Switzerland. This article is an open access article distributed under the terms and conditions of the Creative Commons Attribution (CC BY-NC-ND) license (<https://creativecommons.org/licenses/by-nc-nd/4.0/>).

1. Introduction

The Paris Agreement, an international framework on climate change, was adopted at the Conference of the Parties to the United Nations Framework Convention on Climate Change (COP21) in 2015 and has entered into force in 2016. The first paragraph (a) of article 2 of the Paris Agreement states that the signees will be “holding the increase in the global average temperature to well below 2 °C above pre-industrial levels and pursuing efforts to limit the temperature increase to 1.5 °C above pre-industrial levels, recognizing that this would significantly reduce the risks and impacts of climate change” [1].

In response to the Paris Agreement, all parties to the agreement are required to prepare and submit nationally determined contribution (NDC) targets for greenhouse gas emission reductions every five years, based on their own national circumstances. Based on this agreement, the parties prepared a Long-term Strategies portal [2]. This section describes the long-term

strategies of Japan and Germany, to which the authors belong. Japan aims to reduce greenhouse gas emissions (GHG) by 46% in 2030 (compared to 2013) and to achieve net zero emissions in 2050. Germany, on the other hand, aims to achieve a GHG emission reduction of 65% in 2030 (compared to 1990), net zero in 2045 and negative emissions after 2050.

In Japan, the Cabinet approved the “Long-Term Strategy as a Growth Strategy Based on the Paris Agreement” in October 2021. The energy section of this strategy calls for Japan to use 50–60% renewable energy, 30–40% nuclear power and thermal power with carbon capture, utilization and storage (CCUS), and 10% hydrogen or ammonia as energy in 2050 [3]. In Germany, efforts are aligned with and need to be seen within the context of the goals and measures of the European Union. This is, in particular, the European Green Deal [4], which was put in a legal framework by the European Climate Law [5]. The Green Deal defines both natural gas and nuclear power as green (transition) technologies. The EU supports the erection of CHP plants as long as they adhere to the Emissions Performance Standard of 250 g CO₂/kWh, even if fossil fuels are used [6]. In future, these plants will be converted to burn hydrogen or other carbon-neutral fuels or, alternatively, retrofitted with CCS. Although general directives are defined by the EU, the realization of the goals defined therein is the task of the different countries. Germany plans to generate all of its electricity from renewables in 2050. The electricity will be predominantly generated by a mix of photovoltaics, wind and some geothermal energy; nuclear energy will not be a part of the energy mix, but a number of other countries in the EU are planning new nuclear capacity. Fluctuations will be compensated by combined cycles and combined heat and power plants burning hydrogen or biogas.

The long-term strategies of the two countries indicate that renewable energy sources will continue to grow significantly in order to achieve carbon neutrality. However, as the proportion of renewables—which are subject to load fluctuations—increases, thermal and nuclear power, which have inertia, will be required to stabilize a certain proportion of the power supply. Since nuclear power is a power generation system that is not suitable for adjusting to short-term load fluctuations, thermal power must exclusively play this role, which now accounts for about half of renewable energy.

Currently, the most advanced combined cycle gas turbine (CCGT), which is the most efficient large-scale power generation system, has a thermal efficiency of 64% (LHV), which is about 40% more efficient than coal-fired power generation, and can reduce CO₂ emissions to about one-third of those from coal-fired plants [7,8]. However, even CCGTs will need to undergo further changes and developments in order to be a major source of power generation and achieve carbon neutrality in 2050.

The purpose of this paper is to describe the trend of heat transfer to airfoils and cooling technologies for industrial gas turbines in a carbon-neutral environment. In order to achieve this, it is first necessary to clearly describe the differences in characteristics between industrial gas turbines and aviation jet engines. The first feature of industrial gas turbines is the diversity of fuel types. In particular, small industrial gas turbines are used for cogeneration, which is relatively inexpensive and allows the use of inferior fuels. The second feature is that in industrial gas turbines, there is no weight limit, and any coolant can be used. This feature allows the cooling air extracted from the compressor outlet to cool the turbine blades using a heat exchanger. Additionally, a coolant different from the working fluid, such as water, which has an excellent cooling performance, can be used as well. The third difference is that the industrial gas turbine can be configured with a variety of cycles, some of which are aligned with the second feature. One of these thermal cycles, the CCGT, is already in practical use. Understanding these three major characteristics of industrial gas turbines is necessary to consider future trends in turbine stationary vanes and rotor blades.

In addition to the above features, a carbon-neutral CCGT must have the ability to adjust its electricity output according to load fluctuations, as mentioned above. Considering the increase in cost of new CCUS for conventional natural-gas-fired CCGTs and the increase in production cost of new fuels, such as hydrogen or ammonia, compared to natural gas, it is necessary to further improve the thermal efficiency of the current CCGTs. This

will require increasing the turbine inlet temperature from the current 1600 °C class large industrial gas turbines to the 1900 °C–2000 °C level. This load flexibility is exactly the same as that possessed by aviation jet engines. The major difference is that the airfoils of a large industrial gas turbine are about four times larger than those of an aviation jet engine and have a very large heat capacity—more than four to the third power—so it is necessary to develop new cooling designs.

In this review paper, as a preliminary step to discuss the trend of heat transfer and cooling technologies for industrial gas turbines, we first review cooled airfoils applied to industrial gas turbines. In each stage of development, optimal power generation systems and CHP have been developed for industrial gas turbines taking advantage of the above three characteristics. In addition, there are many thermodynamic cycles that have been realized in demonstration plants but are not yet in practical use. Knowing these legacies, we believe this is a legitimate approach to discussing industrial gas turbines in the carbon-neutral era and the turbine cooling blades, which will be used for them.

Based on the above ideas, the turbine cooling blades researched and developed to date were examined, and the results show that CastCool[®] and wafer and diffusion bonding airfoils are suitable for future industrial gas turbines. In the light of these studies, double-wall cooling developed from the CastCool[®] blade structure is very promising. It is also clear that the ability to fabricate complex turbine cooling structures, such as double-wall cooling (DWC), using additive manufacturing (AM) methods is essential. However, no DWC blades for future ultra-high temperature gas turbines have been shown in the open literature to date, and the fabrication of vanes and blades with simple cooling structures using AM has just begun. Moreover, the standard thickness of AM layers is about 0.6 mm, making it impossible to fabricate elaborate film cooling holes and impingement nozzle holes. Accordingly, this paper reviews the current status of research on DWC blades and the AM method. The fabrication status of double-wall cooling blades is also reviewed, as are heat transfer studies on the cooling methods that comprise this cooling structure, such as internal impingement cooling, full coverage film cooling and effusion cooling. Finally, the trends in carbon-neutral cooling structures for turbine vanes and rotor blades of industrial gas turbines are summarized.

The paper also reviews the results of feasibility and R&D studies of various gas-turbine-based thermal cycles to address fuel diversification and performance improvement. It is also concluded that an oxy-fuel cycle is suitable as a cycle with gas turbines as the main heat source.

Note that wherever stationary vanes and rotor blades are discussed, it is assumed that a “vane” is stationary, and a “blade” rotates. When a statement is applicable to both, the term “airfoils” will be used.

2. Historical Development of Industrial Gas Turbines

2.1. Development of Large Industrial Gas Turbines to Date

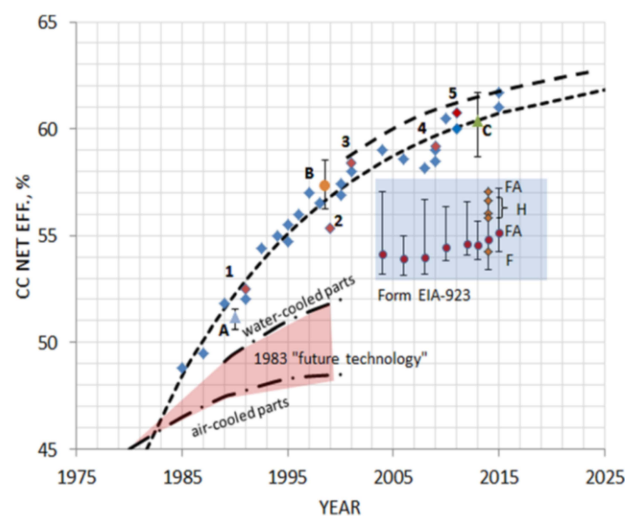
Under the leadership of Aurel Stodola, the world’s first industrial gas turbine was put into commercial operation for power generation in Neuchâtel, Switzerland, in 1939 [9,10]. The gas turbine was manufactured by Brown, Boveri & Company (BBC) with a speed of 3000 rpm, a turbine inlet temperature of 550 °C, a thermal efficiency of 17.4% and an output of 4000 kW. This period coincided with the successful development of the world’s first jet engine for aviation by Whittle and Hans Von Ohain [11,12]. Aero jet engines had made great strides since then. However, improvements in the thermal efficiency of industrial gas turbines could not compete with the speed with which the thermal efficiency of steam turbines improved in the 1950s and 1960s. In the 1960s, steam turbines began to use steam at supercritical pressure and became heat engines with thermal efficiencies exceeding 40% (LHV). On the other hand, large industrial gas turbines were developed with turbine inlet temperatures in the 900 °C class, and the stand-alone thermal efficiency of gas turbines reached the upper half of the 20% range (LHV). Because their thermal efficiency was inferior to that of steam turbines, they were almost exclusively used for peak shaving.

In the 1970s, three aero engine manufacturers began the development of a 1250 °C class aero engine to be installed in the Boeing 747. Aero engines further evolved to 1350 °C. Following this technological trend, four OEMs of large industrial gas turbines (General Electric Corporation (GE), Westinghouse Electric Corporation (WH), Siemens, Brown, Boveri & Company (BBC, later ABB/Alstom)) succeeded in developing a large 1100 °C class industrial gas turbine in the late 1970s.

Various power generation systems and cogeneration thermal cycles using industrial gas turbines as the main engine have been studied [13]. Among these thermal cycles, the combined cycle gas turbine (CCGT), which combines a Brayton cycle gas turbine and a Rankine cycle steam turbine, was found to have a simple equipment configuration and to generate electricity with high thermal efficiency [14,15]. The CCGT was established as a response to the two oil crises that occurred in the 1970s.

One of the early examples of the development of large CCGTs is the combined cycle power plant of Tohoku Electric Power Co. The gas turbine used in this CCGT was a 701 D gas turbine with a frequency of 50 Hz designed and manufactured by Mitsubishi Heavy Industries Ltd. (MHI), Takasago, Japan. The gas turbine was developed by MHI based on the 60 Hz 501D5 gas turbine developed by WH, the turbine inlet temperature of which was 1154 °C [16]. The thermal efficiency of the CCGT using this gas turbine was over 48% (LHV), which was more than 10% higher than the thermal efficiency of the most advanced coal-fired thermal power generation systems of the time. The use of liquid natural gas (LNG) as fuel reduced the carbon dioxide emissions by approximately 20% compared to coal-fired power generation [17]. The development issues included turbine cooling technology to ensure the reliability of the airfoils—even for the long periods between major overhauls—and the combustion technology for a low NO_x combustor that complied with Japanese environmental regulations. The world's first premixing combustor was therefore developed for the 701D.

In response to the strong global demand for CCGTs, gas turbine manufacturers focused on developing larger industrial gas turbines with higher temperatures and pressures. This led to the development of the 1300 °C class F-type gas turbine and the 1500 °C class G- and H-type gas turbines. The thermal efficiency (LHV) of CCGTs using these gas turbines is shown in Figure 1 [18]. Figure 2 also shows the thermal efficiency transition for the case where the gas turbine is used in a simple cycle operation [18]. The symbols A, B, and C in Figure 2 are the same as those in Figure 1, and the symbol D is taken from the cited Reference 20.



(A: TMI 1990 Handbook, B: GTW 1998-99 Handbook, C: GTW 2013 Handbook, 1: Ambarli, Turkey, 2: Tapada do Outerio, Portugal, 3: Mainz Wiesbaden, Germany, 4: Kawasaki, Japan, and 5: Irsching, Germany). Actual U.S. gas-fired GTCC generation data, from U.S. Energy Information Administration Form EIA-923, include some duct-fired units (2014 data are "early release" not final; 2015 data are preliminary until May). For each year, top 20 natural gas-fired GTCC plants are selected. The circles indicate the average efficiency of those (uncorrected); error bars indicate #1 (highest) and #20 (lowest). GT classes for selected plants in 2014 are denoted by diamonds.

Figure 1. Evolution of CCGT efficiency in 1985–2015. CCGT evolution, 1985–2015 [18].

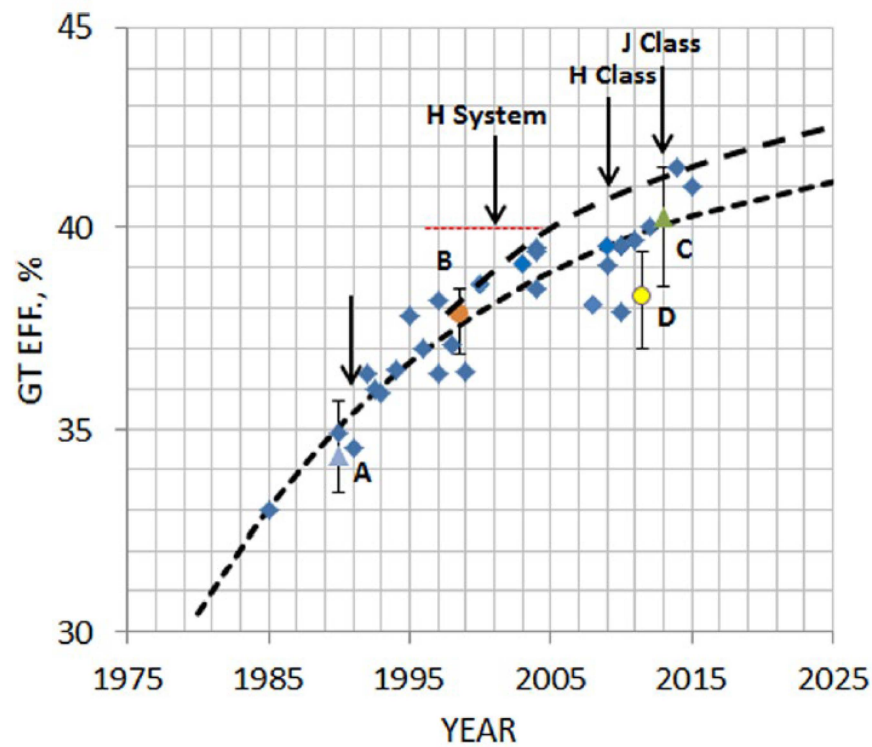


Figure 2. Evolution of large industrial gas turbine efficiencies in 1985–2015 [18].

Table 1 shows the status of development of F-type gas turbines with a turbine inlet temperature of 1300 °C by four OEMs [19,20]. First, GE developed the Frame 7F gas turbine, followed by WH. Both gas turbines had the same turbine inlet temperature, but the cooling design of the first-stage turbine blades was different: GE manufactured large directionally solidified (DS) first-stage rotor blades and used internal cooling with serpentine flow paths and no film cooling. WH and MHI collaborated on the development of the F-type gas turbine. MHI was in charge of the cooling design and the development of the low NO_x combustor. In this design, the first-stage rotor blades were manufactured by CC and used the world’s first film cooling for an industrial gas turbine in the serpentine cooling flow path.

Table 1. Westinghouse, Siemens and ABB react to GE’s “Frame 7F” [19].

Company	Turbine Model	Capacities		Efficiencies (%)		Key Dates Announced	Capacities First Order
		GT	CCGT	GT	CCGT		
GE	Frame 7F	150 MW	230 MW	34.2	53	1987	1987
Westinghouse	501F	150MW	230 MW	35.4	54	1989	1989
Siemens	V94.3	200 MW	300 MW	35.7	54	1990	1992
ABB	GT13E2	164 MW	250 MW	35.7	54.7	1992	1992
	GT24	165 MW	250 MW	37.5	57.5	1993	1993

As can be seen in Table 1, the thermal efficiency of ABB’s CCGT using their GT24/26 frames is remarkably high, even though the turbine inlet temperature is only 1300 °C. The company succeeded in achieving such high efficiency by adopting a reheat cycle. The use of the reheat cycle in gas turbines was proposed by Rice [21–23]. The pressure ratio of the GT24 gas turbine was set as high as 30, so that the gas temperature entering the re-combustor between the high and medium pressure turbines would be low. The design of the secondary combustor required a very sophisticated cooling technology.

Natural-gas-fired CCGTs using F-type gas turbines were highly efficient in power generation and contributed to the reduction in CO₂ emissions, leading to a worldwide

rush to construct such plants. Gas turbine manufacturers all planned to develop high-performance gas turbines, which would achieve next-generation CCGT thermal efficiency of 60% (LHV) [24], and the U.S. DOE's ATS project (1992–2001) was implemented to achieve this. In this project, GE focused on a cooling system with closed-loop steam cooling of the first- and second-stage vanes and blades. The advanced GT with closed-loop steam cooling of the turbine blades at the turbine inlet temperature (TIT) of 1500 °C was called the H class.

The power output and thermal efficiency of a gas turbine are determined by the inlet temperature at the first-stage blades. Therefore, the ratio of air used for combustion to air used for cooling the first-stage vanes is independent of performance and power output, as long as the gas temperature of the first-stage blades is the same. However, as the amount of air used to cool the first-stage vanes increases, the gas temperature in the combustor rises, which increases NO_x emissions. Therefore, the system of using steam extracted from the bottoming cycle to cool the vanes and blades, combustor walls and transition piece walls was a revolutionary method from the standpoint of establishing a low NO_x combustor. In addition, from the perspective of the steam turbine in the bottoming cycle, cooling the high-temperature components of the gas turbine with steam superheats the steam, thereby improving the thermal efficiency of the CC. While the closed steam-cooled GT cycle has the advantage of increasing the thermal output and thermal efficiency of the CCGT, it also poses a difficult problem to solve in terms of the reliability and service life of the steam-cooled components. In addition, any loss of steam to the gas turbine cycle for cooling purposes needs to be compensated for with make-up water. This can become a financial issue because the water in the steam cycle has to be demineralized.

Steam has superior cooling performance compared to air, so the cooling structure of the turbine cooling blade does not need to be complicated to achieve a high cooling performance. GE solved this problem by using large single-crystal castings for the airfoils. Another problem is that the condensation heat transfer coefficient of water vapor is extremely high at about 10⁵ kW/m²K. When the metal temperature of the rotor is lower than the temperature at which water vapor condenses, water flows over the surface of the rotating hot parts, which in some cases may cause thermal deformation of the rotor, resulting in vibration problems. To prevent this, it was necessary to heat the massive rotor of a large industrial GT to a temperature higher than the steam condensation temperature and to start the flow of steam only after the rotating body was warm enough. The need to heat the rotating parts meant that, while the CCGT gained the advantages of high power and high performance, it lost the advantage of being capable of a rapid start-up. However, GE developed the Frame 7H/9H GT [25], which achieved 60% (LHV) thermal efficiency for CCGTs, as shown in Table 2 [19].

Table 2. The GT24 heralds another new generation of gas turbines [19].

Company	Turbine Model	Capacities		Efficiencies (%)		Key Dates	
		GT	CCGT	GT	CCGT	Announced	First Order
ABB	GT24	165 MW	250 MW	37.5	57.5	1993	1993
Westinghouse	501G	230MW	345MW	38.5	58	1994	1997
Siemens	V84.3A	170 MW	245 MW	38	58	1995	1995
GE	Frame 7G	240 MW	350 MW	39.5	58	1995	none
	Frame 7H	n/a	400 MW	n/a	60	1995	2004
	Frame 9H	n/a	480 MW	n/a	60	1995	1998

WH also studied a gas turbine with a closed-loop steam-cooling system in the ATS project. However, they did not finalize the development. Instead, WH opted for a 1500 °C class G-type gas turbine in collaboration with MHI. WH was responsible for the design of the turbine section, and the cooling was developed in cooperation with Rolls-Royce [19]. Figures 3 and 4 show the cooling structure of the first-stage airfoils of this turbine [26].

Siemens acquired the power generation division of WH in 2001. This allowed Siemens to take over the 501F/G design to enhance the GT's high-temperature technology and also made available the steam-cooling technology developed for the U.S. government's ATS program [19].

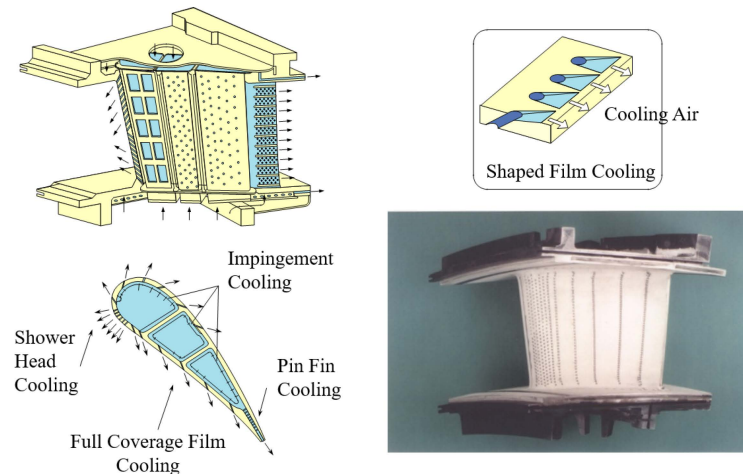


Figure 3. First vane of 1500 °C class G-type gas turbine [26].

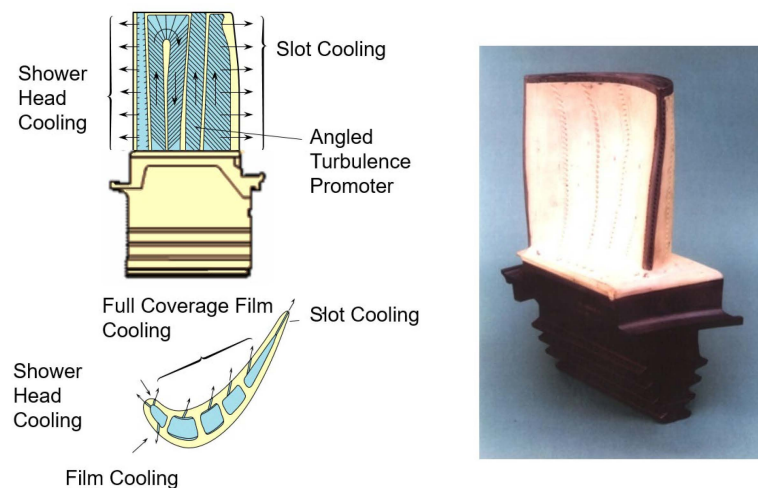


Figure 4. First blade of 1500 °C class G-type gas turbine [26].

In the new millennium, MHI independently developed a J-type gas turbine with a TIT of 1600 °C. This reflected the results of a Japanese national project started in 2004 to develop the technologies needed for a gas turbine with a TIT of 1700 °C. When the TIT of gas turbines was increased, the required parallel increase in coolant consumption counteracted the theoretical improvement in thermal efficiency [27]. In a Japanese national project, a revolutionary film-cooling hole geometry was developed, which significantly reduced the amount of coolant required [28]. The J-type gas turbine used steam to cool the combustor walls and the transition piece. The steam-cooling system was discontinued, and a JAC-type (J-class air-cooled) gas turbine with a TIT of 1650 °C was subsequently developed and employed in a combined cycle plant [8]. GE introduced the HA gas turbine, a fully modified version of the H-system, which had an open-air cooling system [29]. The HA gas turbine uses a system in which all hot components are cooled by air from the compressor discharge. Using the same definition of turbine inlet temperature (i.e., the average total temperature at the inlet of the first-stage vanes) as MHI, the temperature of GE's HA gas turbine is estimated to be 1670 °C [30]. The thermal efficiency of CCGTs

consisting of GE's HA-type gas turbine and MHI's JAC-type gas turbine achieved 64% (LHV). Because of the use of natural gas as fuel and such high thermal efficiency, these CCGTs have succeeded in reducing CO₂ emissions to about one-third of those emitted by state-of-the-art coal-fired power plants.

The history of the development of cooling structures for turbine airfoils used in large industrial gas turbines, described in this section, is described in detail in Ref. [31].

2.2. Development of Small and Medium Industrial Gas Turbines to Date

In this paper, gas turbines with an output of 50 MW or less will be defined as small and medium gas turbines. It is not economical to use small gas turbines of this size in a combined cycle. The amortization time of the investment costs of the steam turbine and steam generator is too long. This does not mean that small turbines are normally used in a simple cycle. Rather, they are used in some form of combined heat and power (CHP) application.

The basis for most small and medium-sized gas turbines was aero engine technology but modified for robustness and simplicity [32]. A multitude of companies have manufactured small and medium-sized gas turbines over the years (see Ref. [33]). Most of these are micro gas turbines with a power output well below 1 MW. These shall not be discussed any further, as they typically do not feature cooled blades and vanes.

In the 1970s, small gas turbines first became popular as a power source for emergency power generation facilities because of their compact size, because they did not require cooling water and because of their short start-up times. Up to the early 1970s, the airfoils could be made of uncooled super heat-resistant alloys, making them cost-competitive with gas engines, which was a factor in their widespread use. In the 1980s, the development of small and medium-sized gas turbines used for CHP applications was started. The gas turbines are thus used to produce electricity in various combinations with hot water, steam, both hot water and steam, or chilled water via absorption chillers. The most distinctive feature of small and medium-sized gas turbines is that they enable the optimal supply of electricity and heat in accordance with the needs of the plant side of the cogeneration system [34].

The development of small and medium-sized gas turbines has depended on competition with gas engines in terms of cost and thermal efficiency. If the power-to-heat ratio (PHR) (total power demand divided by total heat demand) of the application is less than approx. 0.8, the process is called heat-driven, and a gas turbine is usually used. If this ratio is exceeded, the process is considered power-driven, and an internal combustion engine (simple cycle efficiency >45%) is used [35]. Even when the PHR is greater than 0.8, a small gas turbine may be used when high-temperature steam is required. Plants using IC engines cannot generate high-temperature steam due to the inherently low exhaust gas temperature of the engine.

If there is excess steam produced by the exhaust gas boiler, it can be fed into the combustor chamber of the gas turbine, allowing the use of the steam-injected gas turbine (STIG) cycle or Cheng cycle, which enables a variable ratio of electricity to heat [36]. The Cheng cycle is shown in Figure 5.

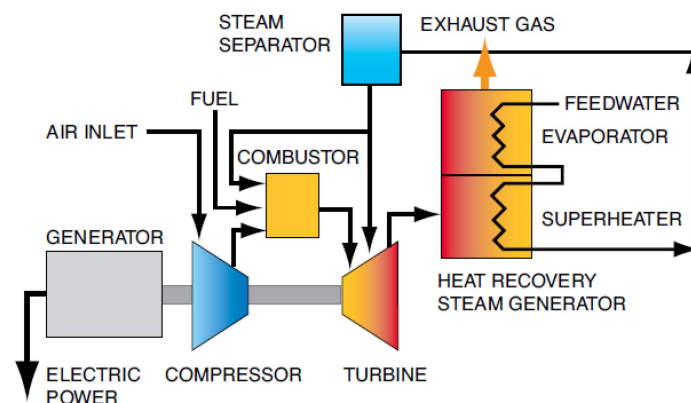


Figure 5. Steam-injected gas turbine cycle (STIG, Cheng cycle) [36].

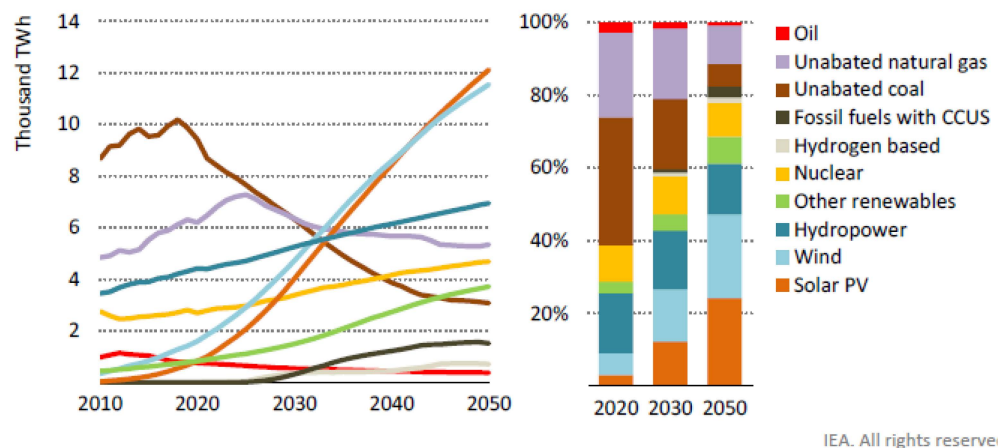
Because most of the applications for small gas turbines are heat-driven, much emphasis is placed upon both the mass and the temperature of the exhaust gas. Therefore, the simple cycle efficiency of the gas turbine is of less relevance, and turbines with a large and hot exhaust gas flow may provide a solution that is superior to that provided by turbines with a higher simple cycle efficiency [37].

Due to cost constraints and the size of small and medium gas turbines, the level of high-temperature technology, expressed primarily in terms of turbine inlet temperature, is at a lower level than that of a similarly sized aircraft jet engine or large industrial gas turbines. However, the turbine inlet temperature of these gas turbines has increased over the years from the 800 °C to 900 °C level, at which uncooled turbine blades are used, up to a TIT of 1300 °C currently in operation [38]. Cleaner fuel is of great importance for these gas turbines; therefore, the development of combustors that can use fuels such as hydrogen and ammonia is the key to success.

Some small and medium gas turbines are still used in simple cycles. This encompasses those used as an emergency back-up, as well as the twin-shaft turbines used in the oil and gas industry as mechanical drives. Neither of these groups shall be discussed here any further because the first fill a niche where, in general, reliability outweighs efficiency, and the second are broadly covered by the discussion of their counterparts used in power generation. This being said, it may well be that small SCGT will become more common again as their importance for load balancing grows: these turbines can start up quicker because no steam cycle is included.

2.3. Integrated Gasification Combined Cycle (IGCC) Technologies

Coal is a very abundant energy source, with reserves that are about four times greater than those of oil and natural gas combined. In 2020, about 85% of the world’s energy consumption came from fossil fuels, of which about 28% came from coal. In the same year, fossil fuels accounted for about 60% of global electricity generation, of which about 35% was coal fueled. As shown in Figure 6, the IAE estimates that the share of fossil fuels in electricity generation in 2030 and 2050 will be 40% and 20%, respectively, and that the share of coal will decrease to about 20% and 8% [39].



Renewables reach new heights in the APC, rising from just under 30% of electricity supply in 2020 to nearly 70% in 2050, while coal-fired generation steadily declines

Note: Other renewables = geothermal, solar thermal and marine.

Figure 6. Global electricity generation by source in the APC [39].

Research on a system to generate electricity from coal in a clean and efficient manner with a gas turbine began in the mid-1960s by GE. In the late 1970s, a coal-fired combined cycle plant was studied with funding from EPRI. In addition, GE studied water-cooled closed-circuit gas turbines under the DOE’s HTTT project. GE considered water cooling

for coal gasification gas turbines because the temperature of the blades should be kept below 538 °C to prevent adhesion of ash to the airfoils and to prevent corrosion of the super heat-resistant alloy. The HTTT project also had a development plan to gradually increase the TIT to 1100 °C, 1400 °C and 1600 °C [40]. In the late 1970s, the development of industrial gas turbines consisting of open-air-cooled circuits with TITs of 1100 °C had begun. However, the amount of air required to cool turbine blades for 1400 °C and 1600 °C class gas turbines using the cooling technology of the time would have been much too high. Furthermore, it was impossible to achieve a metal temperature of 538 °C using air-cooling technology.

GE knew that airfoils made of super heat-resistant alloys with internal water cooling could not meet the design life due to thermal fatigue caused by large temperature gradients in the thickness direction of the walls. Therefore, the company developed airfoils made of a copper alloy. The blades were developed with a system in which cooling water is blown out from the blade tips and collected at the shroud. The details of these problems are elucidated in Ref. [41]. Because of the difficulties encountered in solving problems such as water erosion in the cooling channels and vibration problems caused by boiling of the cooling water, the coal gasification water-cooled gas turbine was never put to practical use. The closed-circuit steam-cooling technology for hot parts used in the project as a back-up for water cooling was later developed by GE and commercialized as the H-system. This was already described in the CCGT section.

In the 1980s, R&D on IGCC using commercial gas turbines was pursued in the United States. The first of these projects was the Coolwater Project [42]. An 1100 °C class gas turbine modified from GE's 7001 E-type was used. Since then, many R&D projects have been conducted in Europe and the United States [43].

In Japan, the IGCC project in Nakoso, using a 701DA gas turbine with a TIT of 1200 °C, was used for power generation. The Nakoso IGCC cycle is shown in Figure 7 and its specifications in Table 3 [44]. The plant achieved a thermal efficiency of 42% (net LHV) or higher after successfully completing 2000 h of continuous operation and 5000 h of endurance testing at an output of 250 MW [45]. Currently, the development of an IGCC plant at Negishi using a 701F gas turbine with a TIT of 1400 °C is underway [43]. As shown in Figure 8, it is considered possible for IGCC to generate electricity with a thermal efficiency of more than 50% (net LHV) using ultra-high-temperature industrial gas turbines with a turbine inlet temperature from 1600° to 1700 °C in the future if clean coal gasified fuel is available [46].

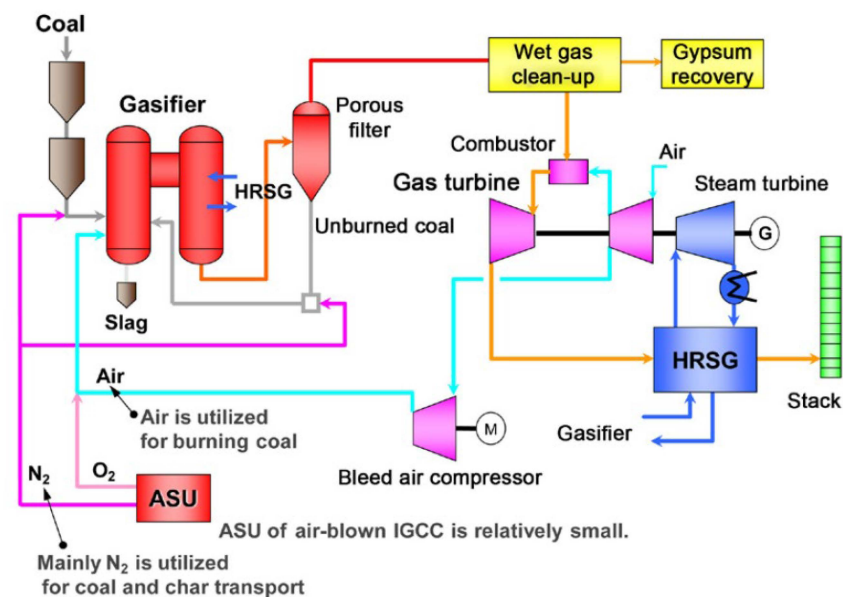


Figure 7. Schematic diagram of an air-blown IGCC demonstration plant [44].

Table 3. Specification of Nakoso IGCC demonstration plant [44].

Capacity		250 MWe Gross	
Coal consumption		approximately 1700 metric tons/day	
System	Gasifier	Air-blown and dry feed	
	Gas treatment	Wet (MDEA) + gypsum recovery	
	Gas turbine	1200°C class (50 Hz)	
Efficiency (Target values)	Gross	48% (LHV)	46% (HHV)
	Net	42% (LHV)	40.5% (HHV)
Flue gas properties (target values)	SOx	8 ppm	
	NOx	5 ppm	(16% O ₂ basis)
	Particulate	4 mg/m ³ N	
EPC		Mitsubishi Heavy Industries (MHI)	

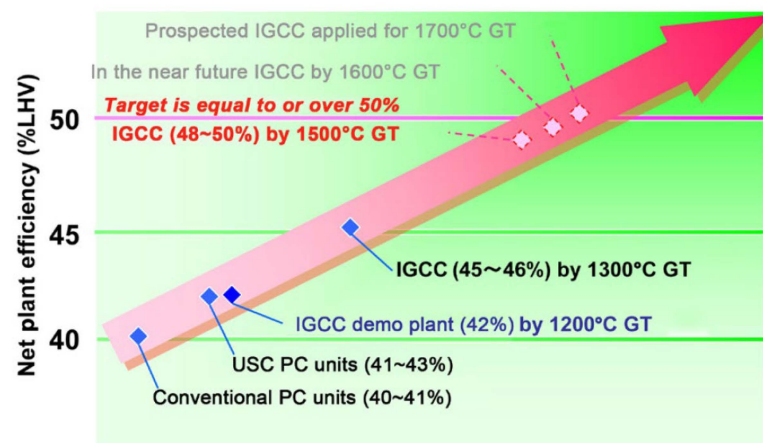


Figure 8. Thermal efficiency improvement of an air-blown IGCC [46].

An IGCC can be established by adding a gasifier, gas clean-up equipment upstream of the currently well-proven combined cycle and, if necessary, air separation. These modifications to the CCGT are considered important in the carbon-neutral era as power generation facilities, which expand the possibilities to burn dirty fuels, such as refinery residues, biomass, edible oil residues and plastic waste.

Coal contains components such as sulphur, chlorine, different alkalis and vanadium, which can cause high-temperature corrosion of hot parts. In an IGCC, the fuel gas for the gas turbine is produced by a gasifier, which converts coal to syngas, and clean-up equipment, which removes corrosive components and ash. The viability of an IGCC as a power generation facility depends on the performance of the gasifier and clean-up equipment. Furthermore, the question is whether the thermal efficiency of IGCC and the total cost of IGCC and associated CCS can compete with other power generation facilities. The gasifier technology, clean-up technology and CCS technology are advancing rapidly. The costs of the fuel cannot be forecast at the moment, but a number of countries will be using fossil fuels for the foreseeable future, and these technologies would still enable a carbon-neutral power generation. However, the cost of IGCC is currently higher than that of other power generation facilities, and research, development and demonstration tests are being conducted only with financial support from governments and other organizations.

2.4. Future Development of CCGTs, or What Is a CCGT in Line with the Carbon-Neutral Era?

In the coming carbon-neutral era, gas-turbine-based power generation facilities will continue to play an important role due to their high energy conversion efficiency and ability to use a variety of fuels.

Let us first consider the specifications an industrial gas turbine used in a carbon-neutral manner should have. When a gas turbine is operated using fossil fuels, the addition of a CCUS facility is mandatory. On the other hand, if hydrogen or ammonia are used as fuels, CO₂ emissions can be reduced to zero, but the unit cost of electricity generation will be considerably higher than that of natural gas. The only way to address these issues is to further improve the thermal efficiency of CCGTs with large industrial gas turbines. We would like to target a thermal efficiency of 70% (LHV), which is approximately 10% higher than the thermal efficiency of current state-of-the-art CCGTs. This implies a TIT from 1900 °C to 2000 °C and a pressure ratio of about 30.

In addition to improving the performance of gas turbines, it is also necessary to consider the functions that industrial gas turbines should have for the environment in which they are used. As mentioned in the Introduction, about half of the electricity generated in a carbon-neutral world will come from renewables. These power sources are susceptible to weather conditions and load fluctuations. In order to provide a stable power supply, thermal or nuclear power generation facilities with inertia is indispensable. The problem of power supply stability has already begun: it is already a challenge for grid operators in countries and power networks where renewable energy dispatch has priority. Figure 9 illustrates the increasing variability of electricity generation in California [47]. The authors of Ref. [47] examine the options for providing flexible distributed generation plants with outputs ranging from 25 MW to 300 MW. The measures proposed assume that large CCGTs are to operate at rated load. In a large CCGT, it is difficult to rapidly change the load on the steam turbine, so it is necessary to develop a CCGT, which can change the load only with the gas turbine while the steam turbine is at or near to rated load. This may mean an extended operation with partial admission or the use of twin-shaft gas turbines.

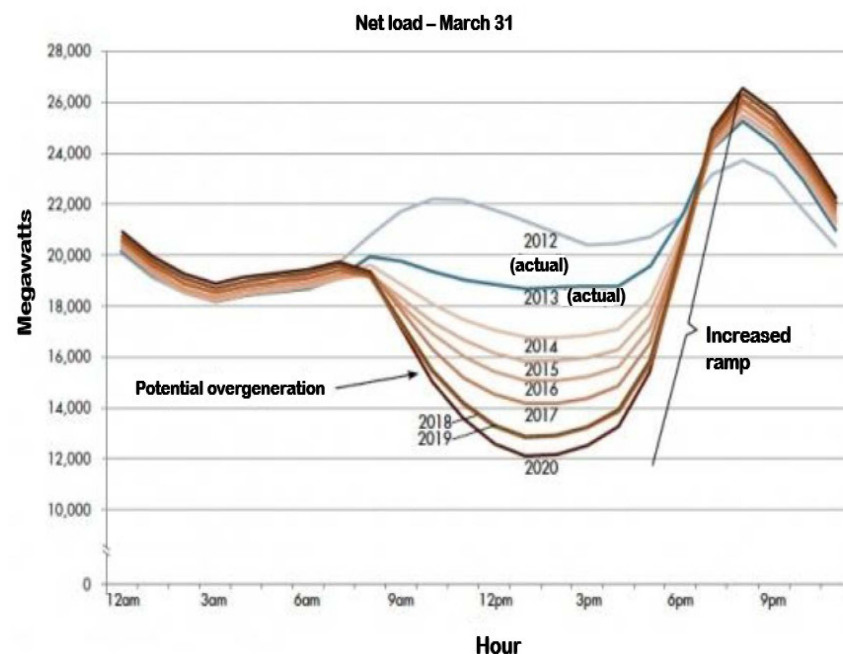


Figure 9. The California ISO “duck curve” illustrating the impact of intermittent renewable power generation [47].

The large industrial gas turbine used in such a CCGT should have the functionality of a jet engine, which can handle rapid load changes. Therefore, the structure of the turbine, from the airfoils to the discs, must be designed to reduce thermal stresses during transient

changes. The current industrial gas turbines used in CCGTs are designed to achieve the highest efficiency at rated load. However, large industrial gas turbines in carbon-neutral applications must maintain high efficiency even at partial load [18].

However, not all large industrial gas turbines need to be capable of following load fluctuations, since there are regional differences in the amount of electricity generated by renewables. In addition, gas turbines used for IGCC must operate at rated load.

For gas-turbine-based power generation facilities, various thermal cycle systems have been studied with the goal of achieving the highest thermal efficiency [48,49]. The results of these studies indicate that complex cycles are required. In particular, the operation of a closed-circuit cooling system is highly efficient, but it is not suitable for the carbon-neutral era because of the time required for the components of the combined plant to achieve thermal equilibrium. Based on a review of the R&D status of gas-turbine-based thermal systems developed to date and the estimation of future specifications, we conclude that a combined cycle consisting of a simple large gas turbine and a steam turbine with cooling of hot parts by the current compressor discharge air is the most suitable for carbon neutrality.

On the other hand, for small and medium-sized industrial gas turbines, the change of fuel to CO₂-free fuels, such as hydrogen or ammonia, means that the current restrictions on the (cooling) design imposed by the possible use of inferior fuels will be removed. This implies that a cooling structure similar to that of airfoils for aero engines with the same geometrical dimensions will be possible. Small to medium-sized gas turbines used as a stand-alone gas turbine—because of its fast start-up and load fluctuation capability—can function as a stabilizer for the power grid. This will enable the TIT of these gas turbines to be increased if the cooled airfoils can be manufactured at a lower cost, leading to a dramatic improvement in thermal efficiency. Since these gas turbines are not used in combined cycle applications, they can be designed for high thermal efficiency with a large pressure ratio and sufficiently low exhaust gas temperature. Simultaneously, small and medium-sized gas turbines are expected to continue to be used as cogeneration systems.

3. Industrial Gas Turbines of the Future

In order to achieve carbon neutrality, one has to either capture any emissions of CO₂ or burn a fuel that does not contain any (additional) carbon. The latter currently means burning either green hydrogen, ammonia based on green hydrogen or bio-fuels. Although the availability [50] and economic feasibility [51] of a green-hydrogen-based society have been called into question, these challenges will probably be overcome, and one has to prepare the technology needed for the carbon-neutral era now and not only when remedies to all objections have been found.

First, we consider the use of industrial gas turbines fueled by CO₂-free hydrogen or ammonia.

Among the various gas turbine cycles, this section discusses those that have been considered for use in the future carbon-neutral era, or advanced gas turbine cycles for which specific plants have been constructed to demonstrate their performance.

3.1. Hydrogen and Ammonia as Gas Turbine Fuels

It is technically possible to produce CH₄ from H₂ and CO₂ (the Sabatier reaction), but this is not economically viable at the moment. Therefore, CO₂-free fuel currently means burning either green hydrogen, ammonia based on green hydrogen or bio-fuels.

Bio-fuels in their pure form may contain contaminants, such as sulphur, but these can be eliminated comparatively easily [52]. This means that the use of these fuels should have little impact on the combustion system and cooling design. The use of hydrogen or ammonia as fuel for gas turbines has long been considered [53,54], and these fuels are expected to be used for gas turbines, boilers, internal combustion engines, industrial furnaces and other existing power and heat sources [55–62]. The main components of a gas turbine can remain largely the same, except for the combustor, which differs from the natural-gas-fired industrial gas turbines currently in operation [63–66]. Apart from

the modifications to the combustion system to take account of the higher flame speed of hydrogen and the long reaction times of ammonia compared to those of methane, the TIT will change as well.

Hydrogen has a calorific value of only 3.0 MJ/m³, but this is equivalent to 120 MJ/kg. Natural gas (“L-gas”), on the other hand, has a calorific value of 31 MJ/m³, which is equivalent to only 32 MJ/kg. This means that the overall mass flow through the turbine, i.e., air and fuel, will decrease when burning H₂. The constituents of the fuel gas also change: there will be no more CO₂, but additional H₂O. The average specific heat capacity of CO₂ is approx. 1.2 kJ/kgK and that of water vapor is approx. 2.4 kJ/kgK. The absolute changes in the mass fraction of the constituents combined with the differences in specific heat cancel each other out, meaning that the heat capacity of the exhaust flow changes only marginally. On the heat transfer side, it has to be taken into account that both CO₂ and water vapor radiate. Again, the changes largely cancel each other out. Nonetheless, the differences in calorific value and overall mass flow lead to changes in the TIT:

- If both the power output and the exhaust gas temperature have to remain constant while burning 100% hydrogen, the TIT increases by several dozens of degrees with the subsequent impact on the average component temperature.
- If both the TIT and the exhaust gas temperature remain constant, the power output of the gas turbine will decrease by more than 10%, but the efficiency will increase slightly and the exhaust gas mass flow substantially.
- If the power output and the TIT remain constant, the exhaust gas temperature will decrease by nearly 20 K, but again, both the gas turbine efficiency will increase slightly and the exhaust gas mass flow substantially.

It is possible to find a thermodynamically optimal solution within the boundaries mentioned above by varying all three parameters. Still, some adjustments to the cooling design will be necessary, especially in combination with the altered design of the combustor, which will lead to a different TIT profile, turbulent length scales and turbulence.

It should be noted that the above discussion is focused solely on the thermodynamic aspects of burning hydrogen. It may be necessary to consider the impact of increased water vapor on the oxidation behavior of alloys and ceramics. Combustion dynamics, NO_x emissions and flashback should also be taken into account. Therefore, a de-rating of the gas turbine may be necessary for other reasons.

The thermo-physical properties and combustion characteristics of hydrogen and ammonia are shown in Table 4 [67]. Hydrogen has a low liquefaction temperature of 20 K, making it difficult to transport and store. In addition, it is necessary to develop a combustor, which will not produce too much thermal NO_x and handle the high turbulent flame speed that can cause flashback. Ammonia, on the other hand, liquefies at about 10 atmospheres at common ambient temperatures, making it easier to handle for transportation and storage than LNG. However, it has a very low turbulent flame speed, and the presence of nitrogen in the fuel may cause fuel NO_x.

Table 4. Thermal properties and fundamental combustion characteristics of ammonia and hydrocarbon fuels [67].

Fuel	NH ₃	H ₂	CH ₄	C ₃ H ₈
Boiling temperature at 1 atm (°C)	−33.4	−253	−161	−42.1
Condensation pressure at 25 °C (atm)	9.90	N/A	N/A	9.40
Lower heating value, LHV (MJ/kg)	18.6	120	50.0	46.4
Flammability limit (Equivalence ratio)	0.63–1.40	0.10–7.1	0.50–1.7	0.5–2.5
Adiabatic flame temperature (°C)	1800	2110	1950	2000
Maximum laminar burning velocity (m/s)	0.07	2.91	0.37	0.43
Minimum auto ignition temperature (°C)	650	520	630	450

Since the production and supply chain for hydrogen and ammonia is still in the early stages of development, the operation of gas turbines using these fuels is still experimental. MHI has operated a CCGT demonstration facility using a 1600 °C J-type gas turbine with 30%_{Vol} of hydrogen mixed with natural gas to demonstrate CCGT power generation [68]. KHI has successfully operated a 2 MW M1A-17 gas turbine with 100% hydrogen fuel at almost full load [69], and IHI has successfully operated a 2 MW IM270 gas turbine with 100% ammonia at full load [70]. In Europe and the United States, 100% hydrogen-fired power plants are currently under construction for CCGTs using large industrial gas turbines, and these power plants are expected to come on line as the infrastructure for hydrogen production and supply is developed.

3.2. Oxy-Fuel and Hydrogen-Oxy Cycle Combustion Turbine

The problem with burning H₂, however, is that hydrogen-fueled combustors, which tend to have higher flame temperatures, are anticipated to emit more NO_x than natural-gas-fired combustors [71] if they use air. Steam cooling can be used to increase the amount of available combustion air and lower the combustion temperature to achieve low NO_x emissions. Carbon-neutral CCGTs will see an additional 200 °C to 300 °C increase in the combustor exit temperature to achieve their efficiency targets. The authors believe that the current combustion system using air as the oxidizer is reaching its limit for low NO_x combustion. A combustion method that does not generate NO_x at all is the oxy-fuel cycle (OFC), which separates oxygen from the air. This cycle was originally proposed for the capture of CO₂ from the combustion of coal in thermal power generation [72,73]. The oxy-fuel cycle can be used for a wide range of fuels, including natural gas, coal gasification gas, biomass, etc. Therefore, it is possible to develop the OFC thermodynamically without difficulty, although it is necessary to redesign the compressor, combustor and turbine based on existing CCGT technology to make them suitable for the cycle. This section describes only the application of the OFC to the CCGT [74].

There is a disadvantage in terms of thermal efficiency, in that additional energy is required for the process of separating oxygen from air. However, by adopting the OFC, the TIT can be increased to 1900 °C–2000 °C, and the gas turbine can be operated without producing any NO_x despite this high combustion temperature. In the future, when hydrogen and oxygen are produced by electrolysis using renewable energy, hydrogen will be used as fuel, and the excess oxygen can be effectively utilized in this cycle.

The cycle diagram of the OFC is shown in Figure 10 [75]. The components of the exhaust gas are CO₂ and water vapor. Capturing CO₂ can be achieved very easily at atmospheric pressure because when water vapor is converted to water in the condenser, gaseous CO₂ remains. When the gaseous CO₂ obtained in this way is recirculated, it becomes a Brayton cycle, whereas when the condensed water is circulated, it becomes a Rankine cycle [76]. In the following section, we will discuss the OFC when the Brayton cycle is employed as a gas turbine.

Different recirculation ratios of H₂O and CO₂ were studied for oxy-fuel CCGTs to find the optimal compressor, combustor and turbine specifications [77]. In the case of a CCGT with CO₂ recirculation, the compressor pressure ratio must be approximately doubled in order to achieve the same exhaust gas temperature in the HRSG as in a natural-gas-fired CCGT. The CCGT power output and thermal efficiency were also studied by calculating an oxy-fuel CCGT with the amount of coolant for the airfoils as a parameter [78,79]. The application of the oxy-fuel's CO₂ circulation system in a natural-gas-fired CCGT with a GE Model 9H gas turbine was studied [80]. According to the results of this study, the thermal efficiency of the OFC was 51.3% (net LHV), which is 8.1% lower than that of a natural-gas-fired CCGT. This lower efficiency compares favorably with the lower efficiency of CO₂ capture using the amine recovery process. However, because it is a CO₂ circulation system, the current 9H gas turbine cannot be used in its present form, and a new design is required for all components. The main flow is a mixed stream of CO₂ and superheated steam, which provides strong radiative heat transfer to the hot parts. The structural integrity of the

cooled airfoils should be evaluated considering the radiative heat transfer. The cooling performance of hot parts in the oxy-fuel CO₂ circulation system is superior to that of air cooling, since carbon dioxide from the compressor discharge is used.

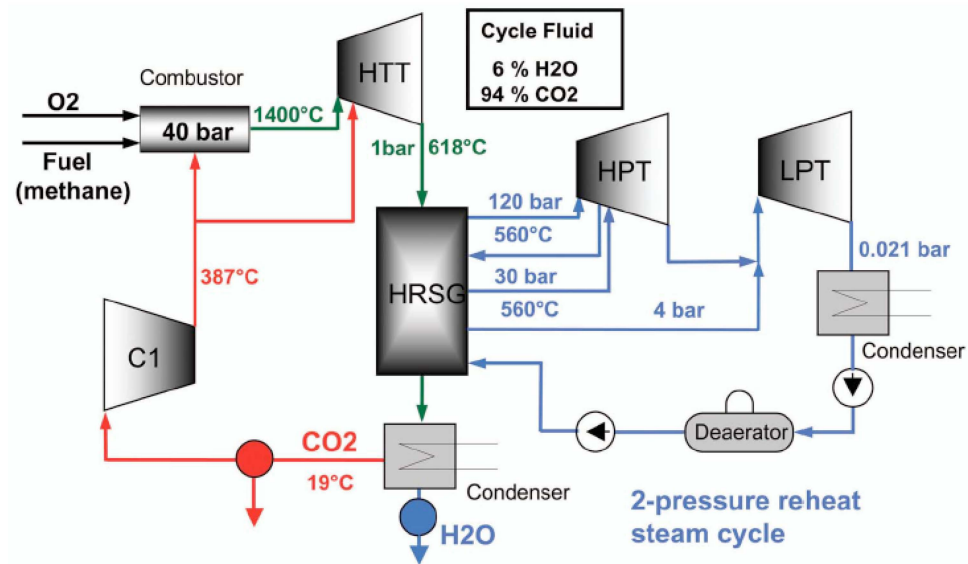


Figure 10. Principle of the flow scheme of the oxy-fuel cycle [75].

Jericha and others at the Graz University of Technology in Austria have proposed a highly efficient combined cycle using hydrogen–oxygen combustion. This cycle was named the “Graz Cycle” by Japanese researchers involved in the WE-NET project [81]. The basic configuration of the Graz cycle is shown in Figure 11 [82], in which natural gas is burned with pure oxygen [83]. This results in a working fluid, which consists exclusively of steam and CO₂, the latter of which can be easily separated from the steam. The exhaust gas is used to generate steam in a regenerative heat exchanger, and the low-pressure steam is used to drive the Rankine cycle and as the compressor inlet steam in the Brayton cycle. Since its inception, a steady stream of publications have refined the concept [75,82,84,85]. Cycle analysis has shown that the thermal efficiency of the Graz Cycle is more than 10% higher than that of a natural-gas-fired CCGT with the same TIT. The Graz Cycle is highly efficient because the exergy losses of combustion are reduced by increasing the combustion pressure and the temperature [85].

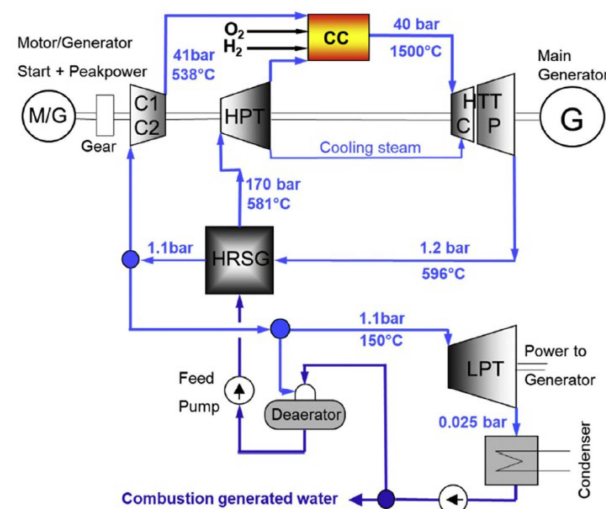


Figure 11. Principle of the flow scheme of the oxy-fuel cycle [82].

A good review of a number of other closed cycles can be found in Ref. [86].

3.3. The HAT Cycle

In the CCGT, the working fluids of the topping gas turbine cycle and the bottoming steam turbine cycle are physically separated. There are, however, many options for converting liquid water to steam and combining it with the working fluid of the gas turbine. The Cheng Cycle for small plants, in which the exhaust heat from the gas turbine is used to generate superheated steam in a heat recovery steam generator (HRSG), was already described.

Recuperated cycles enjoyed a certain popularity some decades ago when the overall pressure ratio of gas turbines was still rather low. The exhaust gas was used to pre-heat the compressor discharge air before it entered the combustion chamber. The heat below the compressor discharge air temperature cannot be recovered from the turbine exhaust gas within the gas turbine cycle. When the TIT is increased to achieve higher performance, it is necessary to increase the pressure ratio accordingly. Therefore, the amount of heat recovered using the recuperator decreases, and the exhaust gas is released into the atmosphere at a higher temperature, resulting in heat loss.

On the other hand, the specific heat of water vapor is about twice as large as that of air, and it has a large heat recovery capacity. Using this property of steam, a relatively low-temperature, high-humidity air can be used for heat recovery in a regenerator. In this case, a cycle can be constructed to recover heat from the exhaust gas down to nearly 100 °C, where the steam condenses at atmospheric pressure [87,88]. A typical example of this high-humidity regenerative gas turbine cycle is the humid air turbine (HAT) cycle shown in Figure 12 [89]. This cycle was developed by Nakamura in 1981 as an application of medium- to low-temperature heat recovery technologies in gas turbines [90]. It was recognized that this cycle can be expected to improve thermal efficiency by approx. 3 to 4 % (absolute value) compared to a normal combined cycle [91]. To achieve its performance, it was necessary to develop a new type of gas turbine with separate compressors and an intermediate cooler. In contrast to the HAT cycle, Hatamiya devised the AHAT cycle; its sequence is shown in Figure 13 [92]. This power generation system aims to achieve high efficiency without the need for the high pressure ratios and high combustion temperatures, which are currently the mainstream of highly efficient combined cycle systems. In the AHAT cycle, intake air is cooled by installing an intake air duct (called an aftercooler), which sprays fine water droplets into the compressor intake air. This lowers the intake air temperature by evaporation before the air reaches the first compressor stages. The remaining water droplets evaporate during the compression process, suppressing the increase in temperature of the air. The compressor discharge air flows into the humidification tower (called a saturator), where it comes into direct contact with hot water and becomes highly humid air. The humidification ratio is about 15 to 20%_{wT} of the intake air flow.

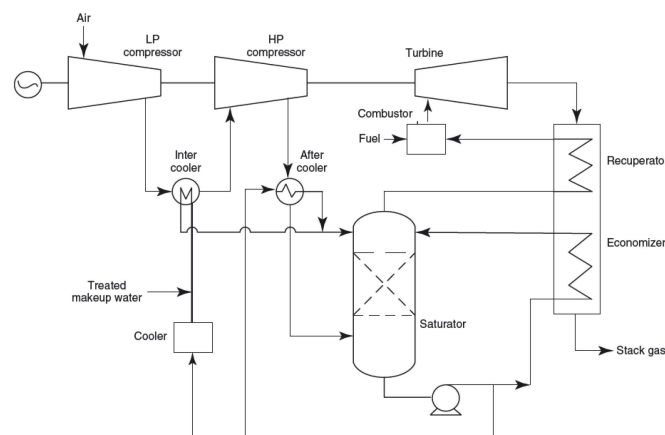


Figure 12. HAT cycle [89].

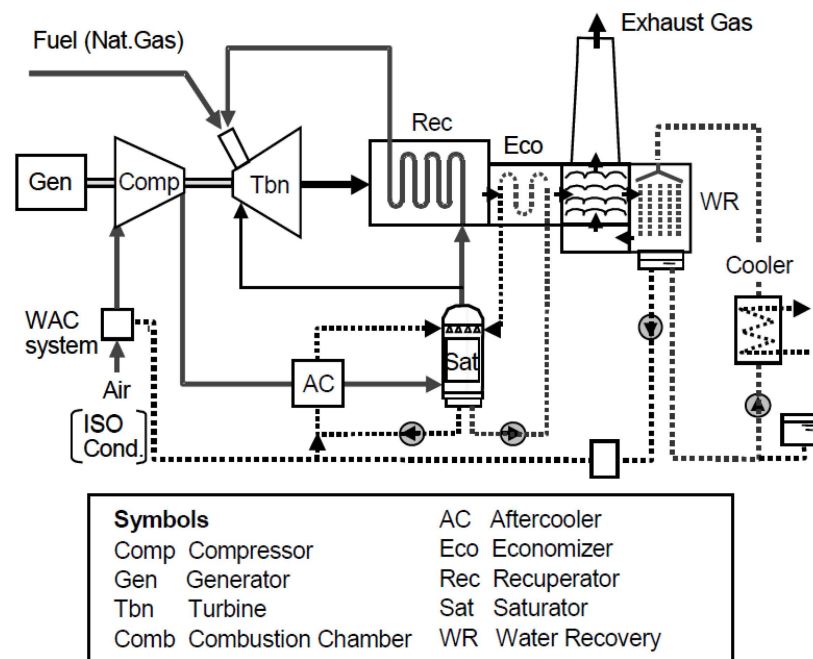


Figure 13. AHAT cycle [92].

Hitachi built an experimental plant to verify whether the cycle concept of the AHAT system and the target performance could be achieved using a 3 MW class gas turbine and conducted demonstration tests [93]. An output of 4.0 MW and a thermal efficiency of 40% LHV were achieved. These results show that if the AHAT cycle is designed under optimal conditions, the power generation efficiency will exceed that of a combined cycle. The difference in efficiency is particularly large for small and medium-sized gas turbines. Figure 14 shows an example of efficiency estimation of an AHAT cycle compared to existing gas turbine power generation systems [92].

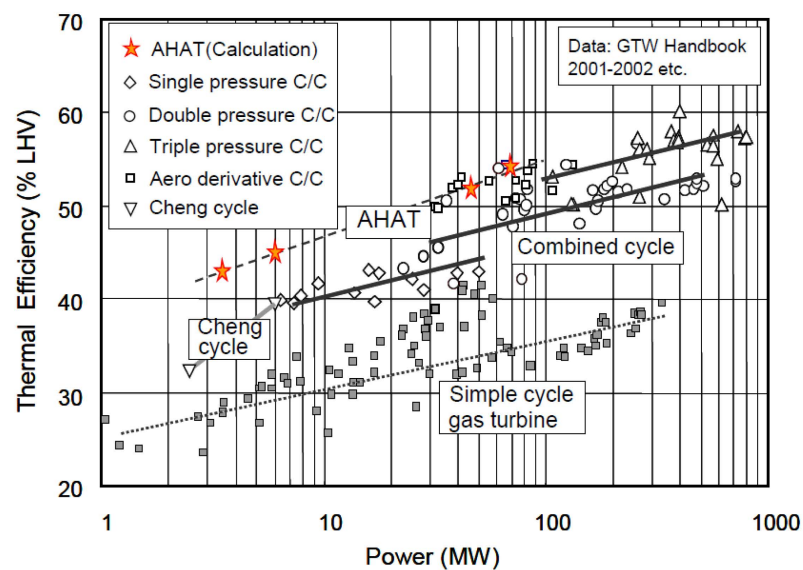


Figure 14. Comparison of thermal efficiencies of gas turbine cycles [92].

The AHAT cycle can be considered one of the best systems for small and medium-sized gas turbines in the carbon-neutral era. Furthermore, it is desirable to consider an AHAT cycle using renewable fuels, such as hydrogen and ammonia, instead of natural gas.

4. Cooling Structure for Gas Turbine Airfoils of Future Importance

Section 2 described the current status of industrial gas turbines in operation. In Section 3, several possible cycles and the preferred or ideal industrial gas turbine cycle for the carbon-neutral era were discussed. This section describes the cooling structures, which should be adopted. First, the current cooling methods for the latest 1650 °C level cooled airfoils are described. Next, the cooling strategies for vanes and blades that have been researched and developed so far are discussed. Then, the cooling structures and production methods that can be applied to airfoils in the carbon-neutral era are described based on those structures and production methods. It should be noted that the quantitative need for cooling will, to some extent, depend on the thermodynamic cycle. Although the temperature will be the same, the exhaust gas compositions will differ, leading to different thermal loads and different cooling requirements.

The first-stage turbine vanes and blades of a 1500 °C class G-type gas turbine are shown in Figures 4 and 5, respectively. The cooling structure of both turbine vanes and blades does not differ significantly from that of a high-pressure turbine of a jet engine with the same TIT. It should be noted, however, that the airfoils of a large industrial gas turbine are approximately four times larger than those of a jet engine. Although not shown in this paper, the cooling air used to cool the turbine rotor blades in the WH-MHI gas turbine does not reflect the fact that the compressor discharge air is taken out of the system and cooled with water from the bottoming cycle. In other words, the air used to cool the blades is cooled to approximately 150 °C. According to Figure 4, this cold cooling air is discharged directly to the outer surface of the blade as film cooling through a short internal cooling channel. In the F-type turbine first-stage blades designed by MHI, the cooling air is used internally as much as possible, and once the temperature has been increased as much as possible, it is discharged from the blade surface as film cooling—a concept unique to industrial gas turbines [31]. All of the blades of the 1500 °C class G-type gas turbine designed by WH were modified by MHI to achieve the optimal cooling geometry for an industrial gas turbine based on the above concept.

Impingement cooling, which is used in vanes, is a method of effectively cooling the vane inner surface at the leading edge and the center section of the airfoil (along the chord). With a serpentine flow passage, which is used in blades, the temperature distribution along the blade height is almost uncontrollable, whereas it can be easily controlled by adopting impingement cooling and adjusting the number of impingement cooling holes.

In the cooling structure of the vane shown in Figure 3, impingement cooling is provided from the inner surface by putting an insert into several cavities in a thin-walled structure. The number of cavities tends to increase as the TIT increases; in the 1150 °C class D-type gas turbine designed by Westinghouse for cooling, the number of cavities in the first-stage vanes was two. However, the number of cavities in the first stage of a 1200 °C class DA-type gas turbine modified by MHI was increased to three. The number of cavities in the first-stage vanes of the 1350 °C class F-type and 1500 °C class G-type turbines is also three, but the number of impingement cavities in the 1600 °C class J-type turbine is five [31]. The increase in the number of cavities is founded in the need to optimize the cooling air supply pressure and the film-cooling outflow velocity on the surface of the vane. The static pressure distribution on the surface varies both along the chord and span, and the cooling is adapted correspondingly. It is possible to form cavities by means of a sealing structure between the insert and the inner surface of the vane, rather than partitions inside the vane, to generate the number of cavities. A tight seal across the span of vanes guarantees a high cooling performance and high reliability. However, as the TIT increases, three-dimensional vane shapes are required to improve aerodynamic performance, making it extremely difficult to design a sealing structure with precise contact between the surfaces. In the combined impingement- and film-cooling section, attention should be paid to the ventral side of the turbine vane. Film cooling on a surface with a small radius of curvature promotes mixing of the film-cooled air with the mainstream due to the Görtler vortices on a concave surface. To avoid this mixing, the pressure surface is composed of sections

with a large radius of curvature. The leading edge of the first-stage vane, on the other hand, has the largest possible leading edge radius to reduce the heat transfer coefficient of the mainstream. Pin-fin cooling is used for the trailing edges of the turbine blades where impingement cooling is not possible due to the difficulty of incorporating inserts.

The cooling structure of the turbine blades shown in Figure 4, which employs film cooling in the tabulated serpentine flow path, is the same as that of a jet engine. The showerhead cooling of the leading edge is designed to distribute the coolant on both sides around the stagnation point. On the other hand, pin-fin cooling is used on the trailing edge of the blades.

The aspect ratio of the serpentine channel of the turbine rotor blade shown in Figure 4, which was designed based on an aircraft engine, is close to unity, which is an excellent cooling design when considered only from the perspective of heat transfer. When WH-MHI designed large industrial gas turbines of the D, F, and G classes, they adopted the same four-stage turbine layout. This implies that the load on the rotor blades increases with the increase in TIT because the load is distributed over the same number of stages. This, in turn, means that the shape of the blade is changing from a reaction type to an impulse type. This tends to increase the aspect ratio of the serpentine channel: the blade becomes thicker, meaning that the surface of the internal divider walls becomes larger than that of the actual inner walls on the pressure and suction sides of the airfoil. Since the ribs of a serpentine channel are generally installed on what is now the short side of the rectangular cross section, a serpentine channel shape with a large aspect ratio is inefficient in terms of cooling.

The improvement of the thermal efficiency of the cycle is roughly in proportion to the amount of coolant reduction, given that the reduction lowers the pumping loss and reduces the temperature of the mainstream less. For this reason, the cooling design of the blades needs to progress to more advanced cooling, which enables a more uniform temperature distribution in spanwise direction and one that is attuned to the creep rupture strength requirements along the blade height. Because the blade rotates by definition, the gas temperature around it can be considered to be the circumferentially averaged value of the mainstream gas temperature. The creep strength of a blade is determined by the centrifugal force acting on it in combination with the average metal temperature of its cross section. For the maximum creep strength to be attained, the gas temperature distribution should be designed in such way that the highest temperature is at about 50 to 60% of the span. Since the blade root has the cross section with the highest centrifugal stress, it must be sufficiently cooled to meet the strength requirements, even though the gas temperature is lower than at the mid-span. The cooling design from the mid-span to the tip of the blade could attain a gradual reduction in the amount of coolant to achieve an average metal temperature, which aligns the creep strength with the decay of centrifugal force. Turbine blade cooling by serpentine channels cannot control the average metal temperature in the blade height direction. However, if a cooling method that combines impingement and film cooling is used for turbine rotor blades, it is possible to achieve this.

Impingement cooling by introducing an insert into the blade is an excellent cooling method in terms of controlling the local metal temperature. However, two problems exist. First, since the inlet angle of a blade changes in the radial direction, the airfoil is twisted. When the blade rotates, the centrifugal force causes it to untwist to some degree. Therefore, the insert must be installed in a location where the relative position of the inner wall and the insert is unlikely to change. Next, the ribbed surface that holds the insert in place and the insert itself must be in contact with each other at a constant pressure. However, even if the sealing surfaces are manufactured very precisely, damage can occur due to fretting wear because of the relative motion caused by the rotational motion and thermal elongation differences. In the high-pressure turbine first-stage blade of the Pratt & Whitney 1250 °C class JT9D-7A jet engine, impingement cooling with a single insert integrated in a single cavity was used. However, PW abandoned the use of impingement cooling for the blade because of the fretting wear mentioned above. For the JT9D-59A, which increased the

turbine inlet temperature of the JT9D engine to 1360 °C, a cooling structure that combines serpentine channels and film cooling was adopted. Impingement cooling of the mid-chord region was no longer used. Currently, impingement cooling remains in use for the leading edge, where impingement nozzles can be produced by precision casting.

The cooling design of the airfoils has its roots in precision casting. From the viewpoint of seeking a cooling structure, which is more reliable, has a higher cooling efficiency and allows local control of the metal temperature, new manufacturing methods that break with this concept need to be conceived. One of the techniques developed for aero engines in the past is cast cooling; another is the wafer and diffusion bonded blade. The airfoils of large industrial gas turbines are thus much larger than those for which these technologies were originally planned, and therefore, one cannot simply apply them. As indicated before, the heat capacity of the airfoils of large gas turbines is much larger, necessitating a modified design that takes the altered thermal stress into account. Because the sizes of the airfoils of small and medium-sized industrial gas turbines and those of aero engines are approximately the same, it is possible to also apply the technology in these industrial gas turbines. Because industrial turbines will be operated more similarly to aero engines in future, the design rules and criteria should converge as well, making these technologies an interesting option. For these smaller gas turbines, the main challenge will be to keep the manufacturing costs down as much as possible.

First, we will discuss cast-cooled airfoils. In combustors for jet engines, the combustor dimensions are reduced to reduce the weight, and diffusion combustion using liquid fuel is the norm. For this reason, designs that can effectively cool the combustor wall with low pressure loss and a small amount of coolant were the focal point of R&D efforts. One combustor wall structure with such a function is Lamilloy[®], which has a double-wall cooling structure [94–96]. It consists of an outer wall, an inner wall (combustion side) and a structure with fins, which promote heat transfer between them. The inner wall and fin structure are fabricated by photo-etching, and the outer wall is diffusion bonded to the inner structure. As the name suggests, CastCool[®] is a high-pressure first-stage blade manufactured by precision casting the cooling structure of Lamilloy[®]. The CastCool[®] first-stage blade is shown in Figure 15 [97,98]; this also gives a good overview of the general features and design of CastCool[®] airfoils. In the CastCool[®] blade, the impingement-cooling and its relative position to the film-cooling holes can be fabricated according to the design intent. This cooling structure allows the impingement-cooling heat transfer coefficient and the film-cooling blow-off rate to be controlled even with fluctuating turbine loads. Furthermore, the combination of the two cooling methods ensures that there is back pressure for the film cooling with no backflow and uniform metal temperatures across the leading edge can be achieved with minimal coolant mass flow. Figure 16 shows an example of the application of the above cooling method, which prevents reverse flow in partial load operation into the cavity of the leading edge [99].

Wafer and diffusion bonding blades are discussed next. The structures of the first-stage blades developed by ERDA, a project spawned by the DOE's HTTT program, are shown in Figures 17 and 18, respectively [100]. Again, these figures were chosen to give an overview of the design of such airfoils in general as well. The first-stage vane was manufactured by forming a fine cooling structure on a thin plate made of a super heat-resistant alloy by photo-etching, then overlapping the wafers in radial direction and integrating them by diffusion bonding. The blade was manufactured in the same way as that of the vane. However, the surfaces are diffusion bonded in the direction where the centrifugal force does not act, i.e., in the axial direction. In the same HTTT project, EPRI developed turbine blades called Shell/Spar. Figure 19 shows the structure of the first-stage Shell/Spar blade [101].

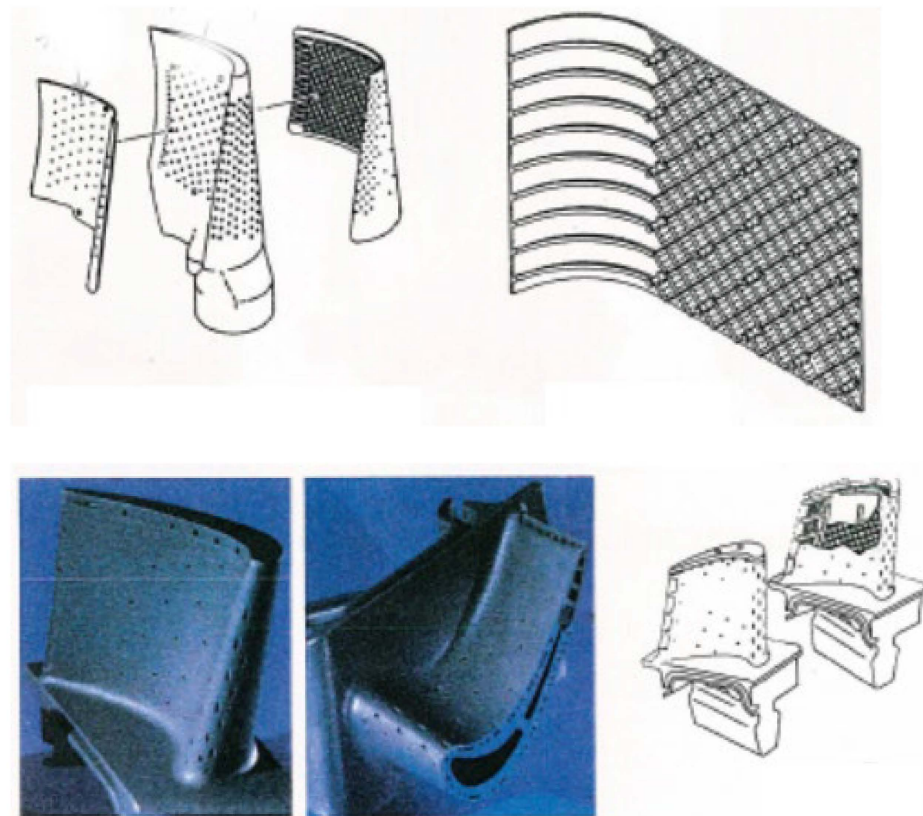


Figure 15. A CastCool® turbine blade [97].

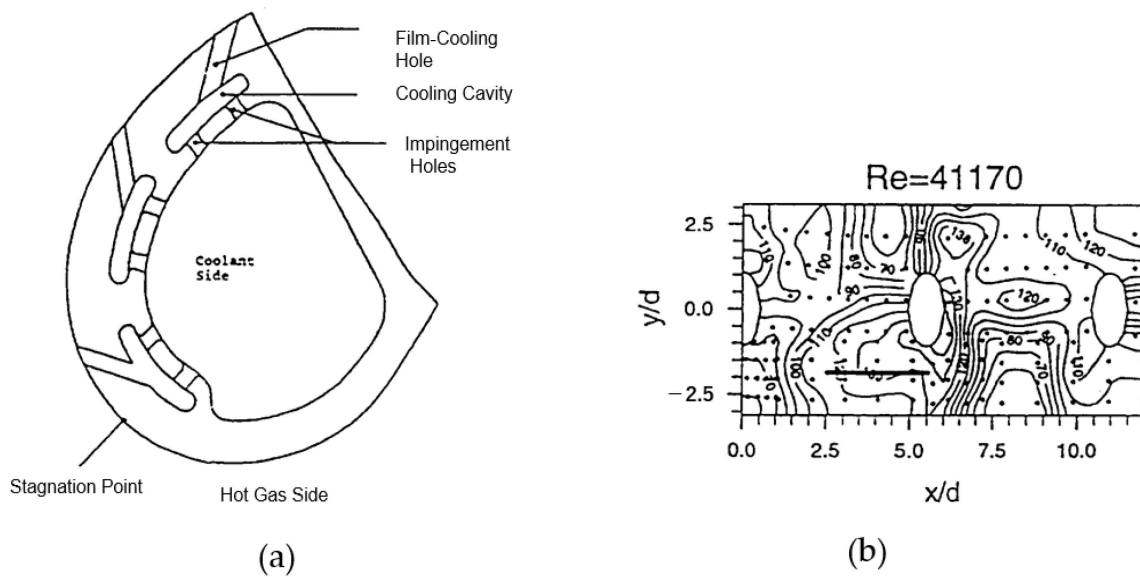


Figure 16. An impingement-cooled leading edge of a CastCool®: (a) Turbine blade with the integrally cast passage; (b) Nusselt number distribution on the target surface [99].

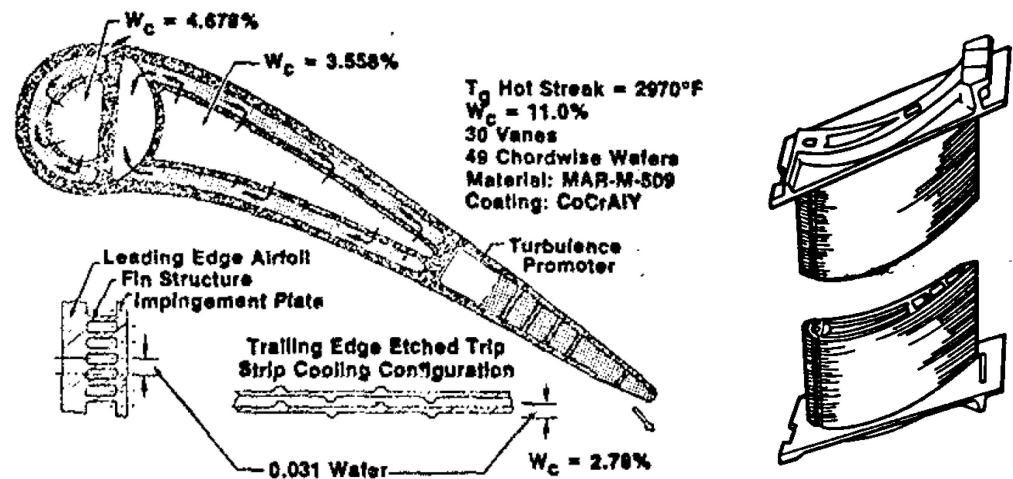


Figure 17. Wafer vane cooling configuration by ERDA—advanced industrial engines [100].

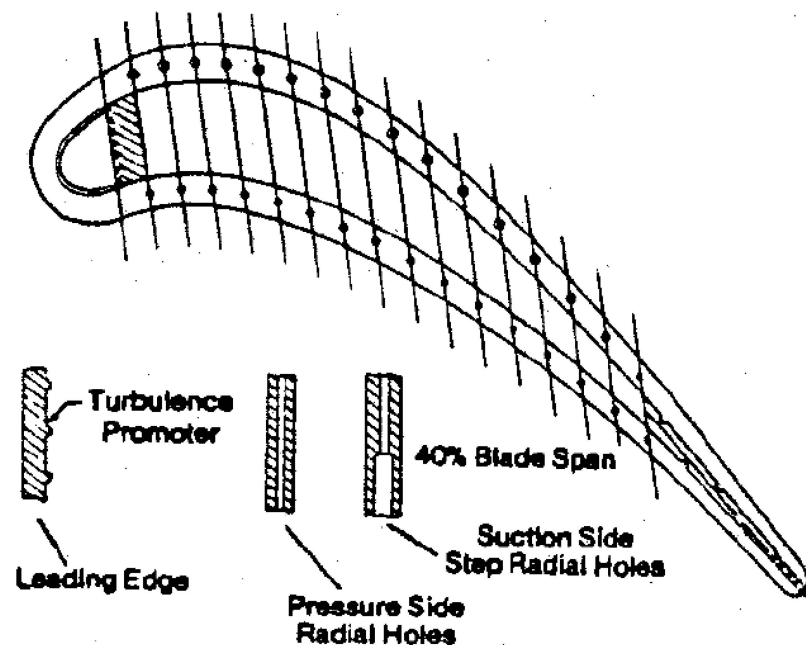


Figure 18. Wafer blade cooling configuration for ERDA advanced industrial engines [100].

The Lamilloy[®] cooling structure described above is currently used for the combustor walls of jet engines. CastCool[®] airfoils have not yet been put into operation. Photo-etching and diffusion bonding offer a superior cooling method, which can improve on the shortcomings of modern cooled airfoils, but they have yet to be commercialized due to their high cost. The only commercialized high-pressure turbine blade produced by wafer and diffusion bonding is operated in the F100 fighter jet engine [102].

Based on this, the cooling structure of the blades used in industrial gas turbines in the carbon-neutral era is considered next. Internal cooling alone will not suffice, even if its efficiency can be increased considerably. A dense effusion-cooling array will be needed to protect the material from the hot gas temperature. As mentioned above, industrial gas turbines are required to function as a regulator to stabilize the power supply. To satisfy this function, they must be able to maintain the thermal fatigue life of the blades and discs even under sudden load fluctuations. In order to improve the reliability of the turbine blades in part-load operation, it is necessary to adopt a cooling structure, which does not allow the mainstream to enter the cooling cavity even if the static pressure distribution around the turbine blades changes. This is contrary to the concept of designing at the point

of maximum film-cooling effectiveness (e.g., film-cooling efficiency reaches its maximum around $M = 0.5$ in the case of circular hole film cooling) by reducing the amount of cooling air. Currently, a design with a certain margin in the back pressure is used to prevent the occurrence of backflow.

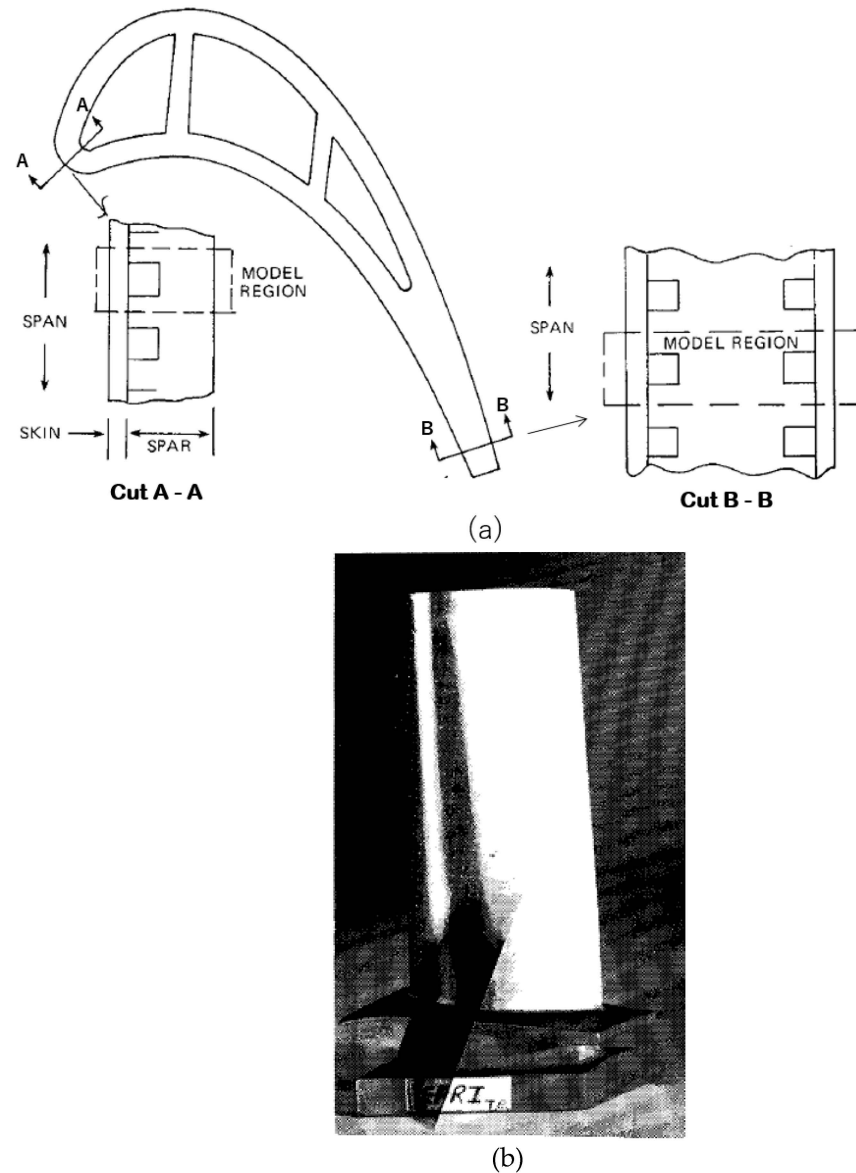


Figure 19. Shell/Spar cooling configuration: (a) Cooling configuration; (b) Fabrication demonstration blade [101].

Cooled blades have evolved in response to increasing turbine inlet temperatures. The authors have proposed a turbine inlet temperature of 1900–2000 °C and a pressure ratio of 30 for large and a TIT of 1500–1600 °C for small and medium-sized gas turbines. Research and development of airfoils suitable for these gas turbines should be pursued intensively. Ron Bunker has proposed “micro” cooling [103,104] and double-wall cooling [105], shown in Figure 20, as the cooling structures for future airfoils for aviation applications. These structures are an evolution of the Shell/Spar and Lamilloy® airfoils described above.

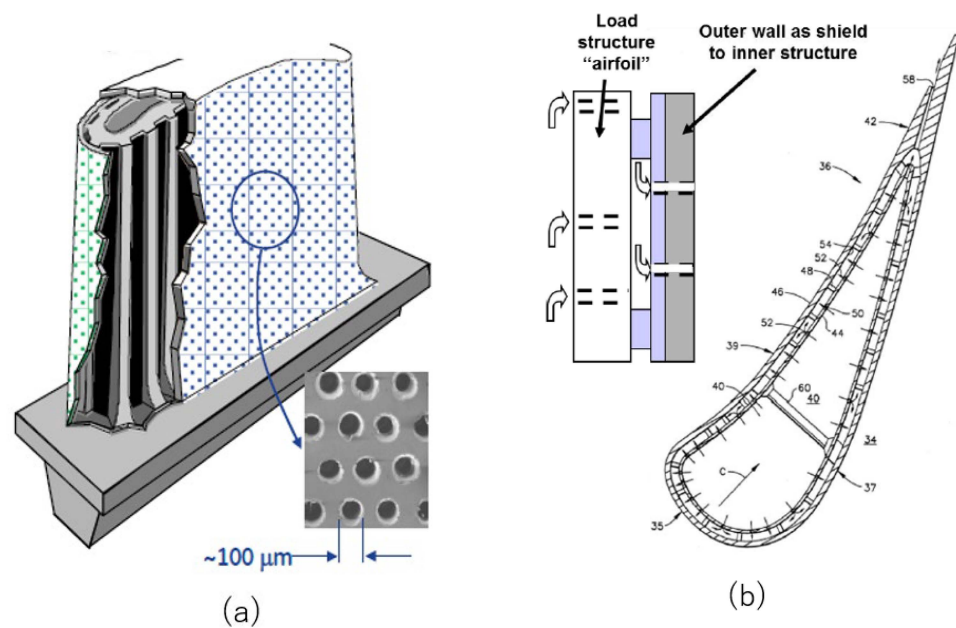


Figure 20. Future of turbine cooling: (a) “Micro” cooling [103,104]; (b) One example of double wall cooling [105].

The technology to fabricate such complex cooling structures out of metal by additive manufacturing (AM) is under development and is already being used to produce high-temperature components for jet engines. The structures manufactured before using all of the different technologies mentioned above can now be made relatively easily and cost effectively. The airfoils of a large industrial gas turbine are approximately four times larger than those of a jet engine. A solid blade would therefore have 4^3 times the heat capacity. Even for such large airfoils, the temperature difference across the airfoil can be reduced, and the transient response time can be modified to keep the metal temperature along the chord constant during rapid load changes. For this, a structure with low heat capacity but high strength needs to be adopted. The response can be delayed by increasing the thickness in the leading edge, where the heat transfer coefficient on the mainstream side is high. The thickness of the pin-fin section at the trailing edge cannot be increased, and therefore, a tight-lattice (or matrix) cooling structure is considered effective. Matrix cooling was originally developed in the former Soviet Union, and it has been used in some modern industrial gas turbines, e.g., in some of Siemens’ Finspong engines and ABB’s GT24/26. Some work has been performed on this in other countries as well (e.g., Refs. [106–108]), but difficulties in manufacturing and relatively high pressure losses have led to a limited number of applications, which might change when these structures can be additively manufactured. An added benefit of this cooling technique is its large heat capacity compared to, for example, pin-fin cooling. This means that, when applied to the trailing edge, the thermal inertia of the leading and trailing edges become more alike. Therefore, internal cooling enables the optimum temperature in the extreme points of the airfoil using complex cooling designs, whereas film cooling keeps the overall level of the structure at an acceptable level.

The manufacturing of turbine vanes and blades with a simple cooling structure using the AM method has already begun. Many studies have been conducted to evaluate the heat transfer characteristics of AM cooling geometries. The current cooling structures that can be produced by AM cannot meet the desired dimensional accuracy or surface roughness. However, as more and more components are produced in this way, the method will be improved to a satisfactory level. With “double-wall cooling”, the insert and blade wall are integrated into a single geometry.

A first additively manufactured DWC (for a sketch of the principle, see Figure 21a) vane was tested in a large frame gas turbine by Ref. [109]. The design itself and the comparison with the traditionally cast vane and the normal cooling design are shown in Figure 21. The AM vane shows a much more homogeneous surface temperature. This can be mainly attributed to the double-wall cooling design adopted in the AM vane, with the higher number of impingement cavities in addition to the overall extension of film cooling over the entire surface. Each row of film-cooling holes is linked to a dedicated internal cavity, allowing for a better distribution of the feed pressure and overall lower blowing ratios. As a result, a very low thermal stress and a thin wall structure, which is highly resistant to transients, is achieved. This being said, it is important to point out that the gas turbine in question belonged to the F class and therefore had a TIT that probably did not exceed 1400 °C, which is a long way from the envisaged 1900 °C. Nonetheless, the feasibility of the concept can be considered proven in principle.

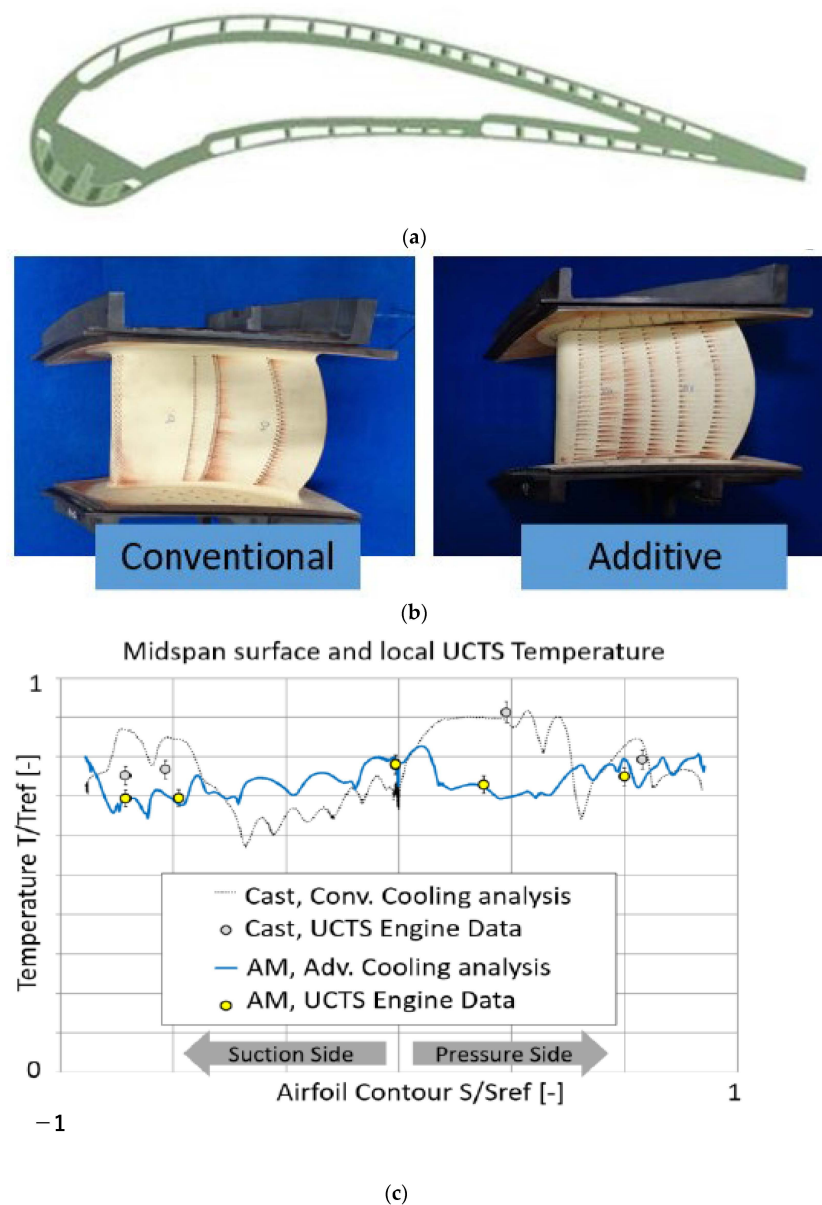


Figure 21. Comparison of cooling effectiveness of F-type gas turbine nozzles [109]: (a) F-type 1st nozzle cooling design concept of 3D printed internal cooling design; (b) Nozzles manufactured by conventional casting and additive manufacturing; (c) Cooling effectiveness distribution results of conventional and additive cooling design.

In the following two sections, research results on the heat transfer characteristics of AM cooling geometries and those of double-wall cooling (not necessarily AM-fabricated specimens) are described.

5. Additive Manufacturing

Additive manufacturing (AM) has been hailed as a game changer in the design of cooling geometries [105] because it will shift the paradigm from design for manufacturing to design for function. The reality is that there are severe restrictions on the geometries, which can be printed; the height of the layers printed is currently typically 0.6 mm (although 0.3 mm is possible). This is being continually reduced, and finer designs will become available in future. A multitude of challenges in the fields of materials' science and manufacturing have precluded the widespread use of the technology in high-temperature applications so far. As the material database is expanded and first long-duration engine trials are conducted, engineers will gain confidence and will expand the array of applications. One significant drawback is that the designers are still caught in old design rules based on design for manufacturing, and humans cannot easily process the complexity a truly innovative design for function would entail. One example of the latter would be a cooling design, which takes account of the stress distribution in a blade. AI/machine learning is not hampered by these restrictions but needs data that offer the required detail, a broader database and, above all, data that are attuned to the possibilities AM has to offer. All of this can be developed on the foundation of the current knowledge of what a good cooling design would be. This may not be the optimal solution at first but can constitute the basis for further development over the next decades. Furthermore, the tools necessary to fully utilize the potential of AM—for example, design tools for hollow, cellular structures instead of solid structures—are still under development. Since the demand from the industry at large, i.e., not only turbomachinery manufacturers, is significant, substantial advances can be expected here as well. Above all, currently, the costs of AM high-temperature components are in the same order of magnitude as those of their cast equivalents when the necessary heat treatment and machining are taken into account. The costs (especially of the printing hardware) will come down gradually but continuously over the next years, making AM components more cost competitive. This, in combination with the superior cooling characteristics it enables, will certainly lead to the breakthrough of this technology in the foreseeable future.

In the following sections, a brief overview of the state of the art of additive manufacturing will be given. This will show the current areas of research, which are concerned with the technology per se and its application in some cooling techniques; it excludes all topics pertaining to machine learning, since this would be a completely different and extensive field altogether.

As mentioned before, the size of the components in small and, to some extent, medium-sized gas turbines also limits the possibilities for a cost-effective and simultaneously innovative cooling design using today's commercial manufacturing techniques. Currently, the TIT of large frame turbines may exceed 1600 °C [110], but it rarely exceeds 1300 °C for the smaller industrial gas turbines. As the limit for the large frames is pushed toward 1900 °C, that of the smaller engines will increase to 1600 °C. The short-term development of completely new cooling schemes for these engines is questionable from an economic point of view. Rather, it may be more viable to optimize existing geometries to reduce costs and incrementally increase their cooling effectiveness. This approach entails the manufacturing by AM of components and geometries, which would normally be investment cast or are very close to such a shape. In the mid-term, i.e., in >10 years' time, the designs of aero engines and large frame turbines will be adapted to small and medium-sized ones.

5.1. Materials' Science

The airfoils designed for AM should, of course, have material properties, which will enable the desired lifetime. These properties are a function of the material temperature,

so a better cooling allows worse material properties, but for now, one would err on the side of caution and define that those of AM materials need to be at least equivalent to cast materials. When discussing the materials' science (or even cooling designs), it should be borne in mind that AM is essentially a form of welding, with all the implications this entails for the material selection and structure. Thus, an additively manufactured airfoil is characterized by the fine granular structure of the metal. In other words, it is the diametrical opposite of the directionally solidified or single-crystal airfoils, which were developed to improve the material characteristics some decades ago: SC materials were developed to give the blades and vanes a higher strength in the direction of the highest load. If AM wants to compete with these materials, it has to be considerably more cost effective and give a cooling effectiveness, which is vastly superior to a cast airfoil to compensate for the decrease in strength via the lower temperature. One cautionary note is in place here: one should consider that the material tests, which are being currently conducted, are on solid materials. However, finite-element analyses based on theories of solid mechanics and material strength do not apply to hollow materials, or such materials, which have inherent gradients. Exactly these tests are envisaged for future airfoils.

Currently, additive manufacturing is being used in a series design of low-temperature components [111], and its suitability for high-temperature components is being evaluated [109,112]. The remaining uncertainties for high-temperature components in particular lie with the printing of materials that contain γ' -phases [113], which are traditionally considered non-weldable. In addition, their susceptibility to cracking is well known and highly dependent on the geometry and the processing parameters [114]. In recent years, attention has turned to what one might call the side effects of additive manufacturing: a more or less distinct influence of the AM process on material properties. This is, first of all, the impact of the printing direction. For nickel-based materials, the properties are best when the samples are printed "in plane", i.e., lying on the plate, whereas this cannot be conclusively said for cobalt-based materials. Second, the effects of roughness also influence the material properties of AM components. As was shown by Ref. [115] and can be seen in Figure 22, when the surface remained "as printed", multiple cracks were initiated because of the cyclic load, and these developed along the grain boundaries, resulting in much faster crack growth and shorter LCF life than for polished samples. For the latter, the crack initialization was limited, and the cracks developed at first within the grains, resulting in a much improved LCF life. The implications for AM components with internal cooling features should be clear.

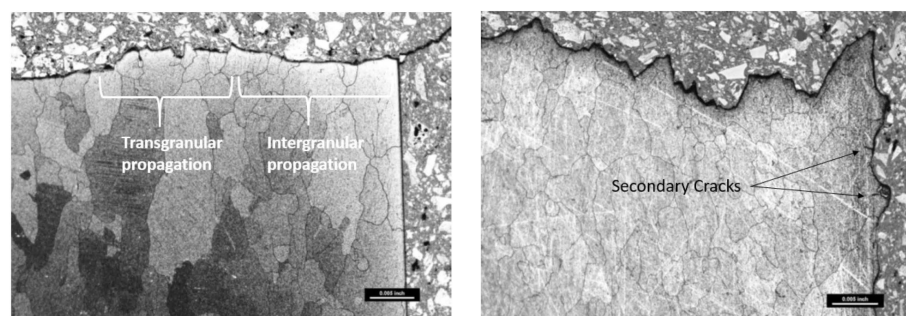


Figure 22. Crack propagation through as-printed and polished AM specimens [115].

A number of materials have been investigated for AM. In general, there is a tendency to move away from cobalt-based alloys (cobalt is an essential component of lithium-ion batteries). Therefore, the majority of the materials have been nickel based. Nonetheless, the vanes used in Ref. [116] were manufactured from MAR M-509 because they were used in direct comparison with cast NGVs, which were also made from this material. Others have investigated IN939 [109], which showed that the material parameters of the AM parts differed dramatically from cast ones or those made of IN738. This last material has received some attention, but its use is still at an experimental stage [117,118]. The main focus has been

firmly on IN718 [113,114,119–122], even though this material does not have the best material properties of the available nickel alloys (but does exhibit a very slow precipitation hardening).

All of these studies used alloy powders, which were either identical in their composition to the alloys used in casting or slightly modified. Recently, completely new alloys have been developed exclusively for AM, e.g., ABD900[®] [123,124]. In Ref. [124], a creep analysis of ABD900[®] was performed, and the results were compared with cast IN939 and IN738. As can be seen in Figure 23, in general, ABD900[®] showed superior values, but an effect of print direction on the results was seen. In addition, the material has a high ductility of approx. 10%, and the creep deformation is about two orders of magnitude higher for transverse than for longitudinal samples. These kinds of materials are the future of AM for high-temperature applications, since they allow for much better weldability, resulting in fewer material defects and better material properties.

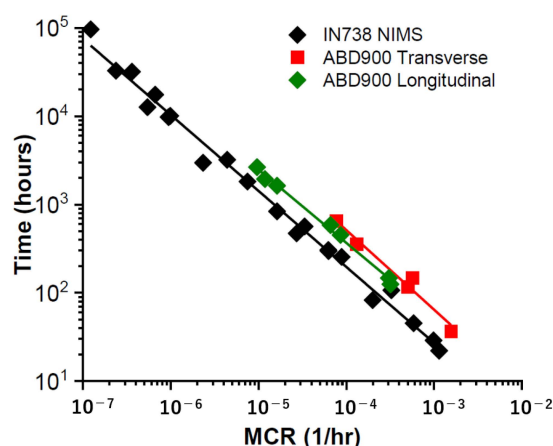


Figure 23. Comparison of creep resistance of different materials including ABD900 with different printing directions [124].

5.2. Impingement Cooling

Additive manufacturing enables the intensification of existing cooling techniques. A major part of the attention is focused on double-wall cooling, as discussed in the next section. However, as mentioned previously, “simple” impingement cooling in an AM blade can also substantially increase the cooling effectiveness and control the temperature profile over the blade height and chord. If the impingement cavity is divided into segments, film cooling can be adjusted to the mainstream pressure profile. This would lead to less structural stress and strain (see also the next section) than DWC with pin fins.

One promising development is the combination of impingement cooling with turbulators. As stated by Ref. [125], roughening or shaping the target wall does not, in general, alter the pressure loss over the impingement system. When using AM, the nozzle and turbulators can be positioned much better and more consistently relative to one another than when combining a cast part and an insert. Two strands of research can be distinguished: one in which the impingement cooling holes are of approximately the same size as the turbulators and one in which the target wall has a “micro-structure”, i.e., the turbulators are significantly smaller than the impingement cooling holes. The combination of impingement with turbulators has been investigated in some detail, e.g., Refs. [126–129]. The value given in Ref. [126] for the increase in area-averaged Nusselt number by rib-like features is 15–20%. A good overview of the potential offered by these innovations, especially considering additive manufacturing, is given in Ref. [130]. The authors cover orifice shape, turbulators and crossflow.

The small cubic turbulators in Ref. [128] fall in the micro-structure category. It is shown that even though the heat transfer of the impinging jet decreases (Nu: −6%), the resulting heat flux will be more than compensated by the increase in target area (+48%). The authors of Ref. [131] showed that increasing the height of the cubic micro-structures can increase

the Nusselt number, but the majority of the improvement comes from the introduction of the structures per se (especially for the higher Reynolds numbers). Some publications from Virginia Tech also looked at this kind of turbulators [132,133]. Three different micro-shapes were investigated: cylindrical, cubic and concentric (see Figure 24). These last ones had a superior heat transfer enhancement for all target plate distances tested (the distance of z/d with the highest enhancement). In Ref. [133], some correlations are given.

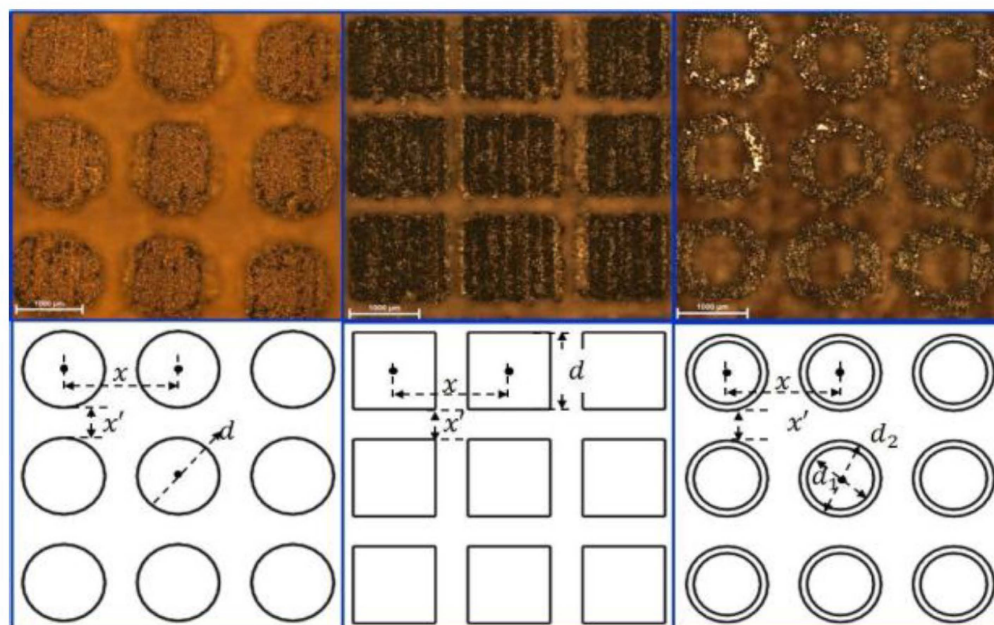


Figure 24. Different micro-roughness shapes on the target plate for impingement cooling, according to Ref. [133].

Takeishi et al. [134] discuss the experimental investigations of several geometrical variations of both circular turbulators and vortex generators (see Figure 25). The turbulators have the highest heat transfer enhancement when they are relatively close to the stagnation point of the impingement cooling. The effectiveness of the vortex generators increases with increasing height, but the investigation was limited to those within or slightly higher than the boundary layer thickness. These showed a very good performance, in line with the results of Ref. [135]. Higher fins extend into the recirculating flow, and this area is thus almost completely ineffective. Radially positioned turbulators were used by Ref. [136] as well. In Ref. [137], the shape of the impingement jets is modified. The holes that had a “V”-shape had the highest heat transfer augmentation but also rather high pressure losses for the coolant. Annerfeldt et al. [127] suggest that shielding the jet from the oncoming crossflow with geometrical features on the target plate may also be beneficial. In Ref. [138], a different approach is chosen, and an AM impingement plate with nozzles is presented. The suggestions from Refs. [136,138] were investigated by Ref. [139]. The combination of dimples with impingement cooling has been suggested, among others, by Ref. [140], but it is not the focal point of current research.

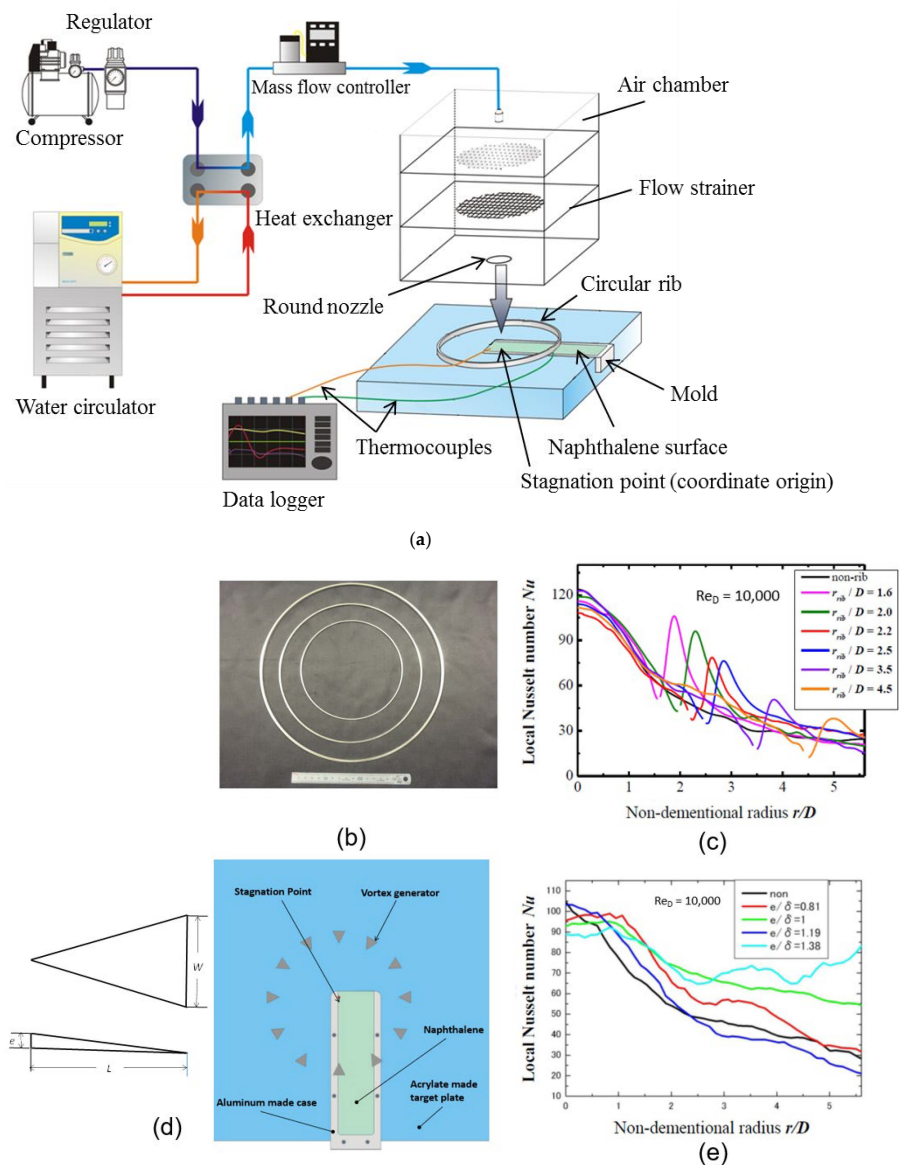


Figure 25. Heat transfer enhancement of impingement cooling using circular ribs and vortex generators [134]: (a) Experimental apparatus, (b) Circular ribs, (c) Nu distribution of circular ribs, (d) Vortex generator and layout of VGs on the target plate, (e) Nu distribution of VGs.

5.3. Internal Cooling

Internal cooling channels have received a considerable amount of attention because they form an essential part of future blade designs. This does not necessarily imply that serpentine channels will remain as dominant as they are today because (as discussed previously) a combined impingement/film-cooled blade would have a superior temperature profile in the spanwise direction. On the one hand, they will remain relevant in the short to medium term for small gas turbines until the newer designs based on aero engine airfoils are applied in industrial turbines. On the other hand, they may be integrated in more sophisticated designs. In fact, one may argue that they are an essential part of advanced impingement/film-cooling configurations.

As pointed out by Ref. [141], a large potential for optimization exists not only for cooled hot gas path components but also for heat exchangers in general. The authors of Ref. [142] considered the heat exchanger designs of various complexities and concluded that more complex designs do not necessarily lead to a better heat transfer performance, i.e., heat transfer per unit pressure loss. This was, to some extent, corroborated by Ref. [143]

whose authors investigated a void filled with a “lattice structure”. Although the intent was to simulate a double-wall cooling geometry, one could imagine integrating such a structure in an internal cooling path as well. The results showed that the more complex structure did increase heat transfer, but it did so at the cost of vastly increased pressure losses. Therefore, the more complex structure had a lower heat transfer performance than the simpler or even traditional geometries. In Refs. [144,145], a traditional serpentine cooling channel was optimized for AM using methods for the prediction of sediment disposal. In the first publication, a turbulated cooling channel was optimized for pressure loss and heat transfer, and Ref. [145] focused on the U-bend. More intricate, V-shaped ribs suitable for AM were investigated in [146].

Moving away from the theoretical considerations into more practical ones, a brief overview of the application of internally cooled AM components in gas turbines is offered. Although the blades would profit most from AM designs (the vanes are already cooled well with impingement cooling), given the concerns about the material properties of AM parts, most work has been done on stationary components [109,116,147–150]. In Ref. [116], additively manufactured NGVs were tested. There were considerable difficulties in printing the very thin insert for the impingement cooling, which points to the limitations with respect to the manufacturability of double-wall cooling designs, which need to be overcome. The test results showed no appreciable difference between the two in terms of surface temperature. In Ref. [147], the showerhead cooling at the leading edge was optimized, taking the possibilities of AM into account. The NGV conceived in Ref. [148] focuses on even more innovative designs, for example, a sweeping-jet cooling. This puts this design more in the realm of large frame gas turbines. In addition, this type of cooling has not been tested in real operation with all the associated vibrations, etc. Therefore, this promising technique will likely only be implemented in the medium to long term. The authors of Refs. [149,150] focused on the casing segment opposite the first-stage blade. They evaluated this from a structural dynamic point of view and showed the impact of including wavy micro-channels in the design. This reduced the average material temperature relative to the baseline design by more than 11%. This points to the practical applicability of the technology.

The authors of Ref. [151] performed a CFD and FE analysis of a design for a non-cooled shrouded AM blade and showed the feasibility of its application. In Refs. [152,153], designs for cooled blades were investigated as well. The former publication investigated a double-wall configuration, matrix cooling and fin cooling for a small gas turbine and gave a first impression on their feasibility. For the latter publication, a number of cooling configurations were conceived as well: impingement, serpentine and double-wall cooling. These were tested under non-rotating conditions, and the double-wall cooling proved to be only slightly better than the conventional ones. The deviations between the prediction and test for the double-wall cooling were non-negligible. This shows that, first, DWC designs are not better by definition and need optimization. Second, this optimization can, for now, not be based on standard CFD because this is validated for and calibrated to conventional cases.

Comparatively little work has been conducted on the additive manufacturing of pin fins. This may be due to the consideration that the size of pin fins is, at least for small gas turbines, in a range where their shape cannot be controlled anymore: their diameter is 1–1.5 mm, while the layer thickness of the AM is approx. 0.6 mm. One investigation [154] showed that the friction losses of AM pin fins far exceeded those of their cast equivalents. This increase is a strong function of the density of the pin-fin array. The heat transfer of AM pin fins increased as well, but not to such an extent that the thermal effectiveness (heat transfer per unit pressure loss) came close to that of cast ones. Other authors [116] did not see any appreciable difference in the temperature within the region with pin fins in additively manufactured and cast NGVs. This may also be attributed to the relative sparsity of the pin-fin array used. One may still envisage more advanced geometries, which have a

higher heat transfer with lower pressure loss, for example, a wavy end wall with inclined pin fins [155,156] (see Figure 26), which cannot be cast but can be additively manufactured.

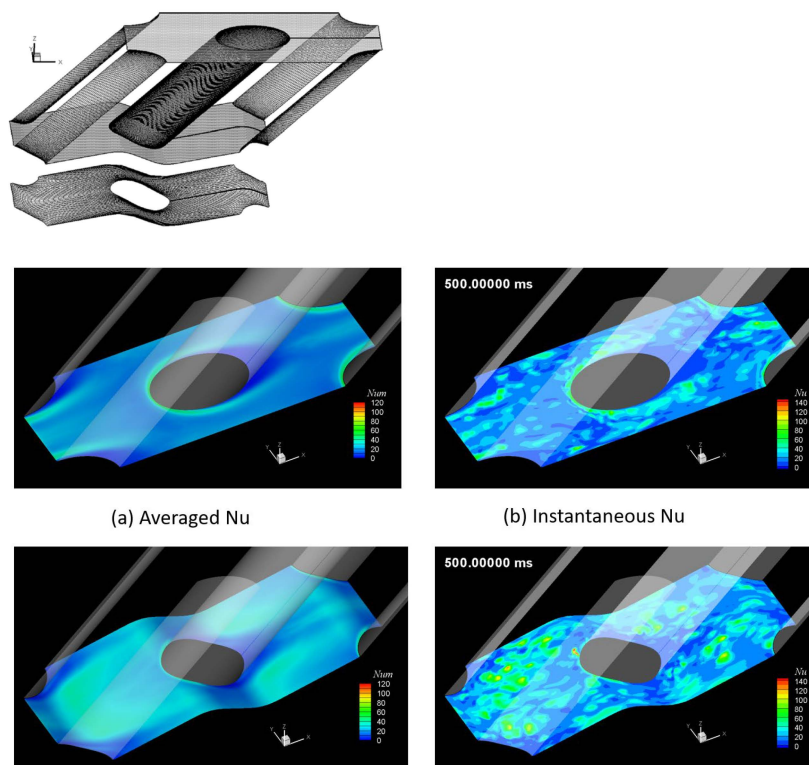


Figure 26. Computational grid and Nusselt number distribution for a pin-fin array with a wavy end wall [155].

In Ref. [157], the hypothesis from Townsend, i.e., that roughness information is not passed on beyond the boundary layer, and therefore, the flow in a channel with walls of different roughness can be simulated using current modeling strategies, is tested. The authors found evidence to support this hypothesis.

5.4. Film Cooling

As the thermal load on turbine airfoils increased, the film-cooling methods applied have been improved, and more efficient film-cooling structures have been developed with less cooling air. Bunker summarizes the historical development of film cooling in Figure 27 (Refs. [104,105]), and the current goal for film-cooling technology applied in DWC is to achieve an overall cooling efficiency of 0.75–0.8.

There is a case to be made that film cooling will become even more important than it is today because of the higher TITs. Therefore, future airfoils will have extensive film or effusion cooling, and it would result in a tremendous cost reduction if the holes could be printed rather than machined.

Effusion cooling can be, somewhat simplified, defined as consisting of a very dense array of small film-cooling holes from which the coolant is ejected at a very low blowing ratio, i.e., $M = 0.5$ or less. It has been employed primarily in combustion chambers, but its use for airfoils has been contemplated for nearly as long as film cooling itself exists. The growing importance and the low blowing ratios require an accurate modeling strategy.

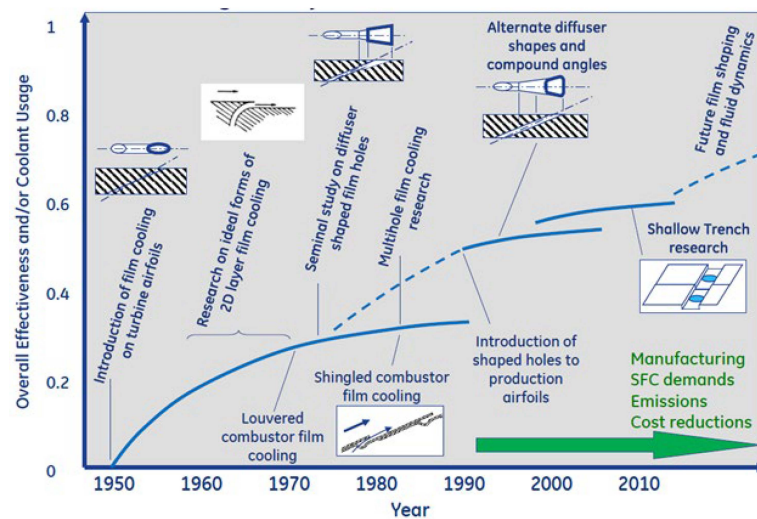


Figure 27. Historical development of film cooling in gas turbines [104,105].

It is not unusual to use Sellers' superposition principle to model film- and effusion-cooling arrays. This method has its deficits, but it works reasonably well on flat plates with a low blowing ratio. Its use for airfoils is disputed, as the flow here shows three-dimensional effects that a simple approach cannot depict. A number of correlations have been developed, but they are typically only valid for the geometry they were developed on. Although CFD is rarely an exact match with experiments, it does a much better job of calculating the heat load on a "random" surface than the two approaches mentioned previously.

Because of the difficulty in meshing large cooling arrays and the computational time this requires, many strategies for modeling effusion cooling as a source term have been developed. Normally, the source terms for mass, momentum, energy and turbulence are required. These can be applied either directly to the wall or as volumetric source terms in the cells of the boundary layer. One overview [158] reported a better prediction of both heat transfer coefficient and film-cooling effectiveness for the volumetric model. The authors of Ref. [159] proposed a source term model in which the in- and outflow were modeled separately and showed good results for low velocity ratios (i.e., attached jets) and low crossflow velocities. The distribution of the sources is often uniform, but Refs. [160,161] presented a set of semi-empirical correlations for the distribution of the source terms over the volume with very good results. Some other approaches have been followed, e.g., Ref. [162] discussed a spectral decomposition of the problem, where the number of simulated holes is reduced, akin to an FFT. Their results were very good, and the approach is especially suitable for very large numbers of holes.

Conjugate simulations are necessary to capture the combined effect of film and internal cooling. In this context, unsteady conjugate simulations, for which pioneering work has been performed by the Osney Laboratory in Oxford [163,164] need to be emphasized. The former proved the possibility of performing unsteady conjugate calculations based on an FFT decomposition of the fluctuating temperature component. Their theoretical considerations show that the mesh near the fluid/solid interface has to be much denser on the solid side than for steady calculations. Their practical calculations showed that not considering the fluctuating component of the flow leads to an over-estimation of the solid temperature, i.e., it is conservative. The authors of Ref. [165] picked up on the issue that the heat flux is not strictly linearly dependent on the difference between the fluid and wall temperatures and suggested a non-linear (basically quadratic) approximation.

The increased use of conjugate methods also triggered some limited interest in designing experiments for validation data, focusing on the Biot number, the ratio of internal to external HTC and bore cooling [165,166].

The rough walls of the cooling holes when using AM were already pointed out, but the inlet to the film-cooling holes is important as well. The latter may not be well defined

when using AM. The inflow into the cooling holes and the flow within the holes themselves need to be modeled properly based on CFD-grade experiments. By the very nature of it, the flow in a hole is difficult to visualize experimentally. The little experimental and ample numerical evidence shows that a separation bubble is formed, which determines the discharge coefficient. Some measurements were recorded, for example by Refs. [167,168] using MRI, and by Ref. [169] using PIV measurement of in-hole flow. The results of Ref. [169] were correlated directly with very high-fidelity LES with very satisfying results.

A good overview of the state of the art of cooling hole manufacturing, which considers the most important commercially available techniques, is given in Ref. [170]. All of these have their drawbacks. Furthermore, one has to bear in mind that manufacturing film-cooling holes in a DWC airfoil will be challenging because, regardless of the manufacturing method (EDM, laser drilling, . . .), it will be difficult to avoid contact between the drilling tool and the backwall. This is understood as the impingement wall, pin fins and divider walls. Therefore, additively manufacturing film-cooling holes seems an attractive alternative. However, it should be borne in mind that the diameter of film-cooling holes is in the same order of magnitude as the layer thickness in AM, especially for small and medium-sized gas turbines. This presents its own challenges when it comes to geometrical accuracy and roughness. The holes will tend to approximate a certain geometry (e.g., round), and, if one takes the layer effect into account, the surface roughness will be in the order of magnitude of the hole diameter.

One strand of research investigates the impact of AM on traditional film-cooling holes [171,172]. The former publication looked at holes with a nominal diameter between 1.26 and 2.45 mm. The cooling holes manufactured using EDM had a significantly lower roughness than the AM holes, and small additively manufactured holes, which were positioned at an angle to the build direction, were almost completely blocked. For the holes that were not blocked, the added roughness in the cooling hole contributed significantly to the overall cooling effectiveness because the heat transfer within the cooling hole increased. The study was extended to a variety of different hole shapes [172] where the susceptibility to deviations between design intent and the achieved geometry was confirmed, as was the influence of roughness on the overall results.

Another strand looks into the possible blockage of smaller holes [173–175]. In the first publication, the impact of hole blockage of small (0.4 mm) cooling holes was investigated based on statistics. In Ref. [174] a number of different cooling hole configurations were tested. Exceptionally, the authors not only tested the thermal performance, but they investigated the tensile strength of the perforated structures as well. Perhaps unsurprisingly, the structures with the largest pitch between the holes showed the highest strength. The thermal investigation was expanded to a number of geometries and investigated experimentally in Ref. [176]. As for the large holes, the internal surface area contributed significantly to the overall cooling effectiveness. AM designs, which completely abandoned classical hole design and resembled packed spheres, a wire mesh or one inspired by blood vessels, were particularly good. Therefore, whereas much of the previous studies pointed toward the limitations that need to be overcome and the impact on existing cooling designs, this last study points the way to truly new ways of thinking.

Double-wall cooling implies the use of film cooling, and conventional film cooling may be applied. One possible improvement on this is swirling film cooling [176]. A swirl can be induced using an inclined impingement nozzle, a vortex generator, etc.; if the double-wall structure has one cavity per film-cooling hole, having the “correct” swirl becomes easier. With this swirl, the film-cooling effectiveness has maximum value at low M . With this combination, the blowing ratio can be reduced from $M = 1.0 \dots 2.0$ to as little as $M = 0.5$.

5.5. Deviations, Tolerances and Roughness

It should be clear from the previous discussions that one of the most important challenges that need to be overcome from a cooling perspective are the deviations from the nominal dimensions of cooling features. In a research environment, more often than

not, scaled-up, ideal geometries are investigated. In real engine manufacturing, tolerances come into play, and these should be taken account of. Heat transfer and wall temperature is given in Ref. [177]. These tolerances arise from the manufacturing process (precision casting) on the one hand and the subsequent machining on the other hand. Both the core itself and its positioning relative to the cast have some variability. In addition, the raw parts have to be fixated for machining, which also causes deviations. This is exacerbated by the sometimes opaque relationship between different parameters that determine the deviations and the fact that these may follow a non-Gaussian distribution. Therefore, these need to be quantified [178,179]. Most of this can be eliminated when AM is used because there are much fewer steps involved. From a cooling perspective, the layer thickness of AM needs to be reduced to allow finer features and reduce the roughness in general. However, the roughness is different on different surfaces, depending on their angle of inclination toward the build direction. This should be reduced as well because this angle cannot always be controlled, and it is difficult to account for it in the design process. As we have seen, it also influences the strength of the component.

Some authors [180] have investigated the factors relevant for AM, such as the different models manufactured on different machines, at different positions on the build plate, with different layer thicknesses and at different angles toward the plate. All of these parameters do have an effect, as does the wall thickness (if it is less than 0.6 mm, an effect can be seen; see also Ref. [116]). In summary, the build location has an appreciable impact on roughness; layer thickness, on the other hand, only has an impact on surfaces where a distinct “stair-stepping” effect occurs. Luckily, the machines do not have a large impact.

The issues with internal surface roughness have led to a large number of both experimental and numerical publications on this issue. The former are the center of attention of the researchers at Penn State University, although others are increasingly making contributions [181–188]. Stimpson et al. [187] emphasize the increased surface roughness in AM parts. In Ref. [188], it is shown that any overhanging features, such as turbulators, are bound to deviate from the nominal geometry due to constraints inherent to AM.

The classification and numerical modeling of roughness is an extremely complicated issue with a long tradition [189]. This research forms the basis for investigations in combination with AM. Much has been achieved by Refs. [181,190] who applied the Aupoix model of roughness to both pressure losses [191] and heat transfer [192], as shown in Figure 28, and validated their results with a substantial amount of data from the Penn State group. Others have, for example, applied the distributed element roughness model to these geometries [193], with reasonable results. This will, in the foreseeable future, lead to numerical models, which are attuned to the peculiarities of AM surfaces. This will then also be the basis for detailed CHT models, which take the heightened heat transfer on AM surfaces into account.

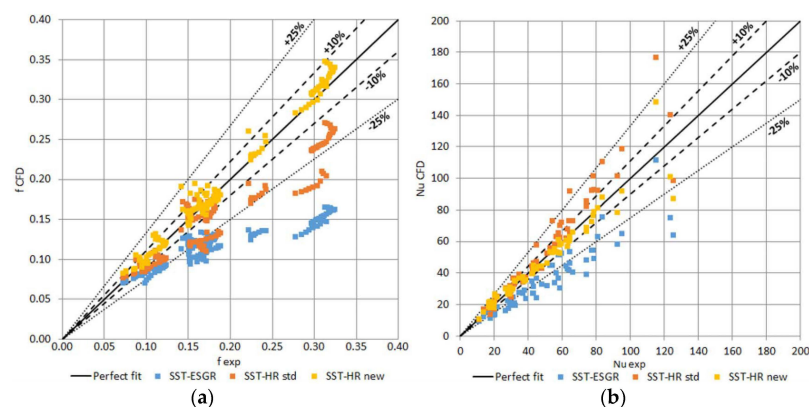


Figure 28. Benchmark on predicted friction factor and Nusselt number [181]: (a) Correlation of calculated versus measured friction factors; (b) Nusselt numbers of experiments and CFD.

6. Double-Wall Cooling

Innovative cycles, as well as cycles with a higher TIT, need airfoils, which are adapted to the changed boundary conditions. The current state of the art of cooled blades is succinctly summarized in Ref. [194]. It consists of serpentine cooling in the leading edge and mid-chord regions and a pin-fin bank in the trailing edge. This is combined throughout with film cooling.

The number of papers in the public domain dedicated to innovative cooling technologies enabled by additive manufacturing is increasing continuously. The majority of these are concerned with double-wall cooling. This concept is not new as such; it creates a void between an inner and an outer (hot gas path) wall, which means that a combination of impingement, pin fin and film cooling can be applied. Similar concepts were pursued in the 1970s, for example, with Lamilloy® [94]. One of the first sets of papers, which discussed potential new designs adapted to the new hot gas path boundary conditions, were Refs. [195,196], where the authors already discussed the advantages of double-wall cooling relative to the classic serpentine cooling; the wall temperature decreased by up to 100 K.

One group who investigated the precursors of double-wall cooling early on was based at Leeds University. The experimental investigation described in Ref. [197] focused on the optimum number of impingement-cooling holes for a given number of effusion-cooling holes. This was found when the number of holes for both cooling techniques was the same, and there was exactly half-a-pitch distance in both streamwise and lateral direction between the impingement- and effusion-cooling holes. In another excellent experimental investigation, Ref. [198], the same group varied the number and size of the effusion-cooling holes. As long as the effusion-cooling jets were attached to the surface ($M < 0.5$), the number of holes had a limited effect. Once the lift-off occurred, the importance of the impingement cooling increased considerably. The concept was also investigated at Yonsei University. The pattern of impingement- and effusion-cooling holes was optimized both experimentally and numerically in Ref. [199], and the effect of crossflow was quantified in Ref. [200]. The authors noted that the effect of the impingement was severely curtailed when the crossflow ratio rose above 0.5, but this is common for normal impingement cooling as well and should not normally occur in combined impingement/film-cooling (DWC) configurations. The same group suggested introducing fins into the space between the impingement- and effusion-cooling plates to increase the heat transfer [201]. Furthermore, they looked at the effects of rotation on the flow in the gap between the two plates [202], which is, of course, highly relevant for the application of DWC to blades. Investigations of this kind gave rise to a number of patents [203–206] before the possibilities of AM were widely recognized.

The double-wall concept has gained more traction with the advent of AM because these geometries can now be much more easily manufactured. Currently, a significant amount of work is being conducted at the University of Oxford [207–211]. As shown in Ref. [209], modeling effusion cooling with Sellers' superposition methodology is challenging, although it does provide a quick (if not entirely accurate) solution. This becomes relevant when modeling double-wall cooling [210]. In this last paper, the authors investigated several geometries and proposed a varying set-up of double-wall cooling, which is adjusted to the local aerodynamic and thermal boundary conditions in the main flow. It should be emphasized here that the experiments were performed at engine-relevant Reynolds numbers, but the test specimens were scaled by a factor 10. When optimizing the interaction of effusion-cooling jets, the stream- and spanwise distances should be varied independently from one another to achieve the best solution [208]. Modeling these complex geometries with CFD or even CHT is still too computationally expensive. Therefore, the group also provided (experimentally validated) simplified models of double-wall cooling geometries [207,211].

For those industrial gas turbines that employ a system, which cools the cooling air using the water of the bottoming cycle, it may be difficult to raise the temperature of the cooling air sufficiently to achieve the optimum thermodynamic and cooling effectiveness with this combination of impingement cooling and film cooling. In such cases, a cooling

mechanism is necessary to increase the temperature to an appropriate level by using the coolant to reduce the temperature of the inner surface of the blade before impingement cooling. Such a cooling structure, which also serves as a supply passage for the impingement air, can be called triple-wall cooling. In addition, it is necessary to design an optimal structure, which satisfies fatigue life, by means of conjugate analysis of the blade surface, cavity including the impingement nozzle, and the internal cooling and rib structure through steady-state and transient thermal analyses.

The efforts of the group at Yonsei University mentioned before continued with emphasis on additively manufactured geometries [212,213]. Tests and simulations were performed on scaled-up sections, in which the impingement-cooling hole simultaneously functions as a pin fin in a multi-layer system. Because the system consists of three plates and two voids, the distance between these plates is a parameter, which can be varied. The highest heat transfer performance was observed in a system where the “cold-side” void was small, and the “hot-side” void was large [212] (see Figure 29).

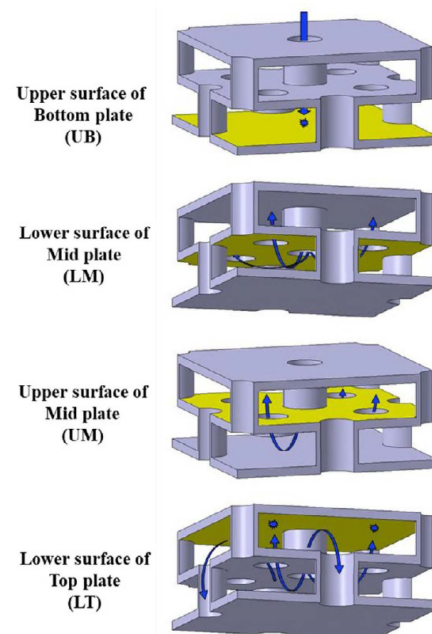


Figure 29. The double-wall cooling configuration conceived by Ref. [213].

An early example of an FE analysis of the effusion wall is Ref. [214]. The creep characteristics of a simulated double-wall specimen were investigated by Ref. [215]. They concluded that the impingement hole and pin-fin distribution were more important for the creep characteristics than the effusion-cooling holes. Elmukashfi et al. [216], on the other hand, investigated the entire system using unit cells (an approach also used for effusion cooling, cf. Ref. [217]) and showed that the area of maximum load changes depending on the relative strength of the various components of the entire system, i.e., impingement, pin fin and effusion cooling. A number of other publications (Refs. [218–222]) also focused on the entire double-wall system applied to a blade. It was shown in Ref. [218] that a significant temperature gradient exists in the double-wall system, which drives thermal stress. The low cycle fatigue of a blade with double-wall cooling is driven by thermal and centrifugal stresses around the cooling holes due to the stress concentration factor, which works here. The same authors discussed the optimization of the resulting stresses in Ref. [219] and recommended spacing the pin fins rather tightly. If the thicknesses of the outer wall increase, the stress here decreases, but it increases in the inner wall. In Ref. [220], the impact of the angle of the cooling hole was evaluated (as a less sharp angle to the outer surface is beneficial). In the last papers of the series (Refs. [221,222]), the authors looked at the convex and concave curvature (see Figure 30) and introduced temperature-dependent

thermo-elastic properties. They point out that the compressive stresses on the pin fins at the hot wall can become exceedingly large, and therefore, a minimum pin-fin diameter is required. In conclusion, the authors suggest a variable ratio of inner and outer wall thicknesses along the chord of the blade.

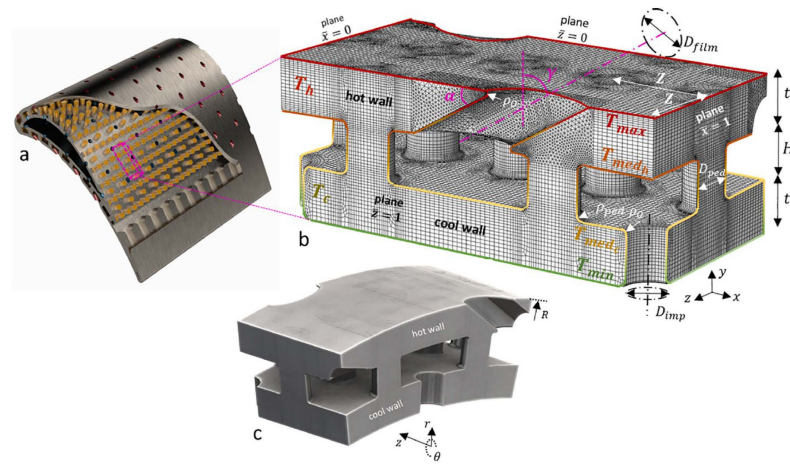


Figure 30. The area considered for the FE analysis in Ref. [221]: (a) A typical double wall transpiration cooling (DWTC) system for a gas turbine blade; (b) Repeating unit cell for a flat DWTC system; (c) Back view of a curved version of the unit cell in (b).

For both FEA and the precise calculation of the temperatures of the coolant and cooling effectiveness of the DWTC, conjugate analyses on life-sized components with the correct surface structuring will be required.

Other work is concerned with the impingement in narrow channels [223]. Here, it is shown that the optimum configuration depends on, for example, jet diameter and spacing, with smaller diameters having a smaller optimum ratio of D/H . Additionally, as seen before, numerical optimization does not always predict the best configuration in practice, even for these relatively simple geometries. Additively manufacturing such micro-channels enables the generation of an angled connection between the individual channels—something, which is investigated in Ref. [224] and shown in Figure 31. The authors show that this enhances heat transfer considerably.

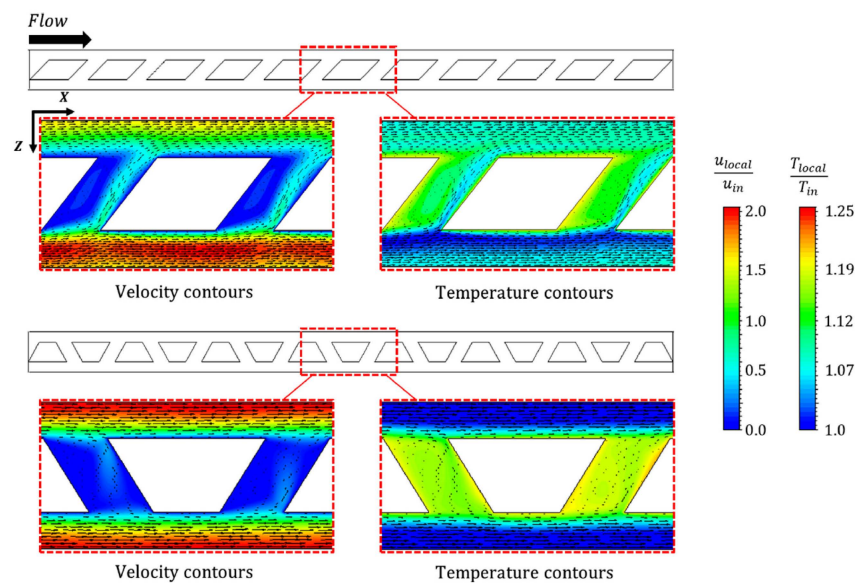


Figure 31. Numerically derived velocity and temperature contours plots along the channel mid-section height in the angled connection between micro-channels [224].

Due to the strong curvature of the walls, the leading edge deserves a separate discussion [131]. The authors of Ref. [225] noted that the pin fins had little influence on the heat transfer on the strongly curved target wall itself, but the heat transfer to the pins depended on their position and size. They suggest that the Lamilloy[®] structure needs to be optimized for the case at hand. The coolant injection into a 90° section of a cylinder representative of a leading edge was investigated in Ref. [226]. The injection angle had a noticeable impact on the heat transfer.

7. Conclusions

The paper discusses the configurations of airfoils for industrial gas turbines used in the carbon-neutral era. First, the evolution of cooling methods for industrial gas turbines, which have come to play a major role in the society as energy conversion equipment, is surveyed. The research status of cooled airfoils, cast-cooled blades, and wafer and diffusion bonded blades, which have not been commercialized but offer high performance and reliability, was also investigated. Research on new gas-turbine-based cycles, such as the use of carbon-free fuels (hydrogen or ammonia), the clean use of fossil fuels (including coal) in the gas turbine cycle, a method that does not generate NO_x when combustion occurs at high temperatures, and a new gas turbine cycle with easy CCS, was discussed. The research and demonstration tests of new cycles using gas turbines were surveyed. As a result, industrial gas turbines and airfoil cooling configurations suitable for the carbon-neutral era were identified.

Industrial gas turbines will become increasingly important as a source of power generation to stabilize fluctuations. For this reason, gas turbines must be able to handle rapid start-up and load fluctuations and maintain a high performance even under partial load. The need to use carbon-free fuel or CCS will increase the unit cost of power generation. To address this issue, it will be necessary to develop high-performance gas turbines with a TIT from 1900 to 2000 °C and a pressure ratio of 30 for large industrial gas turbines and 1500 to 1600 °C for medium-sized gas turbines. The oxy-fuel cycle, which includes hydrogen as a fuel, could be useful as a countermeasure against the generation of NO_x with hydrogen combustion and as a carbon-free power generation system for fossil fuels, including coal.

When burning hydrogen or ammonia, small and medium-sized industrial gas turbines can be used for fast and flexible operation, both in CHP applications and (perhaps more than now) as SCGT. Introducing AM will reduce the manufacturing costs and simultaneously increase cooling effectiveness, enabling larger load gradients than are currently deemed acceptable.

The preferred cooling structure to be used in future industrial gas turbines described above is double-wall cooling. Various DWC cooling structures have been proposed, and their heat transfer characteristics have been investigated. Among them, the structure combining impingement cooling with film cooling or effusion cooling is considered the best. AM is considered the best solution for fabricating these DWC cooling structures. As was pointed out, three major issues need to be addressed: the availability of appropriate materials and the determination of their high-temperature properties, the control of the AM process as such (layer thickness, surface roughness) and the costs. In order to realize DWC blades fabricated by AM, research including conjugate analysis of the cooling structure and lifetime evaluation through steady-state and transient thermal structure analyses should be conducted.

Author Contributions: Conceptualization, K.T.; writing—original draft preparation, K.T. and R.K.; writing—review and editing, K.T. and R.K. All authors have read and agreed to the published version of the manuscript.

Funding: This research received no external funding.

Conflicts of Interest: The authors declare no conflict of interest.

Nomenclature and Acronyms

D	Impingement-cooling hole diameter
d	film-cooling hole diameter
M	film-cooling hole blowing ratio: $\rho_c u_c / \rho_\infty u_\infty$
Nu	Nusselt number
Re	Reynolds number
u	velocity
x	horizontal (in-plane) axis/direction of flat plate
y	horizontal (in-plane) axis/direction of flat plate
z	vertical (out-of-plane) axis/direction of flat plate
δ	boundary layer thickness
ρ	density

Subscripts

c	coolant
f	film
∞	main stream

Abbreviations

ABB	Asea Brown Boveri
AHAT	humid air turbine
AM	additive manufacturing
APC	announced pledges case
ATS	advanced turbine systems
BBC	Brown, Boveri & Company
CC	conventional casting
CC	combined cycle
CCGT	combined cycle gas turbine
CFD	computational fluid dynamic
CHP	combined heat and power
CCS	carbon capture and storage
CCUS	carbon capture usage and storage
COP	Conference of the Parties
DOE	department of energy
DS	dictionary solidified
DWC	double-wall cooling
DWTC	double wall transpiration cooling
EDM	electric discharge machining
EPRI	Electric Power Research Institute
ERDA	Energy Research and Development Administration
FE	Finite element
FEA	finite element analysis
FFT	Fast Fourier Transform
GE	General Electric Corporation
GHG	greenhouse gas emissions
GT	gas turbine
GTW	gas turbine world
HAT	humid air turbine
HHV	high heating value
HRSG	heat recovery steam generator
HTTT	High Temperature Turbine Technology
IEA	International Energy Agency
IGCC	integrated gasification combined cycle
LCF	low cycle fatigue
LNG	liquid natural gas
LHV	low heating value
MHI	Mitsubishi Heavy Industries, Ltd.
MRI	magnetic resonance imaging

NDC	nationally determined contribution
NGV	nozzle guide vane
OEM	original equipment manufacturing
OFC	oxy-fuel cycle
PIV	particle image velocimetry
PHR	power-to-heat ratio
PW	Pratt and Whitney
SCGT	steam-cooling gas turbine
SLM	selective laser melting
STIG	steam-injected gas turbine
TBC	thermal barrier coating
TIT	turbine inlet temperature
UCTS	uniform crystal temperature sensors
VG	vortex generator
WH	Westinghouse Electric Company

References

- United Nations Climate Actions. The Paris Agreement. Available online: <https://www.un.org/en/climatechange/paris-agreement> (accessed on 24 December 2022).
- United Nations Climate Change. Long-Term Strategies Portal. Available online: <https://unfccc.int/process/the-paris-agreement/long-term-strategies> (accessed on 24 December 2022).
- The Government of Japan. The Long-Term Strategy under the Paris Agreement. 2021. Available online: https://unfccc.int/sites/default/files/resource/Japan_LTS2021.pdf (accessed on 9 October 2022).
- Regulation (EU) 2021/1119 of the European Parliament and of the Council of 30 June 2021 Establishing the Framework for Achieving Climate Neutrality and Amending Regulations (EC) No 401/2009 and (EU) 2018/1999 ('European Climate Law'). Available online: <https://eur-lex.europa.eu/legal-content/EN/TXT/?uri=CELEX:32021R1119> (accessed on 24 December 2022).
- A European Green Deal. Striving to Be the First Climate-Neutral Continent. 2019. Available online: https://commission.europa.eu/strategy-and-policy/priorities-2019-2024/european-green-deal_en (accessed on 24 December 2022).
- EIB Group Climate Bank Roadmap 2021–2025. 2020. Available online: <https://www.eib.org/en/publications/the-eib-group-climate-bank-roadmap> (accessed on 24 December 2022).
- GE's 7 HA and 9 HA Plants Rated at More than 61% CC Efficiency. Available online: <https://www.mcilvaineconomy.com> (accessed on 24 December 2022).
- Takamura, K.; Iijima, T.; Wakazono, S.; Hada, S.; Yuri, M.; Kataoka, M. Development of 1650 °C Class Next Generation JAC Gas Turbine based on J Experience. *Mitsubishi Heavy Ind. Tech. Rev.* **2019**, *56*, 1–9. Available online: <https://www.mhi.co.jp/technology/review/pdf/e563/e563020.pdf> (accessed on 11 October 2022).
- ASME. The World's First Industrial Gas Turbine Set at Neuchâtel (1939), An International Historic Mechanical Engineering Landmark, 2 September 1988, Neuchâtel, Switzerland. Available online: <https://www.asme.org/wwwasmeorg/media/resourcefiles/aboutasme/who%20we%20are/engineering%20history/landmarks/135-neuchatel-gas-turbine.pdf> (accessed on 24 December 2022).
- Wettstein, H.E. 80 years open GT development in Baden. In Proceedings of the ASME Turbo Expo 2019, Phoenix, AZ, USA, 17–21 June 2019; Paper No. GT2019-90177. [CrossRef]
- Meher-Homji, C.B. The Development of the Whittle Turbojet. *ASME J. Eng. Gas Turbines Power* **1998**, *120*, 249–256. [CrossRef]
- Meher-Homji, C.B.; Prisell, E. Pioneering turbojet developments of Dr. Hans Von Ohain—From the HeS 1 to the HeS 011. *J. Eng. Gas Turbines Power* **2000**, *122*, 191–201. [CrossRef]
- Horlock, J. *Advanced Gas Turbine Cycles*; Elsevier Science Ltd.: Oxford, UK, 2003, ISBN 0-08-044273-0.
- Horlock, J. *Combined Power Plants Including Combined Cycle Gas Turbine (CCGT) Plants*; Pergamon Press: Oxford, UK, 1992, ISBN 0-08-040502-9.
- Horlock, J. Combined Power Plants—Past, Present, and Future. *J. Eng. Gas Turbines Power* **1995**, *117*, 608–616. [CrossRef]
- Yamakawa, A.; Araki, R.; Saito, I. Design and Construction of Gas-Steam Combined Cycle Plant for Higashi Niigata Thermal Power Station No. 3. In Proceedings of the 1983 Tokyo International Gas Turbine Congress, Tokyo, Japan, 23–29 October 1983; Paper No. IGTC-107.
- Sudo, Y.; Sato, M.; Kobayashi, Y. Construction and Operation of Gas-Steam Combined Cycle Plant for Higashi Niigata Thermal Power Station No. 3. In Proceedings of the ASME 1986 International Gas Turbine Conference and Exhibit, Dusseldorf, Germany, 8–12 June 1986; Paper No. 86-GT-236. [CrossRef]
- Gülen, S.C. Étude on gas turbine combined cycle power plant—Next 20 years. *J. Eng. Gas Turbines Power* **2015**, *138*, 051701. [CrossRef]
- Bergek, A.; Tell, F.; Berggren, C.; Watson, J. Technological capabilities and late shakeouts: Industrial dynamics in the advanced gas turbine industry, 1987–2002. *Ind. Corp. Chang.* **2008**, *17*, 335–392. [CrossRef]
- Ol'khovskii, G.G.; Radin, Y.A.; Mel'nikov, V.A.; Tuz, N.E.; Mironenko, A.V. Thermal Tests of the 9FB Gas Turbine Unit Produced by General Electric. *Therm. Eng.* **2013**, *60*, 607–612. [CrossRef]

21. Rice, I. The Combined Reheat Gas Turbine/Steam Turbine Cycle: Part I-A Critical Analysis of the Combined Reheat Gas Turbine/Steam Turbine Cycle. *J. Eng. Gas Turbines Power* **1980**, *102*, 35–41. [[CrossRef](#)]
22. Rice, I. The Combined Reheat Gas Turbine/Steam Turbine Cycle: Part II-The LM 5000 Gas Generator Applied to the Combined Reheat Gas Turbine/Steam Turbine Cycle. *J. Eng. Gas Turbines Power* **1980**, *102*, 42–49. [[CrossRef](#)]
23. Rice, I. The Reheat Gas Turbine with Steam-Blade Cooling- A Means of Increasing Reheat Pressure, Output, and Combined Cycle Efficiency. *J. Eng. Gas Turbines Power* **1982**, *104*, 9–22. [[CrossRef](#)]
24. Briesch, M.; Bannister, R.; Diakunchak, I.; Huber, D. A Combined Cycle Designed to Achieve Greater Than 60 Percent Efficiency. *J. Eng. Gas Turbines Power* **1995**, *117*, 734–741. [[CrossRef](#)]
25. Pritchard, J. H System™ Technology Update. In Proceedings of the ASME Turbo Expo, Atlanta, GA, USA, 16–19 June 2003; Paper No. GT2003-38711. [[CrossRef](#)]
26. Southall, L.; McQuiggan, G. New 200 MW Class 501G Combustion Turbine. *J. Eng. Gas Turbines Power* **1996**, *118*, 572–577. [[CrossRef](#)]
27. Horlock, J.; Watson, D.; Jones, T. Limitations on Gas Turbine Performance Imposed by Large Turbine Cooling Flows. *J. Eng. Gas Turbines Power* **2001**, *123*, 487–494. [[CrossRef](#)]
28. Takeishi, K.; Komiyama, M.; Oda, Y.; Mori, S.; Kitamura, T. Study on the Thermal and Flow Fields of Shaped Film-Cooling Holes. *Heat Transf. Res.* **2011**, *42*, 83–100. [[CrossRef](#)]
29. Vandervort, C. Advancements in H Class Gas Turbines and Combined Cycle Power Plants. In Proceedings of the ASME Turbo Expo, Oslo, Norway, 11–15 June 2018; Paper No: GT2018-76911. [[CrossRef](#)]
30. Gülen, S. *Gas Turbine Combined Cycle Power Plants*; CRC Press: Boca Raton, FL, USA, 2019, ISBN 9780429244360. [[CrossRef](#)]
31. Takeishi, K. Evolution of Turbine Cooled Vanes and Blades Applied for Large Industrial Gas Turbines and Its Trend Toward Carbon Neutrality. *Energies* **2022**, *15*, 8935. [[CrossRef](#)]
32. Otsuki, Y. Development and History and State of the Art of Kawasaki Gas Turbines. In *Selected Topics in Turbomachinery and Jet Propulsion*; Bohn, D., Ed.; RWTH Aachen University: Aachen, Germany, 2004. Available online: <https://www.ikdg.rwth-aachen.de/cms/ikdg/Studium/Wintersemester/~olev/Ausgewaehlte-Kapitel-der-Turbomaschinen/?lidx=1> (accessed on 24 December 2022).
33. Hunt, R. *The Development and History of the Gas Turbine for Power Generation, Industrial and Marine Purposes*, 1st ed.; Power + Energy Associates Ltd.: Morpeth, UK, 2019, ISBN 13 9781527239401.
34. Saidi, K.; Orth, U.; Boje, S.; Frekers, C. A Comparative Study of Combined Heat and Power Systems for a Typical Food Industry Application. In Proceedings of the ASME Turbo Expo, Düsseldorf, Germany, 16–20 June 2014; Paper No. GT2014-26234. [[CrossRef](#)]
35. Hoops, H.; Saidi, K. A Comparative Study of a Gas Turbine and Gas Engine Regarding Efficiency and Flexibility for Typical Combined Heat and Power Processes. *Gwf Gas Energie* **2017**, *6*, 1–10. Available online: https://www.man-es.com/docs/default-source/energy-storage/orchestrated-heat-and-power/man-es_mgt_technical_paper_preview.pdf?sfvrsn=51cf6dd6_6 (accessed on 11 October 2022).
36. Brun, K.; Kurz, R. *Introduction to Gas Turbine Theory*, 3rd ed.; Solar Turbines Incorporated: San Diego, CA, USA, 2019, ISBN 978-0-578-48386-3.
37. Krewinkel, R. MAN ExpertTalk: Gas Turbine Basics & Applications, Oberhausen. 2021. Available online: <https://www.man-es.com/digitalcenter/MAN-ExpertTalk-center/2021/06/23/webinar/gas-turbines-basics-applications> (accessed on 24 December 2022).
38. Tanaka, R.; Koji, T.; Ryu, M.; Matsuoka, A.; Okuto, A. Development of High Efficient 30MW Class Gas Turbine the Kawasaki L30A. In Proceedings of the ASME Turbo Expo, Copenhagen, Denmark, 11–15 June 2012; Paper No. GT2012-68668. [[CrossRef](#)]
39. IEA. Net Zero by 2050: A Roadmap for the Global Energy Sector—A Special Report by the International Energy Agency, International Energy Agency. 2021. Available online: https://iea.blob.core.windows.net/assets/deebef5d-0c34-4539-9d0c-10b13d840027/NetZeroBy2050-ARoadmapfortheGlobalEnergySector_CORR.pdf (accessed on 24 December 2022).
40. Cohn, A. Water Cooled Gas Turbine Development Summary. In Proceedings of the Joint Power Generation Conference: GT Papers, Denver, CO, USA, 17–21 October 1982; Paper No. 82-JPGC-GT-5. [[CrossRef](#)]
41. Caruvana, A.; Day, W.; Cincotta, G.; Rose, R. System Status of the Water-Cooled Gas Turbine for the High Temperature Turbine Technology Program. In Proceedings of the International Gas Turbine Conference and Exhibit and Solar Energy Conference, San Diego, CA, USA, 12–15 March 1979; Paper No. 79-GT-39. [[CrossRef](#)]
42. Plumley, D. Cool Water Coal Gasification—A Progress Report. *J. Eng. Gas Turbines Power* **1985**, *107*, 856–860. [[CrossRef](#)]
43. Phillips, J.; Booras, G.; Marasigan, J. The History of Integrated Gasification Combined-Cycle Power Plants. In Proceedings of the ASME Turbo Expo, Charlotte, NC, USA, 26–30 June 2017; Paper No. GT2017-64507. [[CrossRef](#)]
44. Asano, A. Case Study: Nakoso IGCC Power Plant Japan. In *Integrated Gasification Combined Cycle (IGCC) Technologies*; Wang, T., Stiegel, G., Eds.; Woodhead Publishing: Kidlington, UK, 2017; pp. 799–816, ISBN 978-0-08-100185-1.
45. Shinada, O.; Yamada, A.; Koyama, Y. The Development of Advanced Energy Technologies in Japan: IGCC—A Key Technology for the 21st Century. *Energy Convers. Manag.* **2002**, *43*, 1221–1233. [[CrossRef](#)]
46. Wang, T.; Stiegel, G. *Integrated Gasification Combined Cycle (IGCC) Technologies*; Woodhead Publishing: Kidlington, UK, 2017, ISBN 978-0-08-100185-1.
47. Welch, M.; Pym, A. Improving the Flexibility and Efficiency of Gas Turbine-Based Distributed Power Plant. In Proceedings of the Future of Gas Turbine Technology, 8th International Gas Turbine Conference, Brussels, Belgium, 12–13 October 2016; Paper No.

- 08-IGTC16. Available online: <https://etn.global/wp-content/uploads/2018/09/Improving-the-flexibility-and-efficiency-of-gas-turbine-based-distrivuted-power-plant.pdf> (accessed on 10 July 2022).
48. Bhargava, R.; Campanari, S.; Montenegro, G.; Bianchi, M.; De Pascale, A.; Peretto, A. High Efficiency Gas Turbine Based Power Cycles—A Study of the Most Promosing Solutions: Part 1—A Review of the Technology. In Proceedings of the ASME Turbo Expo, Berlin, Germany, 9–13 June 2008; Paper No. GT2008-51275. [CrossRef]
49. Bhargava, R.; Campanari, S.; Montenegro, G.; Bianchi, M.; De Pascale, A.; Peretto, A. High Efficiency Gas Turbine Based Power Cycles—A Study of the Most Promosing Solutions: Part 2—A Parametric Performance Evaluation. In Proceedings of the ASME Turbo Expo, Berlin, Germany, 9–13 June 2008; Paper No. GT2008-51277. [CrossRef]
50. Gülen, S. Gas Turbines Fueled by Green Hydrogen: The Numbers Don't Add Up, Gas Turbine World. 2022. Available online: <https://gasturbine.com/gas-turbines-burning-green-hydrogen/> (accessed on 24 December 2022).
51. Bossel, U.; Eliasson, B. Energy and the Hydrogen Economy. 2003. Available online: https://afdc.energy.gov/files/pdfs/hyd_economy_bossel_eliasson.pdf (accessed on 12 July 2022).
52. Becker, C.; Marder, M.; Junges, E.; Konrad, O. Technologies for Biogas Desulfurization—An Overview of Recent Studies. *Renew. Sustain. Energy Rev.* **2022**, *159*, 112205. [CrossRef]
53. Newhall, H.; Starkman, E. *Theoretical Performance of Ammonia as a Gas Turbine Fuel*; SAE Technical Papers; SAE International: Warrendale, PA, USA, 1966; Paper No. 660768. [CrossRef]
54. Verkamp, F.; Hardin, M.; Williams, J. Ammonia Combustion Properties and Performance in Gas-Turbine Burners. *Symp. Combust.* **1967**, *11*, 985–992. [CrossRef]
55. Gupta, R. (Ed.) *Hydrogen Fuel—Production, Transport and Storage*; CRC Press: Boca Raton, FL, USA, 2009, ISBN 978-1-4200-4575-8.
56. Chiesa, P.; Lozza, G.; Mazzocchi, L. Using Hydrogen as Gas Turbine Fuel. *J. Eng. Gas Turbines Power* **2005**, *127*, 73–80. [CrossRef]
57. Winkler-Goldstein, R.; Rastetter, A. Power to Gas: The Final Breakthrough for the Hydrogen Economy? *Green* **2013**, *3*, 69–78. [CrossRef]
58. Capurso, T.; Stefanizzi, M.; Torresi, M.; Camporeale, S. Perspective of the Role of Hydrogen in the 21st Century Energy Transition. *Energy Convers. Manag.* **2022**, *251*, 114898. [CrossRef]
59. Aziz, M.; TriWijayanta, A.; Nandiyanto, A. Ammonia as Effective Hydrogen Storage: A Review on Production, Storage and Utilization. *Energies* **2020**, *13*, 3062. [CrossRef]
60. Cesaro, Z.; Ives, M.; Nayak-Luke, R.; Mason, M.; Bañares-Alcántara, R. Ammonia to Power: Forecasting the Levelized Cost of Electricity from Green Ammonia in Large-Scale Power Plants. *Appl. Energy Part A* **2021**, *282*, 116009. [CrossRef]
61. Yapicioglu, A.; Dincer, I. A Review on Clean Ammonia as a Potential Fuel for Power Generators. *Renew. Sustain. Energy Rev.* **2019**, *103*, 96–108. [CrossRef]
62. Valera-Medina, A.; Xiao, H.; Owen-Jones, M.; David, W.; Bowen, P. Ammonia for Power. *Prog. Energy Combust. Sci.* **2018**, *69*, 63–102. [CrossRef]
63. Pilavachi, P.; Stephanidis, S.; Pappas, V.; Afgan, N. Multi-Criteria Evaluation of Hydrogen and Natural Gas Fuelled Power Plant Technologies. *Appl. Therm. Eng.* **2019**, *29*, 2228–2234. [CrossRef]
64. Nose, M.; Nakamura, S.; Kataoka, M.; Kawakami, T.; Kuroki, H.; Yuri, M. Development of Hydrogen/Ammonia Firing Gas Turbine for Decarbonized Society. *Mitsubishi Heavy Ind. Tech. Rev.* **2021**, *3*, 1–11. Available online: <https://www.mhi.co.jp/technology/review/pdf/e583/e583030.pdf> (accessed on 10 October 2022).
65. Ditaranto, M.; Li, H.; Løvås, T. Concept of Hydrogen Fired Gas Turbine Cycle with Exhaust Gas Recirculation: Assessment of Combustion and Emissions Performance. *Int. J. Greenh. Gas Control* **2015**, *37*, 377–383. [CrossRef]
66. Keller, M.; Koshi, M.; Otomo, H.; Iwasaki, H.; Mitsumori, T.; Yamada, K. Thermodynamic Evaluation of an Ammonia-Fueled Combined-Cycle Gas Turbine Process Operated Under Fuel-Rich Conditions. *Energy* **2020**, *194*, 116894. [CrossRef]
67. Kobayashi, H.; Hayakawa, A.; Somarathne, K.; Okafor, E. Science and Technology of Ammonia Combustion. *Proc. Combust. Inst.* **2019**, *37*, 109–133. [CrossRef]
68. Inoue, K.; Miyamoto, K.; Domen, S.; Tamura, I.; Kawakami, T.; Tanimura, S. Development of Hydrogen and Natural Gas Co-firing Gas Turbine. *Mitsubishi Heavy Ind. Tech. Rev.* **2018**, *53*, 1–6. Available online: https://power.mhi.com/randd/technical-review/pdf/index_66e.pdf (accessed on 4 July 2022).
69. Horikawa, A.; Yamaguchi, M.; Aoki, S.; Fukue, H.; Kusterer, K.; Wirsum, M. 100% Hydrogen Dry Low NO_x Combustor Developments for 2MW Class Gas Turbine and Engine Demonstration Test. *J. Gas Turbine Soc. Jpn.* **2021**, *49*, 1–10. Available online: <https://www.gtsj.or.jp/technical/contents/vol49no4-02.pdf> (accessed on 21 October 2022). (In Japanese)
70. Ito, S.; Uchida, M.; Suda, T.; Fujimori, T. Development of Ammonia Gas Turbine Co-Generation Technology. *IHI Eng. Rev.* **2020**, *53*, 1–6. Available online: https://www.ihico.jp/en/technology/review_library/review_en/2020/_cms_conf01/_icsFiles/afieldfile/2021/01/14/Vol53No1_H.pdf (accessed on 4 July 2022).
71. Ditaranto, M.; Heggset, T.; Berstad, D. Concept of hydrogen fired gas turbine cycle with exhaust gas recirculation: Assessment of process performance. *Energy* **2020**, *192*, 116646. [CrossRef]
72. Zheng, L. (Ed.) *Oxy-Fuel Combustion for Power Generation and Carbon Dioxide (CO₂) Capture*; Woodhead Publishing Limited: Cambridge, UK, 2011, ISBN 978-1-84569-671-9.
73. Stanger, R.; Wall, T.; Spörl, R.; Paneru, M.; Grathwohl, S.; Weidmann, M.; Scheffknecht, G.; McDonald, D.; Myöhänen, K.; Ritvanen, J.; et al. Oxyfuel Combustion for CO₂ Capture in Power Plants. *Int. J. Greenh. Gas Control* **2015**, *40*, 55–125. [CrossRef]

74. Kvamsdal, H.; Jordal, K.; Bolland, O. A Quantitative Comparison of Gas Turbine Cycles with CO₂ Capture. *Energy* **2007**, *32*, 10–24. [[CrossRef](#)]
75. Sanz, W.; Jericha, H.; Bauer, B.; Göttlich, E. Qualitative and Quantitative Comparison of Two Promising Oxy-Fuel Power Cycles for CO₂ Capture. *J. Eng. Gas Turbines Power* **2008**, *130*, 031702. [[CrossRef](#)]
76. Richards, G.; Casleton, K.; Chorpening, B. CO₂ and H₂O Diluted Oxy-Fuel Combustion for Zero-Emission Power. *Proc. Inst. Mech. Eng. Part A J. Power Energy* **2005**, *219*, 121–126. [[CrossRef](#)]
77. Sundkvist, S.; Dahlquist, A.; Janczewski, J.; Sjödin, M.; Bysveen, M.; Ditaranto, M.; Langørgen, O.; Seljeskog, M.; Siljan, M. Concept for a Combustion System in Oxyfuel Gas Turbine Combined Cycles. *J. Eng. Gas Turbines Power* **2014**, *136*, 101513. [[CrossRef](#)]
78. Fiaschi, D.; Manfrida, G.; Mathieu, P.; Tempesti, D. Performance of an Oxy-Fuel Combustion CO₂ Power Cycle Including Blade Cooling. *Energy* **2009**, *34*, 2240–2247. [[CrossRef](#)]
79. Corchero, G.; Timón, V.; Montañés, J. A Natural Gas Oxy-Fuel Semiclosed Combined Cycle for Zero CO₂ Emissions: A Thermodynamic Optimization. *Proc. Inst. Mech. Eng. Part A J. Power Energy* **2011**, *225*, 377–388. [[CrossRef](#)]
80. Amann, J.; Kanniche, M.; Bouallou, C. Natural Gas Combined Cycle Power Plant Modified into an O₂/CO₂ Cycle for CO₂ Capture. *Energy Convers. Manag.* **2009**, *50*, 510–521. [[CrossRef](#)]
81. Jericha, H.; Fesharaki, M. The Graz Cycle – 1500 °C Max Temperature Potential H₂—O₂ Fired CO₂ Capture with CH₄—O₂ Firing. In Proceedings of the ASME Cogen-Turbo Power Conference, Vienna, Austria, 23–25 August 1995; Paper No. 95-GTP-75. Available online: http://www.graz-cycle.tugraz.at/pdfs/grazcycle_asme_1995.pdf (accessed on 7 October 2022).
82. Sanz, W.; Braun, M.; Jericha, H.; Platzer, M. Adapting the Zero-Emission Graz Cycle for Hydrogen Combustion and Investigation of its Part Load Behaviour. *Int. J. Hydrog. Energy* **2018**, *43*, 5737–5746. [[CrossRef](#)]
83. Heitmeir, F.; Sanz, W.; Jericha, H. Graz Cycle—A Zero Emission Power Plant of Highest Efficiency. In *The NETL Gas Turbine Handbook*; Institute for Thermal Turbomachinery and Machine Dynamics, Graz University of Technology: Graz, Austria, 2006; pp. 81–95. Available online: <https://netl.doe.gov/sites/default/files/gas-turbine-handbook/1-3-1-1.pdf> (accessed on 10 July 2022).
84. Mitterutzner, B.; Sanz, W.; Nord, L. A Part-Load Analysis and Control Strategies for the Graz Cycle. *Int. J. Greenh. Gas Control* **2022**, *113*, 103521. [[CrossRef](#)]
85. Yamashita, S.; Yajima, A.; Yoshimura, K.; Nishimura, M. Exergy Analysis on Oxy-hydrogen Combustion Turbine. *J. Gas Turbine Soc. Jpn.* **2017**, *40*, 170–177. Available online: <https://www.gtsj.or.jp/technical/contents/vol45no3-02.pdf> (accessed on 7 October 2022). (In Japanese)
86. Rogalev, N.; Rogalev, A.; Kindra, V.; Zlyvko, O.; Bryzgunov, P. Review of Closed SCO₂ and Semi-Closed Oxy-Fuel Combustion Power Cycles for Multi-Scale Power Generation in Terms of Energy, Ecology and Economic Efficiency. *Energies* **2022**, *15*, 9226. [[CrossRef](#)]
87. Macchi, E.; Consonni, S.; Lozza, G.; Chiesa, P. An Assessment of the Thermodynamic Performance of Mixed Gas-Steam Cycles: Part A—Intercooled and Steam-Injected Cycles. *J. Eng. Gas Turbines Power* **1995**, *117*, 489–498. [[CrossRef](#)]
88. Chiesa, P.; Lozza, G.; Macchi, E.; Consonni, S. An Assessment of the Thermodynamic Performance of Mixed Gas-Steam Cycles: Part B—Water-Injected and HAT Cycles. *J. Eng. Gas Turbines Power* **1995**, *117*, 499–508. [[CrossRef](#)]
89. Rao, A. Evaporative Gas Turbine (EvGT)/Humid Air Turbine (HAT) Cycles. In *Handbook of Clean Energy Systems*; Yan, J., Ed.; Wiley: Hoboken, NJ, USA, 2014. [[CrossRef](#)]
90. Mori, Y.; Nakamura, H.; Takahashi, T.; Yamamoto, K. A Highly Efficient Regenerative Gas Turbine System by New Method of Heat Recovery with Water Injection. In Proceedings of the International Gas Turbine Congress and Exhibition, Tokyo, Japan, 23–29 October 1983; Paper No. IGTC-38.
91. Rao, A.; Francuz, V.; Shen, J.; West, E. *A Comparison of Humid Air Turbine (HAT) and Combined-Cycle Power Plants*; IE-7300 Project 2999-7 Final Report; EPRI: Palo Alto, CA, USA, 1991.
92. Hatamiya, S.; Araki, H.; Higuchi, S. An Evaluation of Advanced Humid Air Turbine System with Water Recovery. In Proceedings of the ASME Turbo Expo, Vienna, Austria, 14–17 June 2004; Paper No. GT2004-54031. [[CrossRef](#)]
93. Araki, H.; Koganezawa, T.; Myouren, C.; Higuchi, S.; Takahashi, T.; Eta, T. Experimental and Analytical Study on the Operation Characteristics of the AHAT System. *J. Eng. Gas Turbines Power* **2012**, *134*, 051701. [[CrossRef](#)]
94. Nealy, D.; Reider, S. Evaluation of Laminated Porous Wall Materials for Combustor Liner Cooling. *J. Eng. Gas Turbines Power* **1980**, *102*, 268–276. [[CrossRef](#)]
95. Sweeney, P.; Rhodes, J. An Infrared Technique for Evaluating Turbine Airfoil Cooling Designs. *J. Turbomach.* **2000**, *122*, 170–177. [[CrossRef](#)]
96. Essman, D.; Vogel, R.; Tomlinson, J.; Novick, A. TF41/Lamilloy[®] Accelerated Mission Test. *J. Aircr.* **1983**, *20*, 70–75. [[CrossRef](#)]
97. Halsey, J.; Warns, R.; Weisbrod, W. Allison Advanced Turbine Systems (ATS) Engine Cycle. In Proceedings of the ASME Turbo Expo, Orlando, FL, USA, 2–5 June 1997; Paper No. 97-GT-195. [[CrossRef](#)]
98. Broomfield, R.; Ford, D.; Bhangu, I.; Thomas, M.; Frasier, D.; Burkholder, P.; Harris, K.; Erickson, G.; Wahl, J. Development and Turbine Engine Performance of Three Advanced Rhenium Containing Superalloys for Single Crystal and Directionally Solidified Blades and Vanes. *J. Eng. Gas Turbines Power* **1998**, *120*, 595–608. [[CrossRef](#)]
99. Gillespie, D.; Wang, Z.; Ireland, P.; Kohler, S. Full Surface Local Heat Transfer Coefficient Measurements in a Model of an Integrally Cast Impingement Cooling Geometry. *J. Turbomach.* **1998**, *120*, 92–99. [[CrossRef](#)]

100. Sellers, R.; Dahlberg, D.; Calvert, G. New Approaches to Turbine Airfoil Cooling and Manufacturing. In Proceedings of the AIAA/SAE 13th Propulsion Conference, Orlando, FL, USA, 11–13 July 1977; Paper No. 77-948. [CrossRef]
101. George, D.; Brown, B.; Cox, A. The Application of Rapid Solidification Rate Superalloys to Radial Wafer Turbine Blades. In Proceedings of the AIAA/SAE/ASME 15th Joint Propulsion Conference, Las Vegas, NV, USA, 18–20 June 1979; Paper No. 79-1226. [CrossRef]
102. Levari, G.; Sauer, J.; Cohn, A. The Design of an Advanced Cooled First Stage for a Full-Scale Utility Combustion Turbine. In Proceedings of the ASME Turbo Expo, London, UK, 18–22 March 1982; Paper No. 82-GT-207. [CrossRef]
103. Bunker, R. Gas Turbine Heat Transfer: 10 Remaining Hot Gas Path Challenges. In Proceedings of the ASME Turbo Expo, Barcelona, Spain, 8–11 May 2006; Paper No. GT2006-90002. [CrossRef]
104. Bunker, R. Turbine Heat Transfer and Cooling: An Overview. In Proceedings of the ASME Turbo Expo, San Antonio, TX, USA, 3–7 June 2013; Paper No. GT2013-94174.
105. Bunker, R. Evolution of Turbine Cooling. In Proceedings of the ASME Turbo Expo, Charlotte, NC, USA, 26–30 June 2017; Paper No. GT2017-63205. [CrossRef]
106. Oh, I.; Kim, K.; Lee, D.; Park, J.; Cho, H. Local Heat/Mass Transfer and Friction Loss Measurement in a Rotating Matrix Cooling Channel. In Proceedings of the ASME Turbo Expo, Orlando, FL, USA, 8–12 June 2009; Paper No. GT2009-59873. [CrossRef]
107. Tsuru, T.; Ishida, K.; Fujita, J.; Takeishi, K. Three-Dimensional Visualization of Flow Characteristics Using a Magnetic Resonance Imaging (MRI) in a Lattice Cooling Channel. *J. Turbomach.* **2019**, *141*, 061003. [CrossRef]
108. Tsuru, T.; Morozumi, R.; Takeishi, K. Study on Thermofluid Characteristics of a Lattice Cooling Channel. *Int. J. Gas Turbine Propuls. Power Syst.* **2020**, *11*, 1–8. [CrossRef]
109. Torkaman, A.; Vogel, G.; Houck, L. Design, Development and Validation of Additively Manufactured First Stage Turbine Vane for F Class Industrial Gas Turbine. In Proceedings of the ASME Turbo Expo, Virtual, 7–11 June 2021; Paper No. GT2021-60201. [CrossRef]
110. Hada, S.; Yuri, M.; Masada, J.; Ito, E.; Tsukagoshi, K. Evolution and Future Trend of Large Frame Gas Turbines a New 1600 Degree C, J Class Gas Turbine. In Proceedings of the ASME Turbo Expo, Copenhagen, Denmark, 11–15 June 2012; Paper No. GT2012-68574. [CrossRef]
111. Bayar, T. The-3D Printing Future Has Arrived. *Power Eng. Int.* **2016**, *24*, 2–7. Available online: <https://www.powerengineeringint.com/coal-fired/equipment-coal-fired/the-3d-printing-future-has-arrived/> (accessed on 22 April 2022).
112. Adair, D.; Kirka, M.; Ryan, D. Additive Manufacturing of Prototype Turbine Blades for Hot-Fired Engine Performance Validation Trials. In Proceedings of the ASME Turbo Expo 2019, Phoenix, AZ, USA, 17–21 June 2019. [CrossRef]
113. Trosch, T.; Strößner, J.; Völkl, R.; Glatzel, U. Microstructure and Mechanical Properties of Selective Laser Melted Inconel 718 Compared to Forging and Casting. *Mater. Lett.* **2016**, *164*, 428–431. [CrossRef]
114. Babu, S.; Raghavan, N.; Raplee, J.; Foster, S.; Frederick, C.; Haines, M.; Dinwiddie, R.; Kirka, M.; Plotkowski, A.; Lee, Y.; et al. Additive Manufacturing of Nickel Superalloys: Opportunities for Innovation and Challenges Related to Qualification. *Metall. Mater. Trans. A* **2018**, *49*, 3764–3780. [CrossRef]
115. Torkaman, A.; Bhattu, R. Low Cycle Fatigue Characterization of Additive Manufactured Specimen with as Printed Surface Roughness Made from Multiple Nickel Based Super Alloy. In Proceedings of the ASME Turbo Expo, Rotterdam, The Netherlands, 13–17 June 2022; Paper No. GT2022-82484. [CrossRef]
116. Krewinkel, R.; Such, A.; Torre, A.; Wiedermann, A.; Castillo, D.; Rodriguez, S.; Schleifenbaum, J.; Blaswich, M. Design and Characterization of Additively Manufactured NGVs Operated in a Small Industrial Gas Turbine. *Int. J. Gas Turbine Propuls. Power Syst.* **2020**, *11*, 36–44. [CrossRef] [PubMed]
117. Risse, J. Additive Manufacturing of Nickel-Base Superalloy IN738LC by Laser Powder Bed Fusion. 2019. Available online: <http://publications.rwth-aachen.de/record/764478/files/764478.pdf> (accessed on 22 April 2022).
118. Menon, N.; Mahdi, T.; Basak, A. Microstructure of IN738LC Fabricated Using Laser Powder Bed Fusion Additive Manufacturing. *J. Turbomach.* **2022**, *144*, 031011. [CrossRef]
119. Stößner, J.; Terock, M.; Glatzel, U. Mechanical and Microstructural Investigation of Nickel-Based Superalloy IN718 Manufactured by Selective Laser Melting (SLM). *Adv. Eng. Mater.* **2015**, *17*, 1099–1105. [CrossRef]
120. Wang, X.; Keya, T.; Chou, K. Build Height Effect on the Inconel 718 Parts Fabricated by Selective Laser Melting. *Procedia Manuf.* **2016**, *5*, 1006–1017. [CrossRef]
121. Wang, Z.; Guan, K.; Gao, M.; Li, X.; Chen, X.; Zeng, X. The Microstructure and Mechanical Properties of Deposited-IN718 by Selective Laser Melting. *J. Alloys Compd.* **2012**, *513*, 518–523. [CrossRef]
122. Mostafa, A.; Rubio, I.; Brailovski, V.; Jahazi, M.; Medraj, M. Structure, Texture and Phases in 3D Printed IN718 Alloy Subjected to Homogenization and HIP Treatments. *Metals* **2017**, *7*, 196. [CrossRef]
123. Waugh, I.; Moore, E.; Greig, A.; Macfarlane, J.; Dick-Cleland, W. Additive Manufacture of Rocket Engine Combustion Chamber Using the ABD[®]-900AM Nickel Superalloy. In Proceedings of the 7th Edition of the Space Propulsion Conference, Virtual Conference, 17–19 March 2021. Available online: https://www.researchgate.net/profile/Iain-Waugh/publication/350278621_Additive_manufacture_of_rocket_engine_combustion_chambers_using_the_ABDR-900AM_nickel_superalloy/links/60588a1c299bf173675caf79/Additive-manufacture-of-rocket-engine-combustion-chambers-using-the-ABDR-900AM-nickel-superalloy.pdf (accessed on 22 April 2022).

124. Bridges, A.; Shingledecker, J.; Clark, J.; Crudden, D. Creep Analysis and Microstructural Evaluation of a Novel Additively Manufactured Nickel-Base Superalloy (ABD[®]-900AM). *J. Eng. Gas Turbines Power* **2023**, *145*, 061005. [CrossRef]
125. Bunker, R.; Dees, J.; Palafox, P. Impingement Cooling in Gas Turbines: Design, Applications, and Limitations. In *Impingement Jet Cooling in Gas Turbines*; Sundén, B., Amano, A., Eds.; WIT Press: Southampton, UK, 2014.
126. Schlünder, E.; Gnielinski, V. Wärme- und Stoffübertragung zwischen Gut und aufprallendem Düsenstrahl. *Chem. Ing. Tech.* **1967**, *39*, 578–584. [CrossRef]
127. Annerfeldt, M.; Persson, J.; Torisson, T. Experimental Investigation of Impingement Cooling with Turbulators or Surface Enlarging Elements. In Proceedings of the ASME Turbo Expo, New Orleans, LA, USA, 4–7 June 2001; Paper No. 2001-GT-0149. [CrossRef]
128. Brakmann, R.; Chen, L.; Weigand, B.; Crawford, M. Experimental and Numerical Heat Transfer Investigation of an Impinging Jet Array on a Target Plate Roughened by Cubic Micro Pin Fins. *J. Turbomach.* **2016**, *138*, 111010. [CrossRef]
129. Oda, Y.; Takeishi, K. Concurrent Large-Eddy Simulation of Wall-Jet Heat Transfer Enhanced by Systematically-Deformed Turbulence Promoter. In Proceedings of the 15th International Heat Transfer Conference IHTC15, Kyoto, Japan, 10–15 August 2014; Paper No. IHTC15-9516. [CrossRef]
130. Dutta, S.; Singh, P. Impingement Heat Transfer Innovations and Enhancements: A Discussion on Selected Geometrical Features. In Proceedings of the ASME Turbo Expo, Virtual, 7–11 June 2021; Paper No. GT2021-59394. [CrossRef]
131. Ren, Z.; Yang, X.; Lu, X.; Li, X.; Ren, J. Experimental Investigation of Micro Cooling Units on Impingement Jet Array Flow Pressure Loss and Heat Transfer Characteristics. *Energies* **2021**, *14*, 4757. [CrossRef]
132. Singh, P.; Zhang, M.; Ahmed, S.; Ekkad, S. Effect of Nozzle-to-Target Spacing on Fin Effectiveness and Convective Heat Transfer Coefficient for Array Jet Impingement onto Novel Micro-Roughness Structures. In Proceedings of the IMECE2018, Pittsburgh, PA, USA, 9–15 November 2018; Paper No. IMECE2018-86501. [CrossRef]
133. Singh, P.; Zhang, M.; Ahmed, S.; Ramakrishnan, K.; Ekkad, S. Effect of Micro-Roughness Shapes on Jet Impingement Heat Transfer and Fin-Effectiveness. *Int. J. Heat Mass Transf.* **2019**, *132*, 80–95. [CrossRef]
134. Takeishi, K.; Krewinkel, R.; Oda, Y.; Ichikawa, Y. Heat Transfer Enhancement of Impingement Cooling by Adopting Circular Ribs or Vortex Generators in the Wall Jet Region of a Round Impingement Jet. *Int. J. Turbomach. Propuls. Power* **2019**, *5*, 17. [CrossRef]
135. Sugimoto, S.; Takeishi, K.; Oda, Y.; Harada, T. A Study on Heat Transfer Enhancement of Jet Impingement Cooling by Turbulence Promoters. In Proceedings of the International Gas Turbine Congress 2007 Tokyo, Tokyo, Japan, 2–7 December 2007; Paper No. TS-116.
136. Domnick, C. Device for Cooling a Component of a Gas Turbine/Turbo Machine by Means of Impingement Cooling. U.S. Patent 11280216, 22 March 2022. Available online: <https://patents.google.com/patent/US11280216B2/en> (accessed on 24 December 2022).
137. Singh, P.; Ravi, B.; Ekkad, S. Experimental Investigation of Heat Transfer Augmentation by Different Jet Impingement Hole Shapes under Maximum Crossflow. In Proceedings of the ASME Turbo Expo, Seoul, Republic of Korea, 13–17 June 2016; Paper No. GT2016-57874. [CrossRef]
138. Krewinkel, R. Gas Turbine Engine Having a Flow-Conducting Assembly Formed of Nozzles to Direct Cooling Medium Onto a Surface. U.S. Patent 10787927, 29 September 2020. Available online: <https://patents.justia.com/patent/10787927> (accessed on 24 December 2022).
139. Yalcikkaya, O.; Durmaz, U.; Tepe, A.; Uysal, U.; Özel, M. Effect of Slot-Shaped Pins on Heat Transfer Performance in the Extended Jet Impingement Cooling. *Int. J. Sci.* **2022**, *179*, 107698. [CrossRef]
140. Khalatov, A.; Nam, C. Aerothermal Vortex Technologies in Aerospace Engineering. *J. Korean Soc. Mar. Eng.* **2004**, *28*, 163–184. Available online: <http://www.koreascience.or.kr/article/JAKO200411922191209.page> (accessed on 24 December 2022).
141. Zhang, C.; Wang, S.; Li, J.; Zhu, Y.; Peng, T.; Yang, H. Additive Manufacturing of Products with Functional Fluid Channels: A Review. *Addit. Manuf.* **2020**, *36*, 101490. [CrossRef]
142. Alsulami, M.; Mortazavi, M.; Niknam, S.; Li, D. Design Complexity and Performance Analysis in Additively Manufactured Heat Exchangers. *Int. J. Adv. Manuf. Technol.* **2020**, *110*, 865–873. [CrossRef]
143. Parbat, S.; Min, Z.; Yang, L.; Chyu, M.-K. Experimental and Numerical Analysis of Additively Manufactured Inconel 718 Coupons with Lattice Structure. *J. Turbomach.* **2020**, *142*, 061004. [CrossRef]
144. Pietropaoli, M.; Ahlfeld, R.; Montomoli, F.; Ciani, A.; D’Ercole, M. Design for Additive Internal Channel Optimization. *J. Eng. Gas Turbines Power* **2017**, *139*, 102101. [CrossRef]
145. Pietropaoli, M.; Montomoli, F.; Gaymann, A. Three-Dimensional Fluid Topology Optimization for Heat Transfer. *Struct. Multidiscip. Optim.* **2018**, *59*, 801–812. [CrossRef]
146. Chen, I.-L.; Sahin, I.; Wright, L.; Han, J.-C.; Krewinkel, R. Heat Transfer in a Rotating, Two-Pass, Variable Aspect Ratio Cooling Channel with Profiled V-Shaped Ribs. *J. Turbomach.* **2021**, *143*, 081013. [CrossRef]
147. Smith, R.; Dutta, S. Conjugate Thermal Optimization with Unsupervised Machine Learning. *J. Heat Transf.* **2021**, *143*, 052901. [CrossRef]
148. Hossain, M.; Ameri, A.; Gregory, J.; Bons, J. Experimental Investigation of Innovative Cooling Schemes on an Additively Manufactured Engine Scale Turbine Nozzle Guide Vane. *J. Turbomach.* **2021**, *143*, 051004. [CrossRef]
149. Wimmer, T.; Rühmer, T.; Mich, Y.; Wanf, L.; Weigand, B. Experimental and Numerical Investigation on an Additively Manufactured Gas Turbine Ring Segment with an In-Wall Cooling Scheme. In Proceedings of the ASME Turbo Expo, Phoenix, AZ, USA, 17–21 June 2019; p. GT2019-90227. [CrossRef]

150. Rühmer, T.; Wimmer, T.; Gampe, U.; Fischer, K.; Haberland, C. Structural Integrity Assessment and Engine Test of an Additive Manufactured First Stage Ring Segment of a Siemens Large Gas Turbine. In Proceedings of the ASME Turbo Expo, Phoenix, AZ, USA, 17–21 June 2019; p. GT2019-90344. [[CrossRef](#)]
151. Pinelli, L.; Amedei, A.; Meli, E.; Vanti, F.; Romani, B.; Benvenuti, G.; Fabbrini, M.; Morganti, N.; Rindi, A.; Arnone, A. Innovative Design, Structural Optimization and Additive Manufacturing of New-Generation Turbine Blades. *J. Turbomach.* **2022**, *144*, 011006. [[CrossRef](#)]
152. Magarramova, L.; Kinzburskiy, V.; Vasilyev, B. Novel Designs of Turbine Blades for Additive Manufacturing. In Proceedings of the ASME Turbo Expo, Seoul, Republic of Korea, 13–17 June 2016; Paper No. GT2016-56084. [[CrossRef](#)]
153. Straub, D.; Ramesh, S.; Searly, M.; Robey, E.; Floyd, T.; Roy, A.; Ames, F. Frmance of Additively Manufactured Internally Cooled Airfoils for Small Industrial Gas Turbines. In Proceedings of the ASME Turbo Expo, Rotterdam, The Netherlands, 13–17 June 2022; Paper No. GT2022-83333. [[CrossRef](#)]
154. Kirsch, K.; Thole, K. Pressure Loss and Heat Transfer Performance for Additively and Conventionally Manufactured Pin Fin Arrays. *Int. J. Heat Mass Transf.* **2017**, *108 Pt B*, 2502–2513. [[CrossRef](#)]
155. Takeishi, K.; Oda, Y.; Miyaka, Y.; Motoda, Y. Convective heat Transfer and Pressure Loss in Rectangular Ducts with Inclined Pin-Fin on a Wavy Endwall. *J. Eng. Gas Turbines Power* **2013**, *135*, 061902. [[CrossRef](#)]
156. Saglam, S.; Fujitai, J.; Takeishi, K.; Oda, Y. Three-dimensional Velocity Field Measurements of a Rectangular Channel with an Inclined Pin-Fin Array on a Flat and Wavy Endwall Using Magnetic Resonance Velocimetry. In Proceedings of the Asian Congress on Gas Turbines 2018, Morioka, Japan, 22–24 August 2018; Paper No. ACGT2018-TS78.
157. McClain, S.; Hanson, D.; Cinnamon, E.; Snyder, J.; Kunz, R.; Thole, K. Flow in a Simulated Turbine Blade Cooling Channel with Spatially Varying Roughness Caused by Additive Manufacturing Orientation. *J. Turbomach.* **2021**, *143*, 071013. [[CrossRef](#)]
158. Mazzei, L.; Andereini, A.; Facchini, B. Assessment of Modelling Strategies for Film Cooling. *Int. J. Numer. Methods Heat Fluid Flow* **2017**, *27*, 1118–1127. [[CrossRef](#)]
159. Zhang, Z.; Chen, Z.; Su, X.; Yuan, X. Non-Uniform Source Term Model for Film-Cooling with the Internal Cross Flow. In Proceedings of the ASME Turbo Expo, Virtual, 22–26 June 2020; Paper No. GT2020-14404. [[CrossRef](#)]
160. Kamp, T.; Völker, S.; Zehe, F. A Model for Cylindrical Hole Film Cooling: Part I—A Correlation for Jet-Flow with Application to Film Cooling. *J. Turbomach.* **2012**, *134*, 061010. [[CrossRef](#)]
161. Kamp, T.; Völker, S. A Model for Cylindrical Hole Film Cooling: Part II—Model Formulation, Implementation and Results. *J. Turbomach.* **2012**, *134*, 061011. [[CrossRef](#)]
162. He, L. Block-Spectral Approach to Film-Cooling Modeling. *J. Turbomach.* **2012**, *134*, 021018. [[CrossRef](#)]
163. He, L.; Oldfield, M. Unsteady Conjugate Heat Transfer Modelling. *J. Turbomach.* **2011**, *133*, 031022. [[CrossRef](#)]
164. Maffulli, R.; He, L. Impact of Wall Temperature on Heat Transfer Coefficient and Aerodynamics for Three-Dimensional Turbine Blade Passage. *J. Therm. Sci. Eng. Appl.* **2017**, *9*, 041002. [[CrossRef](#)]
165. Dyson, T.; Winka, J.; Helmer, D. Conjugate Scaling in the Presence of Bore Cooling. In Proceedings of the ASME Turbo Expo, Montreal, Canada, 15–19 June 2015; Paper No. GT2015-43625. [[CrossRef](#)]
166. Stewart, W.; Dyson, T. Conjugate Heat Transfer Scaling for Inconel 718. In Proceedings of the ASME Turbo Expo, Charlotte, NC, USA, 26–30 June 2017; Paper No. GT2017-64873. [[CrossRef](#)]
167. Issakhanian, E.; Elkins, C.; Eaton, J. In-Hole and Mainflow Velocity Measurements of Low-Momentum Jets in Crossflow Emanating from Short Holes. *Exp. Fluids* **2012**, *53*, 1765–1778. [[CrossRef](#)]
168. Milani, P.; Gunady, I.; Ching, D.; Banko, A.; Elkins, C.; Eaton, J. Enriching MRI Mean Flow Data of Inclined Jets in Crossflow with Large Eddy Simulations. *Int. J. Heat Fluid Flow* **2019**, *80*, 108472. [[CrossRef](#)]
169. Peterson, S.; Plesniak, M. Short-Hole Jet-in-Crossflow Velocity Field and Its Relationship to Film-Cooling Performance. *Exp. Fluids* **2002**, *33*, 889–898. [[CrossRef](#)]
170. Li, Z.; Wei, T.; Guo, Y.; Sealy, M. State-Of-Art, Challenges, and Outlook on Manufacturing of Cooling Holes for Turbine Blades. *Mach. Sci. Technol.* **2015**, *19*, 361–399. [[CrossRef](#)]
171. Stimpson, C.; Snyder, J.; Thole, K.; Mongillo, D. Effectiveness Measurements of Additively Manufactured Film Cooling Holes. *J. Turbomach.* **2018**, *140*, 011009. [[CrossRef](#)]
172. Snyder, J.; Thole, K. Performance of Public Cooling Geometries Produced Through Additive Manufacturing. *J. Turbomach.* **2020**, *142*, 051009. [[CrossRef](#)]
173. Yang, L.; Min, Z.; Parbat, S.; Chyu, M.-K. Effect of Pore Blockage on Transpiration Cooling with Additive Manufacturable Perforate Holes. In Proceedings of the ASME Turbo Expo, Oslo, Norway, 11–15 June 2018; Paper No. GT2018-75310. [[CrossRef](#)]
174. Min, Z.; Parbat, S.; Yang, L.; Chyu, M.-K. Thermal-Fluid and Mechanical Investigations of Additively Manufactured Geometries for Transpiration Cooling. In Proceedings of the ASME Turbo Expo, Phoenix, AZ, USA, 17–21 June 2019. [[CrossRef](#)]
175. Min, Z.; Huang, G.; Parbat, S.; Yang, L.; Chyu, M.-K. Experimental Investigation on Additively Manufactured Transpiration and Film Cooling Structures. *J. Turbomach.* **2019**, *141*, 031009. [[CrossRef](#)]
176. Takeishi, K.; Komiyama, M.; Oda, Y.; Egawa, Y. Aerothermal Investigations on Mixing Flow Field of Film Cooling With Swirling Coolant Flow. *J. Turbomach.* **2014**, *136*, 051001. [[CrossRef](#)]
177. Bunker, R. The Effects of Manufacturing Tolerances on Gas Turbine Cooling. *J. Turbomach.* **2009**, *131*, 041018. [[CrossRef](#)]
178. Högnér, L.; Voigt, M.; Mailach, R.; Meyer, M.; Gerstberger, U. Probabilistic Finite Element Analysis of Cooled High-Pressure Turbine Blades—Part A: Holistic Description of Manufacturing Variability. *J. Turbomach.* **2020**, *142*, 101008. [[CrossRef](#)]

179. Högner, L.; Voigt, M.; Mailach, R.; Meyer, M.; Gerstberger, U. Probabilistic Finite Element Analysis of Cooled High-Pressure Turbine Blades—Part B: Probabilistic Analysis. *J. Turbomach.* **2020**, *142*, 101009. [[CrossRef](#)]
180. Wildgoose, A.; Thole, K.; Subramanian, R.; Kersting, L.; Kulkarni, A. Impacts of the Additive Manufacturing Process on the Roughness of Engine Scale Vanes and Cooling Channels. *J. Turbomach.* **2023**, *145*, 041013. [[CrossRef](#)]
181. Mazzei, L.; Soghe, R.; Bianchini, C. Calibration of a Computational Fluid Dynamics Methodology for the Simulation of Roughness Effects on Friction and Heat Transfer in Additively Manufactured Components. *J. Turbomach.* **2022**, *144*, 081002. [[CrossRef](#)]
182. Wildgoose, A.; Thole, K. Heat Transfer and Pressure Loss of Additively Manufactured Internal Cooling Channels with Various Shapes. *J. Turbomach.* **2023**, *145*, 071011. [[CrossRef](#)]
183. Snyder, J.; Stimpson, C.; Thole, K.; Mongillo, D. Build Direction Effects on Microchannel Tolerance and Surface Roughness. *J. Mech. Des.* **2015**, *137*, 111411. [[CrossRef](#)]
184. Stimpson, C.; Snyder, J.; Thole, K.; Mongillo, D. Roughness Effects on Flow and Heat Transfer for Additively Manufactured Channels. *J. Turbomach.* **2016**, *138*, 051008. [[CrossRef](#)]
185. Kirsch, K.; Thole, K. Heat Transfer and Pressure Loss Measurements in Additively Manufactured Wavy Microchannels. *J. Turbomach.* **2016**, *139*, 011007. [[CrossRef](#)]
186. Lüscher, P.; Deflorin, M.; Vogesser, M.; Stuber, M.; Galoul, V.; Ko, M. Internal Heat Transfer Measurement on Metal-Based Additively Manufactured Channels Using a Transient Technique. In Proceedings of the ASME Turbo Expo, Rotterdam, The Netherlands, 13–17 June 2022; Paper No. GT2022-79547. [[CrossRef](#)]
187. Stimpson, C.; Snyder, J.; Thole, K.; Mongillo, D. Scaling Roughness Effects on Pressure Loss and Heat Transfer of Additively Manufactured Channels. *J. Turbomach.* **2016**, *139*, 021003. [[CrossRef](#)]
188. Ferster, K.; Kirsch, K.; Thole, K. Effects of Geometry and Spacing in Additively Manufactured Microchannel Pin Fin Arrays. *J. Turbomach.* **2018**, *140*, 011007. [[CrossRef](#)]
189. Bons, J. A Review of Surface Roughness Effects in Gas Turbines. *J. Turbomach.* **2010**, *132*, 021004. [[CrossRef](#)]
190. Mazzei, L.; Soghe, R.; Bianchini, C. Calibration of a CFD Methodology for the Simulation of Additively Manufactured Components Accounting for the Effects of Diameter and Printing Direction on Friction and Heat Transfer. In Proceedings of the ASME Turbo Expo, Rotterdam, The Netherlands, 13–17 June 2022; Paper No. GT2022-82391. [[CrossRef](#)]
191. Aupoix, B. Improved Heat Transfer Predictions on Rough Surfaces. *Int. J. Heat Fluid Flow* **2015**, *56*, 160–171. [[CrossRef](#)]
192. Aupoix, B. Roughness Corrections for the k - ω Shear Stress Transport Model: Status and Proposals. *J. Fluids Eng.* **2014**, *137*, 021202. [[CrossRef](#)]
193. Altland, S.; Yang, X.; Thole, K.; Kunz, R.; McClain, S. Application of a Distributed Element Roughness Model to Additively Manufactured Internal Cooling Channels. In Proceedings of the ASME Turbo Expo, Rotterdam, The Netherlands, 13–17 June 2022; Paper No. GT2022-81218. [[CrossRef](#)]
194. Town, J.; Straub, D.; Black, J.; Thole, K.; Shih, T. State-of-the-Art Cooling Technology for a Turbine Rotor Blade. *J. Turbomach.* **2018**, *140*, 071007. [[CrossRef](#)]
195. Chyu, M.-K.; Siw, S.; Karainov, V.; Slaughter, W.; Alvin, M. Aerothermal Challenges in Syngas, Hydrogen-Fired, and Oxyfuel Turbines—Part II: Effects of Internal Heat Transfer. *J. Therm. Sci. Eng. Appl.* **2009**, *1*, 011003. [[CrossRef](#)]
196. Chyu, M.-K.; Alvin, M. Turbine Airfoil Aerothermal Characteristics in Future Coal–Gas-Based Power Generation Systems. *Heat Transf. Res.* **2010**, *41*, 737–752. [[CrossRef](#)]
197. Dabagh, A.; Andrews, G.; Husain, R.; Husain, C.; Nazari, A.; Wu, J. Impingement/Effusion Cooling: The Influence of the Number of Impingement Holes and Pressure Loss on the Heat Transfer Coefficient. *J. Turbomach.* **1990**, *112*, 467–476. [[CrossRef](#)]
198. Andrews, G.; Dabagh, A.; Asere, A.; Bazdidi-Therani, F.; Mkpadi, M.; Nazari, A. Impingement/effusion cooling, Heat Transfer and Cooling in Gas Turbines, AGARD-CP-527, 1993; p. 30.1–30.10. Available online: <https://www.sto.nato.int/publications/AGARD/Forms/AllItems.aspx?RootFolder=%2Fpublications%2FAGARD%2FAGARD-CP-527&FolderCTID=0x0120D5200078F9E87043356C409A0D30823AFA16F60B00B8BCE98BB37EB24A8258823D6B11F157&View=%7B7E9C814C-056A-4D31-8392-7C6752B2AF2B%7D> (accessed on 24 December 2022).
199. Cho, H.; Rhee, D.; Goldstein, R. Effects of Hole Arrangements on Local Heat/Mass Transfer for Impingement/Effusion Cooling with Small Hole Spacing. *J. Turbomach.* **2008**, *130*, 041003. [[CrossRef](#)]
200. Rhee, D.; Choi, J.; Cho, J. Flow and Heat (Mass) Transfer Characteristics in an Impingement/Effusion Cooling System with Crossflow. *J. Turbomach.* **2003**, *125*, 74–82. [[CrossRef](#)]
201. Hong, S.; Rhee, D.; Cho, H. Effects of Fin Shapes and Arrangements on Heat Transfer for Impingement/Effusion Cooling with Crossflow. *J. Heat Transf.* **2007**, *129*, 1697–1707. [[CrossRef](#)]
202. Hong, S.; Cho, H. Effect of Rotation on Heat/Mass Transfer for an Impingement/Effusion Cooling System. *J. Heat Transf.* **2010**, *132*, 114501. [[CrossRef](#)]
203. Dailey, G.; Evans, P.; McCall, R. Cooled Aerofoil for a Gas Turbine Engine. Europe Patent EP 1 022 432 B1, 23 March 2005.
204. Lutum, E.; Semmler, K.; Wolfersdorf, J. Cooled Blade for a Gas Turbine. US Patent 2001/0016162 A1, 23 August 2001.
205. Liang, G. Stator Vane with Near Wall Integrated Micro Cooling Channels. US Patent 8,414,263 B1, 9 April 2013.
206. Liang, G. Turbine Airfoil with Multiple Near Wall Compartment Cooling. US Patent 7,556,476 B1, 7 July 2009.
207. Ngetich, G.; Ireland, P.; Murray, A.; Romero, E. A Three-Dimensional Conjugate Approach for Analysing a Double-Walled Effusion-Cooled Turbine Blade. *J. Turbomach.* **2019**, *141*, 011002. [[CrossRef](#)]

208. Courtis, M.; Murray, A.; Coulton, B.; Ireland, P.; Mayo, I. Influence of Spanwise and Streamwise Film Hole Spacing on Adiabatic Film Effectiveness for Effusion-Cooled Gas Turbine Blades. *Int. J. Turbomach. Propuls. Power* **2021**, *6*, 37. [[CrossRef](#)]
209. Murray, A.; Ireland, P.; Wong, T.; Tang, S.; Rawlinson, A. High Resolution Experimental and Computational Methods for Modelling Multiple Row Effusion Cooling Performance. *Int. J. Turbomach. Propuls. Power* **2018**, *3*, 4. [[CrossRef](#)]
210. Murray, A.; Ireland, P.; Romero, E. Experimental and Computational Methods for the Evaluation of Double-Wall, Effusion Cooling Systems. *J. Turbomach.* **2020**, *142*, 111003. [[CrossRef](#)]
211. Murray, A.; Ireland, P.; Romero, E. An Experimentally Validated Low-Order Model of the Thermal Response of Double-Wall Effusion Cooling Systems for High-Pressure Turbine Blades. *J. Turbomach.* **2021**, *143*, 111015. [[CrossRef](#)]
212. Bang, M.; Kim, S.; Park, H.; Kim, T.; Rhee, D.; Cho, H. Impingement/Effusion Cooling with a Hollow Cylinder Structure for Additive Manufacturing: Effect of Channel Gap Height. *Int. J. Heat Mass Transf.* **2021**, *175*, 121420. [[CrossRef](#)]
213. Bang, M.; Kim, S.; Choi, S.; Sohn, H.; Cho, H. Impingement/Effusion Cooling with a Hollow Cylinder Structure for Additive Manufacturing. *Int. J. Heat Mass Transf.* **2020**, *155*, 119786. [[CrossRef](#)]
214. Hahn, W.; Urner, G. Verbundvorhaben Schadstoffe in der Luftfahrt: Untersuchungen zur Kühlung von Brennkammererelementen. Forschungsbericht BMFT-20 T 9104t, 1995.
215. Li, L.; Wan, H.; Gao, W.; Tong, F.; Sun, S. Investigation on Creep Characteristics of Nickel-Base Single Crystal Alloy Double Wall Cooling Specimen. In Proceedings of the ASME Turbo Expo, Oslo, Norway, 11–15 June 2018; Paper No: GT2018-76285. [[CrossRef](#)]
216. Elmukashfi, E.; Murray, A.; Ireland, P.; Cocks, A. Analysis of the Thermomechanical Stresses in Double-Wall Effusion Cooled Systems. *J. Turbomach.* **2020**, *142*, 051002. [[CrossRef](#)]
217. Laschet, G.; Krewinkel, R.; Hul, P.; Bohn, D. Conjugate analysis and Effective Thermal Conductivities of Effusion-Cooled Multilayer Blade Sections. *Int. J. Heat Mass Transf.* **2013**, *57*, 812–821. [[CrossRef](#)]
218. Skamniotis, C.; Courtis, M.; Cocks, A. Multiscale Analysis of Thermomechanical Stresses in Double Wall Transpiration Cooling Systems for Gas Turbine Blades. *Int. J. Mech. Sci.* **2021**, *207*, 106657. [[CrossRef](#)]
219. Skamniotis, C.; Cocks, A. Minimising Stresses in Double Wall Transpiration Cooled Components for High Temperature Applications. *Int. J. Mech. Sci.* **2021**, *189*, 105983. [[CrossRef](#)]
220. Skamniotis, C.; Cocks, A. Designing Against Severe Stresses at Compound Cooling Holes of Double Wall Transpiration Cooled Engine Components. *Aerosp. Sci. Technol.* **2021**, *116*, 106856. [[CrossRef](#)]
221. Skamniotis, C.; Cocks, A. Thermal and Centrifugal Stresses in Curved Double Wall Transpiration Cooled Components with Temperature Dependent Thermoelastic Properties. *Int. J. Solids Struct.* **2022**, *234–235*, 111273. [[CrossRef](#)]
222. Skamniotis, C.; Cocks, A. 2D and 3D Thermoelastic Phenomena in Double Wall Transpiration Cooling Systems for Gas Turbine Blades and Hypersonic Flight. *Aerosp. Sci. Technol.* **2021**, *113*, 106610. [[CrossRef](#)]
223. Stoakes, P.; Ekkad, S. Optimized Impingement Configurations for Double Wall Cooling Applications. In Proceedings of the ASME Turbo Expo, Vancouver, BC, Canada, 6–10 June 2011. [[CrossRef](#)]
224. Panse, S.; Ekkad, S. Forced Convection Cooling of Additively Manufactured Single and Double Layer Enhanced Microchannels. *Int. J. Heat Mass Transf.* **2021**, *168*, 120881. [[CrossRef](#)]
225. Luo, L.; Zhang, Y.; Wang, C.; Wang, S.; Sunden, B. On the Heat Transfer Characteristics of a Lamilloy Cooling Structure with Curvatures with Different Pin Fin Configurations. *Int. J. Num. Methods Heat Fluid Flow* **2021**, *31*, 1268–1394. [[CrossRef](#)]
226. Yu, Z.; Xu, T.; Li, J.; Ma, L.; Xu, T. Comparison of a Series of Double Chamber Model with Various Hole Angles for Enhancing Cooling Effectiveness. *Int. Commun. Heat Mass Transf.* **2013**, *44*, 38–44. [[CrossRef](#)]

Disclaimer/Publisher’s Note: The statements, opinions and data contained in all publications are solely those of the individual author(s) and contributor(s) and not of MDPI and/or the editor(s). MDPI and/or the editor(s) disclaim responsibility for any injury to people or property resulting from any ideas, methods, instructions or products referred to in the content.